STUDIES ON SOME VISIBLE LASING TRANSITIONS IN PULSED XeIV LASER

By
RAMA CHARI

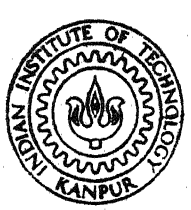

DEPARTMENT OF PHYSICS
INDIAN INSTITUTE OF TECHNOLOGY, KANPUR
NOVEMBER, 1984

STUDIES ON SOME VISIBLE LASING TRANSITIONS IN PULSED XeIV LASER

A Thesis Submitted
In Partial Fulfilment of the Requirements
for the Degree of
DOCTOR OF PHILOSOPHY

By
RAMA CHARI

to the
DEPARTMENT OF PHYSICS
INDIAN INSTITUTE OF TECHNOLOGY, KANPUR
NOVEMBER, 1984

PHY - 1984 - D - CHA - STU

CERTIFICATE

This is to certify that the work presented in this thesis titled 'Studies on Some Visible Lasing Transitions in Pulsed Xenon Ion Laser' is the original work of Ms. Rama Chari, done under my supervision and it has not been submitted elsewhere for a degree.

Dr G Chakrapani
Assistant Professor
Department of Physics
Indian Institute of Technology
KANPUR - 208016

ACKNOWLEDGEMENTS

I am deeply grateful to Dr. G. Chakrapani for introducing me to this field and for his constant help and guidance throughout the work.

I am thankful to Dr. T.M. Srinivasan, Dr. G.N. Rao and Dr. O.P. Katyal for their helpful advice from time to time. I wish to thank Dr. Y.V. Chalapati Rao and Sri K.M.S. Prasad for the loan of the boxcar-integrator.

Dr. A.A. Tagliaferri, La Plata, Argentina and Dr. William C. Martin, N.B.S., U.S.A. have very kindly supplied the latest spectroscopic information on these transitions. I thank Prof. L. Minnhagen, Lund Institute of Technology, Sweden for his helpful advice.

The cooperation of the lasers and spectroscopy group, I.I.T. Kanpur and the help given by Dr. P.B.K. Sarma in the beginning of the work is appreciated. I thank the members of the glass blowing workshop and the Physics workshop.

I wish to thank Alika, Pramila and Raghuram for their help in the preparation of the thesis, Mrs. B. Rukmini and Mr. R.N. Srivastava for the neat typing and Mr. S. Qasim Husain for preparing the tracings.

I wish to express my deep sense of gratitude to my mother and my sisters Akka and Vijaya for their continuous encouragement, guidance and help in all matters.

Rama Chari

CONTENTS

List of Tables

List of Figures

SYNOPSIS

Studies on Some Visible Lasing Transitions in Pulsed Xe IV Laser

RAMA CHARI

Department of Physics
Indian Institute of Technology Kanpur
India

This thesis presents the results of some studies on seven visible transitions in the short-pulse Xe IV laser. The wavelengths of these transitions are 4954.13A, 5007.8A, 5159.08A, 5260.19A, 5352.92A and 5955.67A.

The first six chapters form the main part of the thesis and describe the various studies made on the pulsed Xe IV laser.

The first and the introductory chapter includes a brief review of the general characteristics of gaseous ion lasers along with a short history of their development. The Xe IV laser is the most powerful one in the pulsed laser family capable of delivering a few kilowatts of peak power in a suitably designed system. However, no systematic study of the performance of this laser has so far been made to our knowledge; the chief reason for this is probably the non-availability of relevant information on the spectroscopic and other physical parameters of the transitions.

In the second chapter, the experimental techniques used in fabrication of the pulsed Xe IV laser and in carrying out the

different experiments are described. The output of the laser in different wavelengths has been measured using a photo-diode or an energy meter in conjunction with a gated integrator. Threshold gain measurements on the various transitions have been made by introducing known losses in the cavity. For studying the effect of axial magnetic fields on the laser output, a pulsed magnetic field drive circuit has been developed to drive a solenoidal magnet. This has enabled us to reach fields as high as 5 KG, though fields beyond 2 KG were found unnecessary due to the quenching of laser action.

The effect of different laser parameters on the power output is discussed in Chapter 3. The various parameters considered are the gas pressure, excitation voltage, energy storage capacitor, the diameter and length of the plasma tube. It has been found that the optimum pressures for individual lines are different from the pressure at which the total all-line power output is maximum. Further, the variation of the optimum pressure for any particular line with the plasma tube diameter is distinctly non-linear although the all line optimum pressure shows a linear dependence on tube diameter. The relative power distribution in the different lines is also a function of pressure; the lines at 5395A and 5955A dominate the spectrum at the highest operating pressures while the line at 4954A is the strongest at very low pressures. The operating pressure range, which depends on the tube diameter to some extent, is from nearly 30 microns down to less than 1.5 microns. The laser efficiency is found to

increase with increasing tube diameter though the rate of this increase is marked only upto diameters of 4 mm. The laser operation is not very strong in tubes of small bore. However, in tubes of larger diameter the inversion is observed to exist mostly near the tube axis. This indicates that wall-collisions play a significant role in quenching the laser action.

The results of small signal gain measurements on these transitions are presented in Chapter 4. To our knowledge these are the highest values repoted so far. The variation of the gain coefficient with various laser parameters has been studied. Our results further support the conclusions given in Chapter 3 about the excitation processes. An attempt to study the saturation behaviour of this laser has also been made. It is found that the power output is linearly proportional to the small signal gain coefficient, indicating that the transitions are homogeneously broadened. However, attempts to fit the experimentally observed variation of power output with varying operating gain to the existing theoretical formulation have failed.

A discussion of the probable excitation mechanisms involved in this laser is presented in Chapter 5. From the observed current dependence of the output power in this case it is interpreted that two excitation processes are more probable. The main process is a two-step electron impact excitation from the neutral atom ground state to the upper laser level. The intermediate level probably belongs to Xe III though it is not necessarily the ion ground state. At high pressures and

currents another excitation process becomes significant which involves a four step excitation alongwith some cascade processes. This mechanism contributes to the double peak formation in the laser pulse. The quenching of the first peak is probably due to collisional de-excitation of the upper laser level and we believe that recombination and collisional de-excitation at the tube walls can contribute significantly to the quenching of laser action.

The effect of axial magnetic fields on the laser output is described in Chapter 6. During these studies the laser has been operated both with and without a Brewster window in the cavity and the variation in the power as well as the polarization of the output has been studied. The power in all the lines has been observed to decrease monotonically with increasing magnetic field except for a very small enhancement at very low fields (10 G). This continuous reduction in power output with increasing magnetic field is similar to that observed in the 4579A line of a pulsed Ar^+ laser by Birnbaum. A tentative explanation for the behaviour observed in the present work is given. The Faraday rotation produced by the medium is observed to first increase to a peak value and then decrease with increasing magnetic field. The ellipticity, which is very small, shows a similar variation.

In the seventh and the final chapter, the conclusions arrived at on the basis of these various studies are enumerated alongwith the limitations of the present work and the immediate follow-up work undertaken.

CHAPTER 1

INTRODUCTION

Gaseous ion lasers are among the most important practical sources of coherent radiation in the ultraviolet, visible and near infrared. Operating in both pulsed and cw modes, they find numerous uses in experiments in basic sciences as well as in various industrial and technological applications. All the important ion lasers can broadly be divided into two groups depending on whether the active ion is from one of the noble gases viz., Ar, Ne, Kr, Xe or from a metal vapor viz., Cd, Hg, Zn, Cu, Se, Mg, Au etc. Apart from these lasing has been observed in some other ionised gaseous media also. However, among ion lasers, the noble gas ion lasers have been more widely studied and developed and are in extensive use at present.

1.1 Historical Background of Noble Gas Ion Lasers

The first noble gas ion laser to be reported was the pulsed Argon ion laser, which was independently and almost simultaneously discovered by Bridges [1], Convert et al. [2,3] and Bennett et al. [4]. These initial observations showed that this laser had several strongly lasing transitions in the blue and green regions of the spectrum. Optical gains of several dB/m and long pulse (> 1 ms) output of several watts were reported [4]. Bridges [5] extended the pulsed ion laser operation to cover the whole visible spectrum with singly ionised Krypton and Xenon lasers. Continuous operation on many previously reported transitions in Ar II, Kr II and Xe II was reported by Gordon et al. [6]. Several new lasing transitions were discovered in the near infrared by Sinclair [7] and Horrigan et al [8]; in the visible by Bloom and Bell [9] and Birnbaum and Stokes [10]; and in the ultraviolet by Dana et al. [11]. Bridges and Chester [12] reported 118 visible and ultraviolet laser transitions in seven elements while Cheo and Cooper [13] observed 55 ultraviolet transitions in 6 elements. A survey of the literature up to 1980 [14] indicates that the number of noble gas ion laser transitions has been further increased to as many as 236, many of which have yet to be identified.

Comprehensive reviews of noble gas ion lasers have been given by Paananen [15], Kitaeva et al. [16], Bridges and

Chester [17], Davis and King [18] and Dunn and Ross [19]. The spectroscopy of ion laser transitions has been reviewed by Bridges and Chester [20] and Willett [21], while Bridges et al. [22] have reviewed the ion laser plasmas.

Most of the early ion laser transitions were reported in the pulsed mode. In nearly all of them lasing occured only during the exciting current pulse,indicating that electron impact was the dominant mechanism involved in exciting the upper levels. In addition, lasing action in discharge afterglow was observed by Laures et al. [23,24,25] on Kr II transitions in a He-Kr discharge and on Xe II transitions in a Ne-Xe discharge. In these cases the excitation mechanism was attributed to energy/charge transfer processes. However, this latter class of transitions has turned out to be of academic interest only due to the extremely low power output. This is explained to be due to the fact that in a conventional plasma discharge, the lower levels of these transitions are excessively populated through electron collisions.

The noble gas ion laser transitions identified so far involve various types of transitions among singly and multip ionized species. A common characteristic of all these trans tions is that the strongest laser lines are also the stronge lines observed in the spontaneous spectrum. This has been confirmed for Argon lines by Minnhagen [26] and is found to be true for Xenon lines also based both on the available

spectral data [27] and the observations of relative spontaneous intensities in the present work. For atomic lines which follow the LS-coupling approximation, this observed characteristic implies that the strongest laser lines should satisfy the preferred LS-coupling selection rules viz., $\Delta J = \Delta L$, especially $\Delta J = \Delta L = +1$ and no change in core or total spin [21]. The rule $\Delta J = \Delta L$ apparently has wider applicability than the other rules; many transitions involving core or spin change obey it [28].

Transitions violating the LS-coupling rules require a more general model. For Ar II transitions, Statz et al. [29] have made calculations using intermediate coupling schemes and found that the J_c1-coupling approximation is more valid in these cases. It is expected that this model will also prove to give a more appropriate description of laser lines originating from levels of higher energy or belonging to heavier gases such as Krypton and Xenon.

1.2 Excitation Mechanisms

The dominant excitation mechanism of noble gas ion lasers is thought to be due to various processes involving electron impact. The exact nature of these processes varies with the actual transition under study. Individual theoretical and experimental studies have to be made on each laser to determine the exact contribution of different electron

impact process in exciting the respective upper levels. Till now, the bulk of such studies has been aimed at the Ar^+ laser, primarily because of its practical importance.

The following five different excitation processes have been proposed for the Ar^+ laser:

a. Direct excitation from the neutral atom ground state to the upper laser level.

b. Excitation to an intermediate metastable state followed by excitation from this state to the upper laser level.

c. Excitation to the ion ground state followed by excitation from this state to the upper laser level.

d. Excitation to the ion ground state, from there to a level higher than the upper laser level followed by radiative cascade to the upper laser level.

e. Excitation to the ion ground state, from there to an intermediate ion metastable state, followed by excitation from the ion metastable to the upper laser level.

Generally, the actual excitation involves more than on of the above mentioned processes. The relative importance of these processes in different discharge conditions is decided by the various plasma parameters. The more important of these parameters are neutral and charged particle temperature densities, spatial distribution within the plasma tube and longitudinal and radial drift velocities. Some of these

parameters like gas density, mean free path, gas temperature etc., can be directly deduced from experimental conditions, while the others require a theoretical model of the discharge to derive them from experimental conditions. Different theories for high and low pressure ion laser plasmas have been proposed [18]. Experimental measurements of some plasma parameters have been made, mainly on the Ar^+ laser. However, considerable information regarding the excitation mechanisms has been derived from the observations of the current dependence of output power, gain or the spontaneous emission from the upper laser level and from the levels cascading into it [30,31,32]. The current dependence of these factors is predicted from simple rate equation models. No such detailed studies have so far been made on the Xe IV laser. In the present work we have tried to approach this problem in a qualitative way.

The following is a brief summary of the broad conclusions reached about the excitation and quenching mechanisms in different kinds of noble gas ion lasers:

A. Singly Ionised Lasers: As far as the excitation is concerned, the dominant process in short pulse lasers is a sing step one from the neutral atom ground state. In cw lasers, the excitation is mainly through a multi-step process involving the ground or metastable states of the ion. The ion ground state can be populated either directly from the neutr

atom ground state or via a neutral metastable state. Radiative cascade from higher lying levels contributes a significant proportion of the pumping, particularly at high current densities [33].

In the case of long pulse lasers (5 μs), the excitation processes involved are not very clear. In these lasers, multiple-pulse laser output in different time regions of the exciting current pulse have been frequently observed. The first pulse is generally ascribed to a single step excitation from the neutral atom ground state; while the second pulse could be due to a two step excitation involving either the ion ground state or the neutral metastable states. The actua excitation process again depends on the plasma conditions which vary from system to system. Also, the relevant plasma parameters vary during the laser pulse so that quantitative analysis is difficult [34,35].

In both cw and pulsed lasers, saturation and eventual quenching of laser output occurs as the current density is increased or the pressure is varied from some optimum value. The following mechanisms have been proposed for saturation and quenching at high current densities:

a. Increased excitation of the lower laser level by electron collisions.

b. Electron destruction of the upper laser levels.

c. Resonance trapping of the vuv radiation between the lower laser level and the ion ground state.

d. Reduction of the neutral atom density due to a high degree of ionization.

e. Reduction of singly charged ion density due to a high degree of multiple ionization.

f. Contamination of the discharge caused by high current densities.

The quenching of the laser oscillation due to change in pressure can be explained as follows. If the pressure is too high, the electron energy distribution shifts to lower values of electron temperature which will upset the balance between the rates of excitation to the upper and lower laser levels. Higher pressures can also increase the resonance trapping of the radiation from the lower laser level. Reduction of pressure causes the plasma electron temperature to rise however reducing the total ion density; again this leads to a decrease in the population inversion.

B. Multiply Ionised Lasers: Several excitation mechanisms have been proposed for these lasers. Koozekanani [36] calculated the cross sections for simultaneous double-ionization and excitation in Ar, Ne and Kr by fast electrons (>100 eV) using the 'sudden perturbation' approximation. These cross sections are very small so this (single step) process may not be very significant.

Levinsen et al. [37] have studied some Ar III and Ar IV laser transitions and propose that the multiply ionized levels are excited from the next lower ion ground state, that is

$$Ar^{n+} + e^- \rightarrow Ar^{(n+1)+*} + 2e^-$$

This process is analogous to the single-step excitation in singly ionized lasers and can therefore be expected to be of importance under conditions of high electron temperature such as are obtained in high current pulsed lasers. However, in cw excitation, the electron temperatures are too low for this process to be significant. The following process proposed by Bridges and Chester is more likely

$$Ar^{n+} + e^- \rightarrow Ar^{n+*} + e^-$$

However, very little diagnostic information is available about such high current density plasmas. So it is difficult to ascertain the exact contribution of each mechanism in the actual excitation process.

Quenching at high current densities occurs in these lasers, though such high current densities are obtainable only with pulsed discharges. The quenching mechanisms may be similar to those in singly ionized lasers. The effect of pressure change is similar to that present in singly ionized lasers.

1.3 The Xenon IV Laser

Among the lasing transitions in multiply ionized species a set of lines belonging to Xenon, most probably to Xe IV, are the most powerful lines in the pulsed mode. These include the seven lines in the visible and two in the ultraviolet part of the spectrum. There are a few more lines which are comparatively weaker.

Lasing action in Xenon ion transitions was first observed by Bridges [5], Heard and Peterson [38] and Dana and Laures [39] who obtained lasing in Xe II. Further work of Bridges and Chester [12] on the pulsed Xenon ion laser showed that this laser had four more strong and characteristic lines with measured wavelengths at 5159.04Å , 5260.17Å, 5352.89Å and 5394.59Å. These lines could not be assigned to any of the known energy levels of Xenon but were found to be powerful enough to lase even in tubes as short as 10 cm. Dahlquist [40] reported laser action in Xenon with discharge conditions different from those reported in earlier works. In his study oscillation was observed on nine wavelengths, out of which six could not be identified. These six included three of the lines reported previously by Bridges and Chester [12]; the additional three being at 4954.2Å, 5007.8Å and 5955.7Å. However, the line at 5260.1Å was wrongly assigned to Xe II.

All these lines had earlier been observed in the spontaneous spectrum of Xenon by Humphreys at National Bureau of Standards, U.S., who had also studied their intensity dependence on excitation energy. This study did not give any definite assignment for these lines (unpublished work).

In earlier works, these lines were tentatively assigned to Xe III [40] because of their high current thresholds. cw operation on five of these lines was obtained by Bridges and Mercer [41]. They used a tungsten disc bore tube (46 cm x 2.3 mm) operated up to 1500 Amp/cm^2 with an axial magnetic field greater than 700 gauss. Along with these unclassified lines, laser oscillation on some classified Xe III lines was also obtained. It was found that the two groups of lines behave differently. The classified set (Xe III lines) almost reached saturation at the highest currents used (64 amp) while the power output in the unclassified lines was still increasing. It was found that these unclassified lines operate at higher optimum pressures and magnetic fields compared to the Xe III lines. Another observation reported in the study was that the Xe III lines momentarily decrease in output with +dB/dt while the intensity of the unclassified lines increases momentarily. Based on these facts, it was suggested that the unclassified lines may belong to the Xe IV spectrum.

Further, Bridges and Mercer attempted to use a correlation spectroscopic technique to determine the origin of these

lines. It is to be noted that no classification of Xenon ion lines in the higher ionization states has been made so far. Bridges and Mercer showed that all the five lines reported by them originated from five different upper levels and none of these upper levels correspond to the upper level of any of the identified transitions in Xe II or Xe III. However, several definite correlations were observed with some of the lines observed by Humphreys in his unpublished work. The uv laser transition at 330.8 nm, which had earlier been tentatively assigned to Xe IV showed a modest degree of out of phase correlation with at least three of the strongest unclassified lines suggesting that it originated from the same multiplet and was coupled through second order effects.

The cw output in these unclassified transitions was found to be very much lower compared to Argon at the currents used (0.5 watts in Xenon lines vs. 10 watts in Argon lines). In contrast, pulsed operation has been observed to give very much higher peak powers compared to Ar II lines [42,43]. The lower pressures used in pulsed operation would favour early saturation of the lower ionization states and a shifting of the excitation to higher ionization states. These observations are consistent with the suggestion that these lines belong to the Xe IV spectrum.

Ring-shaped beam formation under conditions of high discharge currents and pressures was observed in three of

these transitions namely, 5353Å, 5260Å and 4954Å by Cheo and Cooper [44]. Radiation trapping was proposed as the possible mechanism for this behaviour, though no definite proof was given. Somewhat similar behaviour has been noticed in the present work and is discussed in Chapter 5 and 6.

Gallardo et al. [45] made a systematic study of the spontaneous emission from Xenon and measured the wavelengths accurate to ± 0.03Å. This work cleared up the controversy about the 5260Å line. It was found that there are two lines, one at 5260.43Å observed earlier by Heard and Peterson [38] and belonging to the Xe II spectrum; the other line at 5260.17Å was the one observed earlier by Dahlquist [40] and Bridges and Chester [12]. This line belongs to the set of unclassified lines tentatively assigned to Xe IV. Bridges and Chester later checked their data and confirmed this fact [46].

An attempt to assign the ionic species responsible for the green lines was made by Lluesma et al. [47] by studying the variation of the spontaneous emission intensity in these lines with changing excitation voltage. The spontaneous emission from a conventional pulsed laser tube (bore dia., 2.3 mm) was photographed between 2400Å and 8700Å. The variation in the intensities of spectral lines as a function of excitation energy was carefully analysed. Twenty two unclassified lines including the seven mentioned above were studied. It was found that lines belonging to different ionization

states behave differently. Based on this, all these unclassified lines were assigned to Xe IV.

Davis and King [48] correlated the threshold and quenching currents of ion laser transitions with the degree of ionization. By comparing the behaviour of the unclassified Xenon transitions with known Argon and Neon ion laser transitions they concluded that the unclassified Xenon lines most probably belong to Xe IV.

Hoffmann and Toschek [49] studied the time dependence of the spontaneous emission from a pulsed Xenon ion laser. The delay between the initiation of the discharge current and the spontaneous emission in different wavelengths was correlated with the ionic state. On this basis, the unclassified Xenon lines were assigned to Xe IV.

The operation of small bore ($\leqslant 3$ mm) pulsed Xenon ion laser was first studied by Simmons and Witte [43]. In that study the behaviour of six blue and green lines was investigated. It was observed that all the six lines were considerably more intense than the Ar II 5145Å line and operated with higher output power in the long-pulse mode (5-50 μs) also.

Papayoanou et al. [50] investigated the operation of wide bore (> 7 mm) tubes and obtained an empirical equation relating the all-line optimum pressure to the tube bore

diameter. Since different lines can have different optimum pressures, it is not necessary that they should vary in the same way with tube diameter. We have investigated the variation of optimum pressures of each line with varying tube diameter and our results are discussed in Chapter 3.

The highest output power reported so far in these lines is 80 KW by Gunderson and Harper [51]. They used a 17 mm i.d. quartz tube. Multiple peaks with pulse widths of the order of 200 ns were observed. Ring-shaped formation in the output beam was also reported.

Laser action in high current pinched Xenon discharges was studied by Papayoanou and Gumeiner [52,53] on five of the blue-green lines and three uv lines. The authors used streak camera pictures of the laser pulses together with oscilloscopic pictures of the current pulse and concluded that the laser action begins and is sustained during the dynamic portion of the pinch, reaching its peak intensity near the time where the collapsing plasma attains its minimum radius.

They further measured the time dependence of the electron density in the plasma by using interferometric techniques [53]. From their studies, they obtained a qualitative picture of the radial dependence of the evolving electron density which is consistent with a collapsing plasma. Estimating the temporal variation of the degree of ionization, the authors concluded that the plasma was fully ionized and that

the laser lines originated from levels in triply or even higher ionized species.

Long-pulse operation ($>$ 50 μsec) in six lines viz., 4954Å, 5008Å, 5260Å, 5353Å, 5395Å and 5955Å was reported by Sasaki and Saito [32]. Double-pulse output similar to that reported in Ar and Kr ion lasers [13,57,58] was obtained. It was also noted that the fill pressures used ($\sim$ 0.1 mm Hg) were very much higher than those used in short-pulse lasers. The authors proposed that out of the two laser pulses, the first one could be due to a single-step excitation while the second one due to a multi-step excitation.

The beam properties of pulsed Xenon ion laser viz., the mode composition, the spatial and temporal coherence, the divergence of the output beam and the pulse to pulse stability were studied by Moskalenko et al. [56] using a commercial pulsed ion laser tube.

It has been shown that the application of an axial magnetic field in an ion laser leads to an enhancement of the charged particle density near the tube axis. This reduces the axial electric field and hence the electron temperature. Due to this the output power will either decrease or increase, depending on the relative contributions by the change in electron temperature, electron and ion number densities and their spatial distribution to the excitation process.

Little diagnostic work has been reported so far on the actual effect of magnetic field on ion laser plasmas. However, it was observed that as far as charged particle diffusion is concerned, the effect of increasing the magnetic field is similar to that of increasing the pressure of the gas [57,58]. This has been confirmed for the cw Ar^+ laser by Gorog and Spong [59]. The effect of axial magnetic field on glow discharge plasmas has been discussed theoretically by Forrestand Franklin [57,58].

The magnetic fields required for pulsed lasers are found to be generally an order of magnitude lower compared to those used in cw lasers. Ahmed et al. [60] studied this aspect in both pulsed and cw Ar^+ lasers and concluded that this is due to the fact that gas pumping is less effective in pulsed lasers. In heavier gases, like Krypton and Xenon, the optimum magnetic fields are expected to be lower than in Argon.

Besides affecting the plasma parameters of the laser, the axial magnetic field can also affect the laser output through Zeeman splitting in the transition. This causes the output radiation to break up into left and right circularly polarised light, and introduces circular dichroism in the medium [61]. With Brewster windows attached to the laser plasma tube this results in the output becoming elliptically polarised. Further, the polarisability of the medium is in

general different for the two circularly polarised components, there by producing Farady rotation also in the output. It can be shown that the amount of rotation depends on the gain in the medium [62].

This magnetically induced anisotropy in gaseous gain media has so far been studied by Terekhin and Fridrikhov [63] for the 3.39μ transition in a He-Ne laser; by Fork and Patel [64] for the 2.026μ transition of atomic Xenon in a He-Xe laser and by Sinclair [61] and Fotiadi and Fridrikhov [65] for the 4880Å transition in the Ar^+ laser.

The only work reported so far, on the effect of externally applied axial magnetic field in the Xenon ion laser is by Ames [66]. He studied the variation of all line output power with magnetic fields up to 684 gauss at different pressures. No investigation on the behaviour of individual lines was made. Probably Brewster windows were employed in his laser, though not explicitly mentioned.

1.4 Summary of the Present Work

This work comprises of studies of the following characteristics of the pulsed Xenon ion laser. The experimental techniques developed and used in the present course of experiments are briefly discussed in Chapter 2.

A detailed parametric study of seven visible transitions viz., 4945Å, 5008Å, 5160Å, 5260Å, 5353Å, 5395Å and 5955Å

has been made. Specifically, the effect of gas pressure, excitation voltage, energy storage capacitor and the diameter and length of the plasma tube on the laser output is discussed in detail in Chapter 3.

The small signal gain coefficients of each of these seven transitions have been measured under different operating conditions and the results are presented in Chapter 4. Gain saturation on these transitions is also discussed in this chapter.

An attempt has been made in Chapter 5 to understand qualitatively the excitation mechanism for this least studied laser system.

A study of the magnetic field effect on all five of the seven transitions has been taken up. This includes the study of the variation in the laser output with magnetic field through its effect on the plasma parameters as well as through the induced anisotropy. A detailed discussion of these results is given in Chapter 6.

The summary of results obtained in this work is given in the concluding chapter along with the discussion of the major limitations present due to total lack of any information on the spectroscopic properties of these transitions. The immediate program of work already initiated in an attempt to resolve at least a few of the dilemmas in understanding the behaviour of this laser is also mentioned.

CHAPTER 2

EXPERIMENTAL TECHNIQUES

The active medium of an ion laser generally consists of a low pressure discharge plasma. A discharge with the required characteristics can be produced in many ways. These include pulsed and cw discharges using electrodes with hot or cold cathodes, pulsed and cw RF discharges using induction coupling, pulsed dc discharges using electrodeless magnetic induction coupling, pinched discharges, E-beam generated plasmas and many more.

Pulsed operation of lasers enables high peak currents to be easily reached; transitions in higher ionization states can thus be excited without much difficulty. Many of the transitions which either do not lase or lase weakly in cw operation due to current limitation, can be excited in the pulsed mode.

The design requirements of pulsed and cw lasers differ considerably. In cw operation, the discharge is run either at low currents (a maximum of few tens of amperes) in a capillary of 2 to 4 mm diameter or at high currents ($\backsim$100 amp) in wider bore (>1 cm) tubes. It is usually further confined by applying a longitudinal magnetic field. Since the efficiency of these lasers is low, typically much less than 1 percent, almost all the input power of several kilowatts is dissipated as heat; thereby necessiating cooling of the plasma tube.

On the other hand, pulsed lasers have the advantage that the average input power is much less. However the peak output power is nearly an order of magnitude higher or more. Thus thermal loading is not a problem, at least at a low repetition rate. Simple glass discharge tubes can be used, though sometimes quartz tubes are used. The pressures used in pulsed lasers are an order of magnitude lower compared to those used in cw lasers. The effect of gas pumping is not severe and the laser can be operated even without a gas return path between the anode and the cathode ends of the plasma tube.

The peak currents in pulsed laser discharges usually range between a few hundreds of amperes to a few kilo amperes. It has been found that in the domain of high peak currents (>500 amp) cold cathodes offer a definite advantage over large, current-limited thermionic cathodes. In the earlier tubes with cold cathodes large anode to cathode voltages were required for reliable operation. Later designs using a pellet

of Indium melted around the cathode junction alleviated this problem. This is thought to be due to the low work function of Indium combined with the extended irregular cathode surface formed by the Indium metal through its high sputtering rate [67].

2.1 Experimental Set-up for Parametric Studies

The plasma tubes used in the present work have been made of pyrex glass with Indium cathodes constructed by melting a pellet of spectroscopically pure Indium metal around tungsten pins. The processing of the tubes involved the following steps. Before attaching a tube to the vacuum station, it is cleaned thoroughly to remove dirt and grease by using sodium hydroxide and chromic acid. The tubes are thoroughly washed with distilled water, dried and finally rinsed with GR grade acetone. Then the tube is connected to the vacuum station and windows are attached to it by an epoxy resin (Varian Associates - Torr Seal). The tube is processed by degassing it at more than 150°C, while simultaneously evacuating it. The vacuum system consists of an oil diffusion pump with an LN trap attached and backed by a rotary pump. The degree of vacuum attainable in this system is about 10^{-6} torr.

After this initial processing, the discharge tube is filled with Xenon at a suitable pressure and the discharge is run at a rep-rate of a few pulses per second for several hours.

This process releases the contaminating gases adsorbed by the glass walls of the plasma tube as well as the electrodes. After running the discharge for some hours the tube is flushed out and refilled. This process is repeated several times to ensure the level of contamination in the plasma tube to be negligible.

Xenon is highly adsorbed by glass. Due to this, in the initial stages the pressure in the plasma tube fluctuates markedly while the discharge is running. However, by filling and pumping out several times the pressure in the tube stabilises. To further ensure that during the experiments the level of contamination due to discharge produced impurities is low, the tubes are flushed out and refilled after several hours of continuous operation. As the parameters like pressure and excitation voltage are changed the discharge is allowed to stabilise at the new operating point. This has ensured that during the course of one set of experiments, the performance of the laser is stable and reproducible.

The pressures indicated in the present work are manifold pressures measured during the experiment. These have been continuously monitored by a calibrated CVC pirani gauge connected to the plasma tube on the cathode side through a side arm. We believe that our pressure measurements are accurate to $\pm$ 1 micron.

The experimental setup used for the parametric studies is given in Figure 2.1. Six plasma tubes of different bore diameters but otherwise similar geometry have been used in this study. The bore diameters chosen are 10, 8, 6.3, 4, 2.7, and 1.5 mm. Each plasma tube used has an active length of 100 cm ($\pm$ 1 cm) between electrodes and a total length of 125 cm. The extra length is provided to separate the windows from the electrodes so that the former would not be contaminated by sputtering from the electrodes.

The optical cavity has been formed using mirrors of equal radii of curvature of 2 meters, separated by 145 cm. Two sets of mirrors have been used in our experiments. One set consists of a pair of Spectra Physics mirrors normally used with their model 165 Argon ion laser. These mirrors are referred to as the Ar^+ mirrors in the rest of the report. The second set is a pair of He-Ne mirrors and is referred to as the He-Ne mirrors. The actual reflectivities for both the mirror sets at the operating wavelengths have been measured by carefully measuring their transmittances.

The excitation energy for the discharge has been supplied by discharging a 1.0 μF capacitor charged from a variable DC power supply. This power supply is operated from a servo-stabiliser which has a rated stability of 1 percent. The voltage to which the capacitor is charged has been measured with an HP VTVM-model No. 4108, with a high voltage probe.

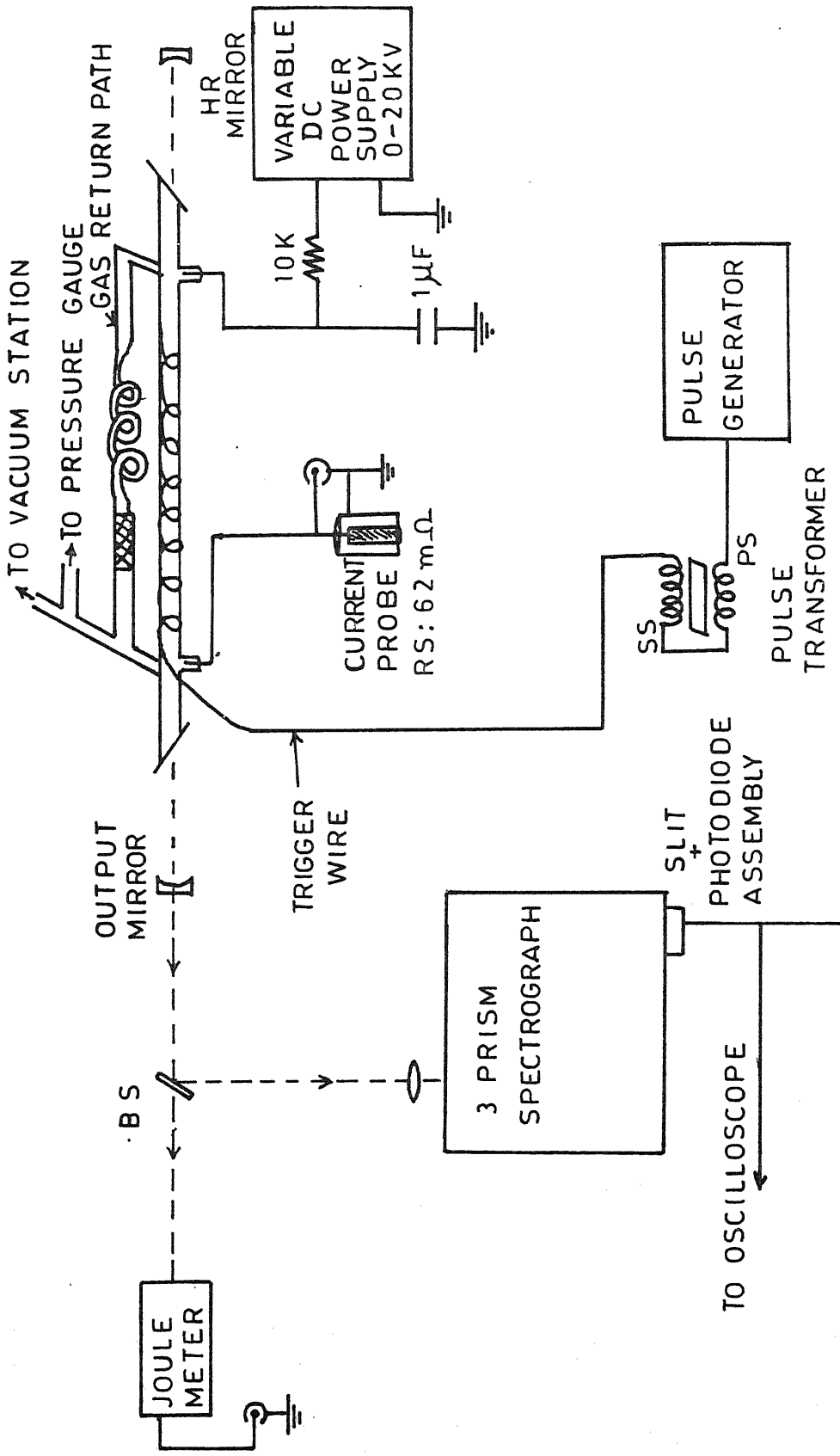

FIG.2.1 BLOCK DIAGRAM OF THE EXPERIMENTAL SET-UP

We believe that all our voltage measurements are accurate to better than ± 5 percent.

To initiate the discharge, a high voltage (15 KV) pulse is applied to the tube walls through a copper wire wound round it for nearly three quarters of its length, commencing from the cathode end. This pulse comes from an EG and G pulse transformer No. TS. 185, the primary of which is fed with a 300 volts pulse generated in a variable PRF pulse generator. The detailed circuit schematic is given in Figure 2.2. The circuit is designed with an NE 555 for timing; its timing capacitor is charged from a constant current generator consisting of two transistors connected in the current-mirror configuration to ensure linear charging of the capacitor. Use of high stability resistors and a low-leak capacitor in the timing circuit ensures a stable pulse repetition rate, which could be varied from 1 pulse in 5 sec to 50 pps. However, during the experiments the laser is operated at a rate of 1-2 pps, so that thermal and gas pumping effects are negligible and gas contamination is minimum. Environmental stability is improved by carrying out the experiments in an air-conditioned laboratory.

The current through the plasma tube has been measured with a low-inductance, low-resistance coaxial probe, specifically fabricated for this purpose and connected in series with the plasma tube at the cathode end. The estimated bandwidth

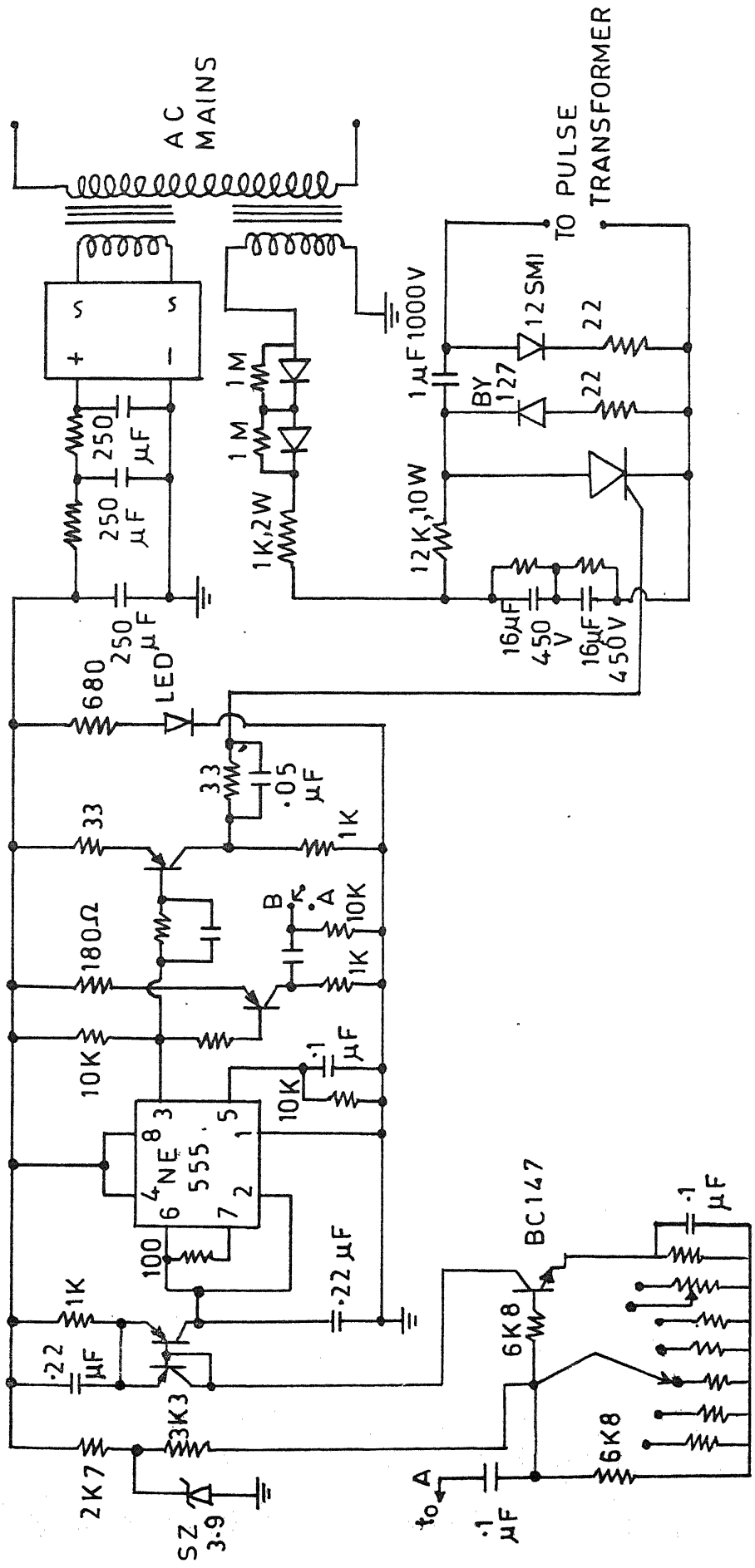

FIG. 2.2 PULSE GENERATOR CIRCUIT

of the probe is about 1 GHz. Its resistance is 62 milli ohms (± 1mohm) and it has adequate thermal dissipation capacity.

The output of the laser has been divided into two parts by a calibrated beamsplitter. One of the beams is made to fall on a pyro-electric joule meter (Molectron Corporation's model No. J3-05) the output of which is a measure of the all-line energy in the laser pulse. The other beam has been used to measure individual outputs at the wavelengths of interest. For this, the beam is focussed on to a medium-resolution, high throughput 3 prism spectrograph (Carl Zeiss JENA). A slit and a calibrated PIN photodiode (HP 5082-4207) have been attached at the exit of the spectrograph. Both the throughput and the polarisation sensitivity of the spectrograph at all the seven wavelengths have been carefully measured several times during the course of the experiments.

The PIN photodiode has been used with a reverse bias of 20 volts. The photocurrent as measured at the cathode across a one kilo ohm resistor has been monitored on a Tektronix Oscilloscope (model No. 545A, rise time 10 nsec.). For measurements, the signal has been fed to a high-resolution boxcar integrator (PAR model 160) used as a gated integrator, with the aperture fixed or scannable depending on the experiment. In the fixed-gate mode, the aperture time has been kept constant (5 μsec) throughout, so that the data from different sets of experiments can be directly compared. For recording

the temporal variation of the laser output or the discharge current, the boxcar has been used in the high resolution scan mode with an aperture time of 10 nsec. The output signal from the boxcar is recorded with a strip-chart recorder. The entire detection system has been carefully calibrated at all the seven wavelengths several times during the course of the experiments. In view of this, we believe that our measurements of power and energy output of the laser are accurate to much better than 15 percent.

2.2 Experimental Setup for Gain Measurements

Small-signal gain at each wavelength has been measured by inserting variable losses in the laser cavity and adjusting the loss till lasing just stops. For this, fixed losses have been introduced by using different calibrated attenuators (metal coated quartz substrates used as neutral density filters). Intermediate and continuous loss variation has been introduced by using a laser quality calcite prism polariser in the cavity. By rotating this polariser about the laser axis, a known amount of loss can be introduced. Use of Brewster windows at the plasma tube ends results in a plane polarised output from the laser. Due precautions have been taken to ensure that these attenuators do not introduce any optical feedback in the cavity. All the attenuators have been carefully calibrated at all the seven wavelengths. The

Brewster losses at the windows have been estimated before attaching the latter to the plasma tubes. This has been done by a comparison with known losses in an already working laser.

2.3 Experimental Set-up for Studying the Effect of Magnetic Field

For studying the effect of axial magnetic field on the laser output, a tube of dia. 6.3 mm has been chosen with non-Brewster terminations. However, the two windows have been tilted along two mutually orthogonal directions by approximately one degree to avoid both etalon effects and polarisation selection within the cavity. The active length of the discharge is 65 cm. A solenoid of approximately the same length has been used to produce a pulsed axial magnetic field in the plasma tube. End corrections for the field have been made while specifying the results.

To generate high enough magnetic fields without producing excessive heating, a pulsed current has been used to drive the solenoid. Fields up to 5 KGauss have been obtained with this technique. The detailed schematics of the circuits are given in Figures 2.3 and 2.4. The current through the coil is a damped sinusoid with a half period of 5 msec. Due to the nature of the switching circuit used and the damping provided in the coil, no negative cycle of the current is produced. The laser is switched on when the magnetic field

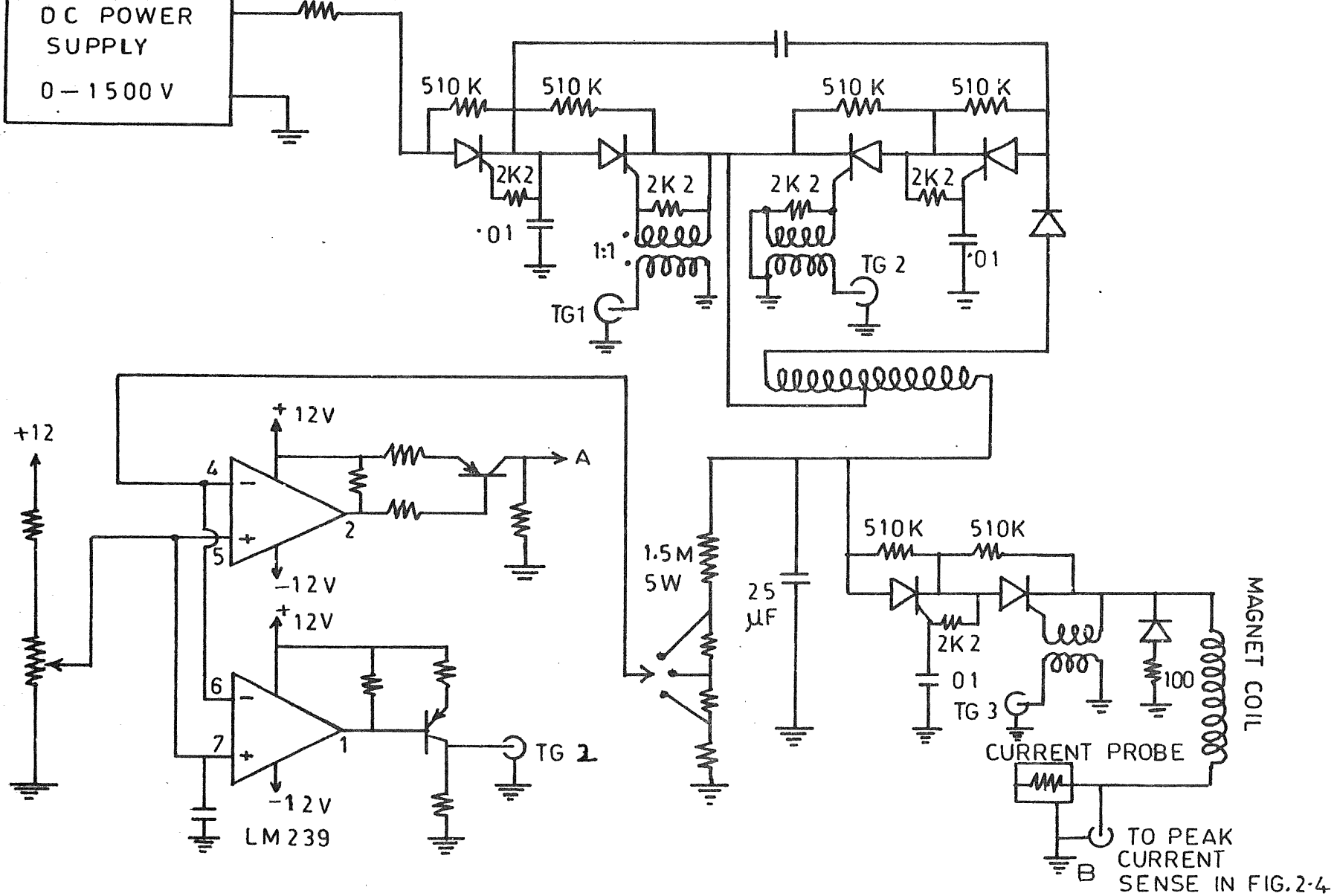

FIG. 2.3 SCHEMATIC DIAGRAM OF PULSED MAGNETIC FIELD POWER SUPPLY.

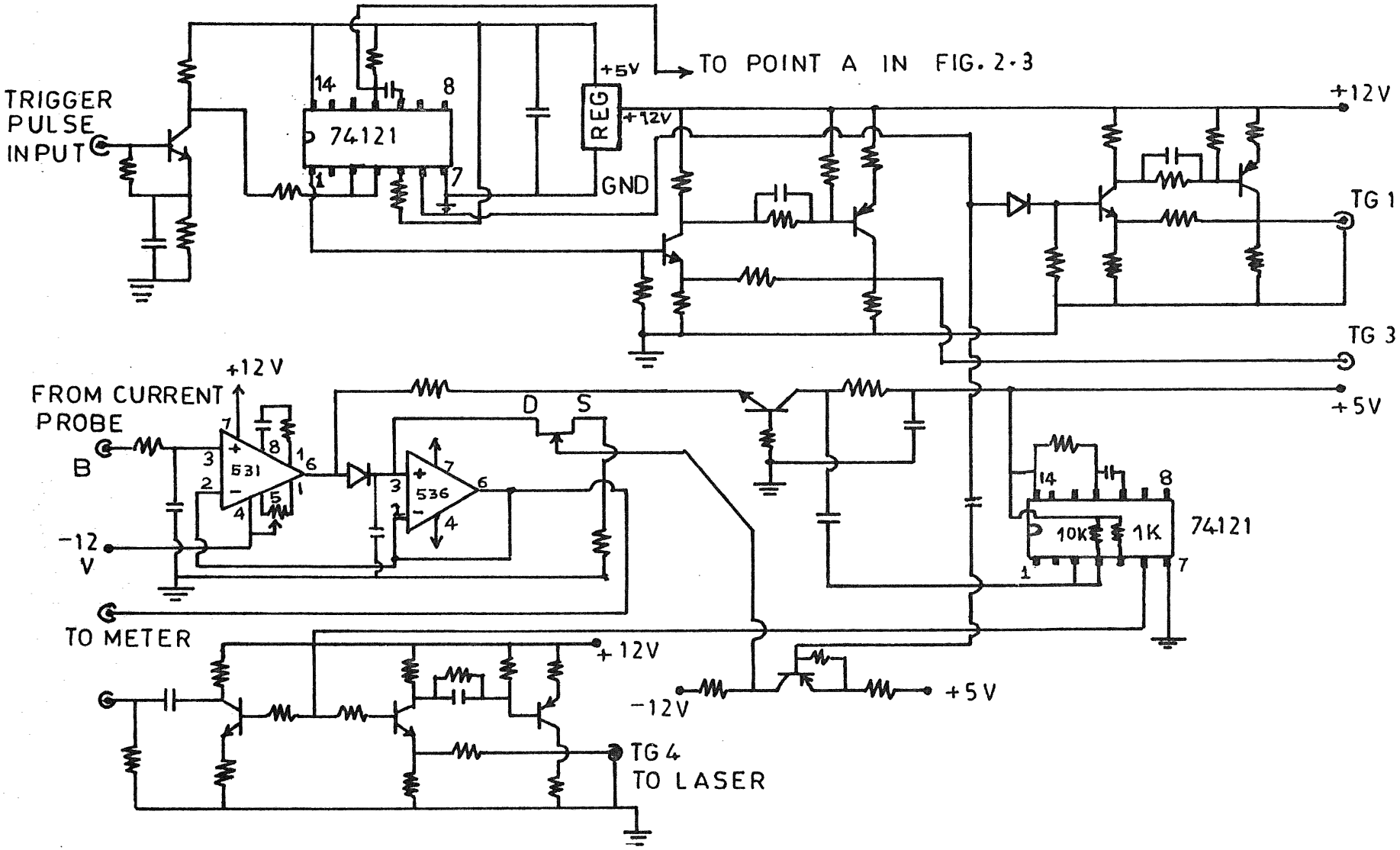

FIG. 2.4 SCHEMATIC DIAGRAM OF THE PULSED MAGNETIC FIELD SWITCHING CIRCUIT.

reaches its peak value. This has been achieved by detecting the peak of the field current with a peak detector which in turn triggers the laser. Since the width of the plasma current pulse is three orders of magnitude smaller than the half-period of the magnetic field pulse, we assume that the field is constant during the operation of the laser and stays at its peak value. The peak value of the magnetic field is always measured in terms of the current passing through the coil. This current has been measured by using a current probe similar to the one used for measuring the plasma current which has been described above. The magnetic field has been calibrated against the current through the solenoid using a Hall probe Fluxmeter, to an accuracy of better than 10 percent.

For measurement of magnetically induced Farady rotation and ellipticity in the active medium near the lasing transitions, an additional quartz window has been inserted in the laser cavity at Brewster angle. A laser quality prism polarizer has been used to detect the nature of the polarisation of the output radiation at all the seven wavelengths. The direction of the major axis and the ratio of the major and minor axes have been measured. More details of this experimental procedure are given in Chapter 6.

CHAPTER 3

PARAMETRIC PROPERTIES OF PULSED XENON ION LASER

Lasing action on some of the more powerful Xe IV transitions was reported as early as in 1964 [5], however, very little parametric study was reported on this laser. All the reports made so far by different authors are the results of experiments performed under different experimental conditions, thereby making a comparison of results difficult. In view of this, a detailed parametric study on this laser has been undertaken, in which the laser power output dependence on various parameters like tube bore diameter, plasma tube length, excitation voltage and energy storage capacitor has been investigated. This study has taken a considerable amount of time and effort and

we believe that this is the first exhaustive report on the parametric properties of this ion laser.

The transitions studied in this work are the following: 4954.13Å, 5007.8Å, 5159.08Å, 5260.19Å, 5352.92Å and 5955.67Å [27]. Simmons and Witte [43] have reported the operation of small bore (1.5 mm - 3.0 mm i.d.) lasers, while Papayoanou et al. [49] have studied laser operation in larger diameter tubes (7.5 mm - 12 mm i.d.). To our knowledge, the operation of this laser has not been studied in the diameter range of 3 mm to 7 mm. It is to be noted that, in the Ar^+ laser the highest electrical efficiency has been obtained in a tube of diameter 6.3 mm [22]. With this in view and to have a better comparison of the results with tubes of different diameters, we have studied laser action in tubes of diameter 1.5 mm, 2.7 mm, 4 mm, 6.3 mm, 8 mm and 10 mm. The length of the tubes, the cavity geometry and the excitation conditions have been kept the same. The details of the experimental set-up have already been given in Chapter 2.

Most of the data has been taken with a capillary length of 100 cm ($\pm$ 1 cm) between the electrodes; however, for the 6.3 mm and 4 mm tubes additional data has been taken for a length of 60 cm. For discharge excitation, a 1 μF capacitor charged up to 7 KV is discharged through the plasma tube, the limit on the voltage being decided by the discharge stability. With 6.3 mm and 4 mm tubes 0.1 μF and 0.3 μF capacitors have also been used.

3.1 Power Output Variation with Pressure and Plasma Tube Geometry

Typical curves showing the power output variation with pressure are given in Figures 3.1 to 3.9. Each curve shows a distinct maximum. Figure 3.1 gives the variation of all-line output power with pressure, for different initial electrical fields, E, in the 6.3 mm tube. The optimum pressures for the same E are found to be different for the two mirror sets. For the same tube, the power output variation with pressure for individual lines is given in Figures 3.2 - 3.5. The data for all lines except 5955Å have been taken with Ar^+ mirrors, while that for 5955Å with He-Ne mirrors.

Similar behaviour has been observed with other tubes and in each case, the optimum pressures for the all-line output as well as the individual lines have been obtained. The data for different tubes with a single excitation voltage are plotted in Figures 3.6 to 3.9. For a given tube and wavelength, the optimum pressure increases with excitation energy. This behaviour is similar to that reported in other ion lasers [4].

The distribution of the total output power in different wavelengths is found to be dependent on pressure. At the all-line optimum pressure this distribution in a 6.3 mm tube is as given in Table 3.1. Similar behaviour is exhibited by other tubes. Table 3.1 shows that the transition at 5353Å is the

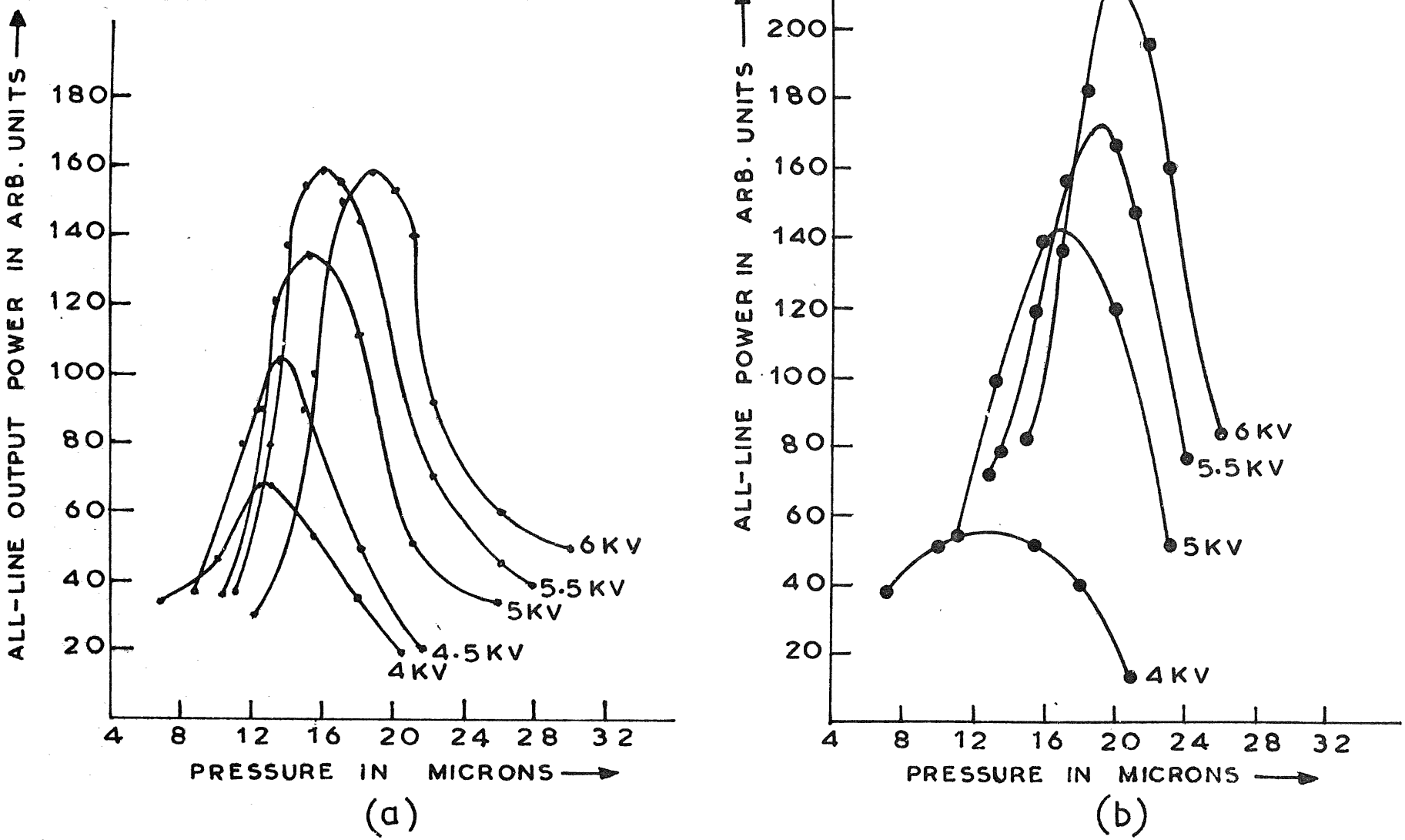

FIG.3.1 ALL-LINE POWER OUTPUT IN 6·3 mm. TUBE Vs PRESSURE FOR DIFFERENT EXCITATION VOLTAGES.
(a) Ar+MIRRORS (b) HE-NE MIRRORS

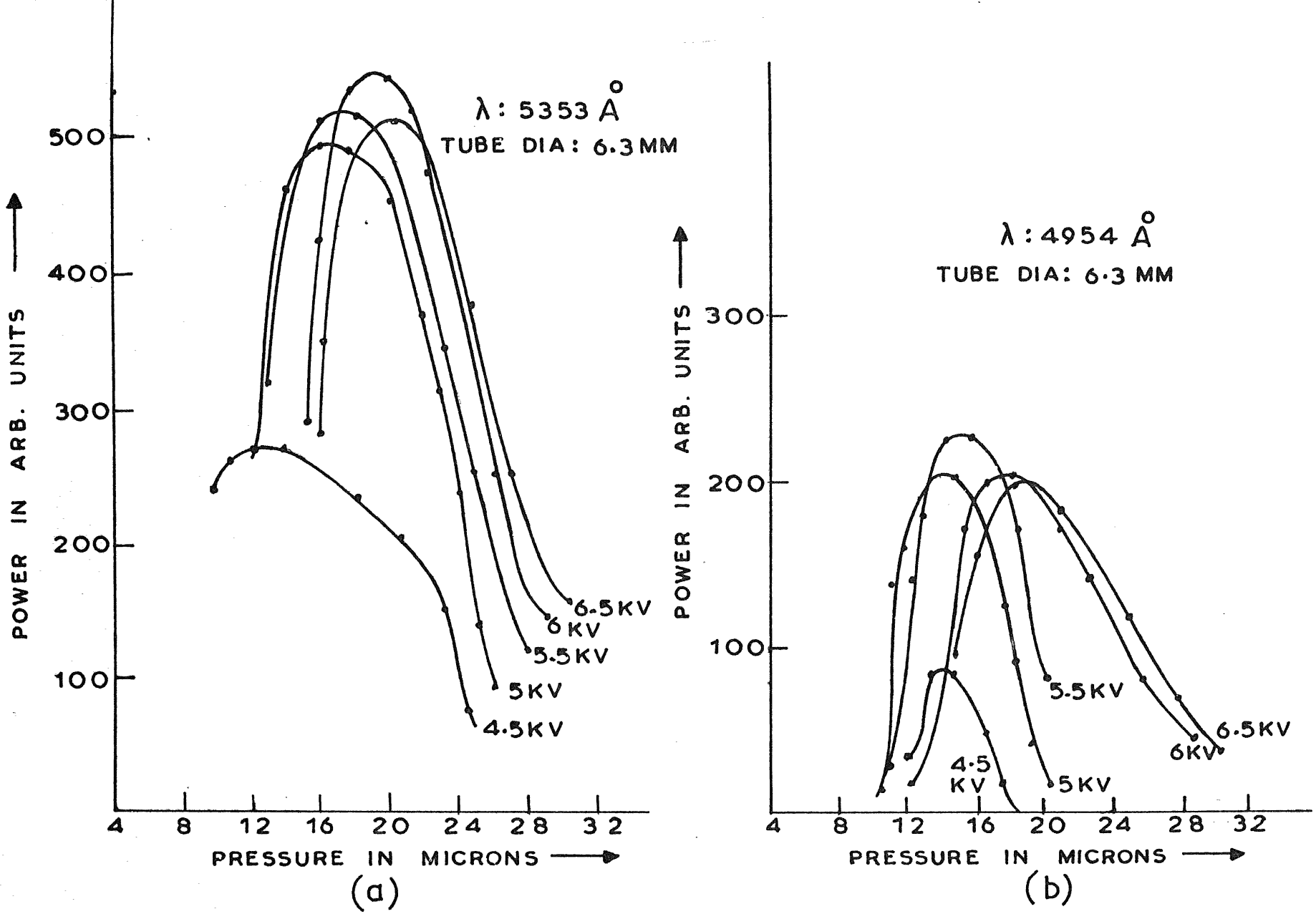

FIG. 3.2 POWER OUTPUT IN DIFFERENT WAVELENGTHS Vs PRESSURE, FOR DIFFERENT EXCITATION VOLTAGES.

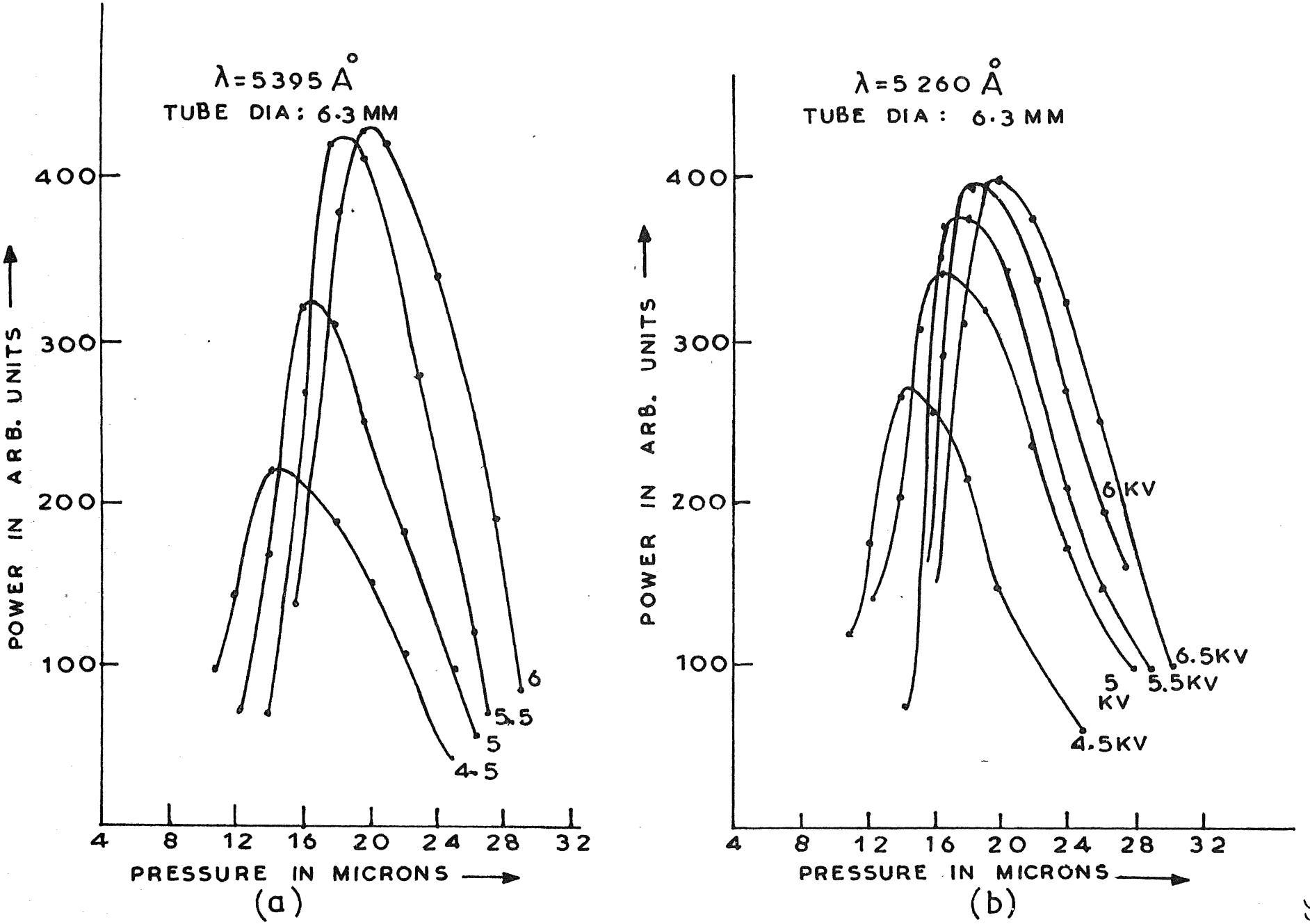

FIG.3.3 POWER OUTPUT IN DIFFERNT WAVELENGTHS Vs PRESSURE, FOR DIFFERENT EXCITATION VOLTAGES.

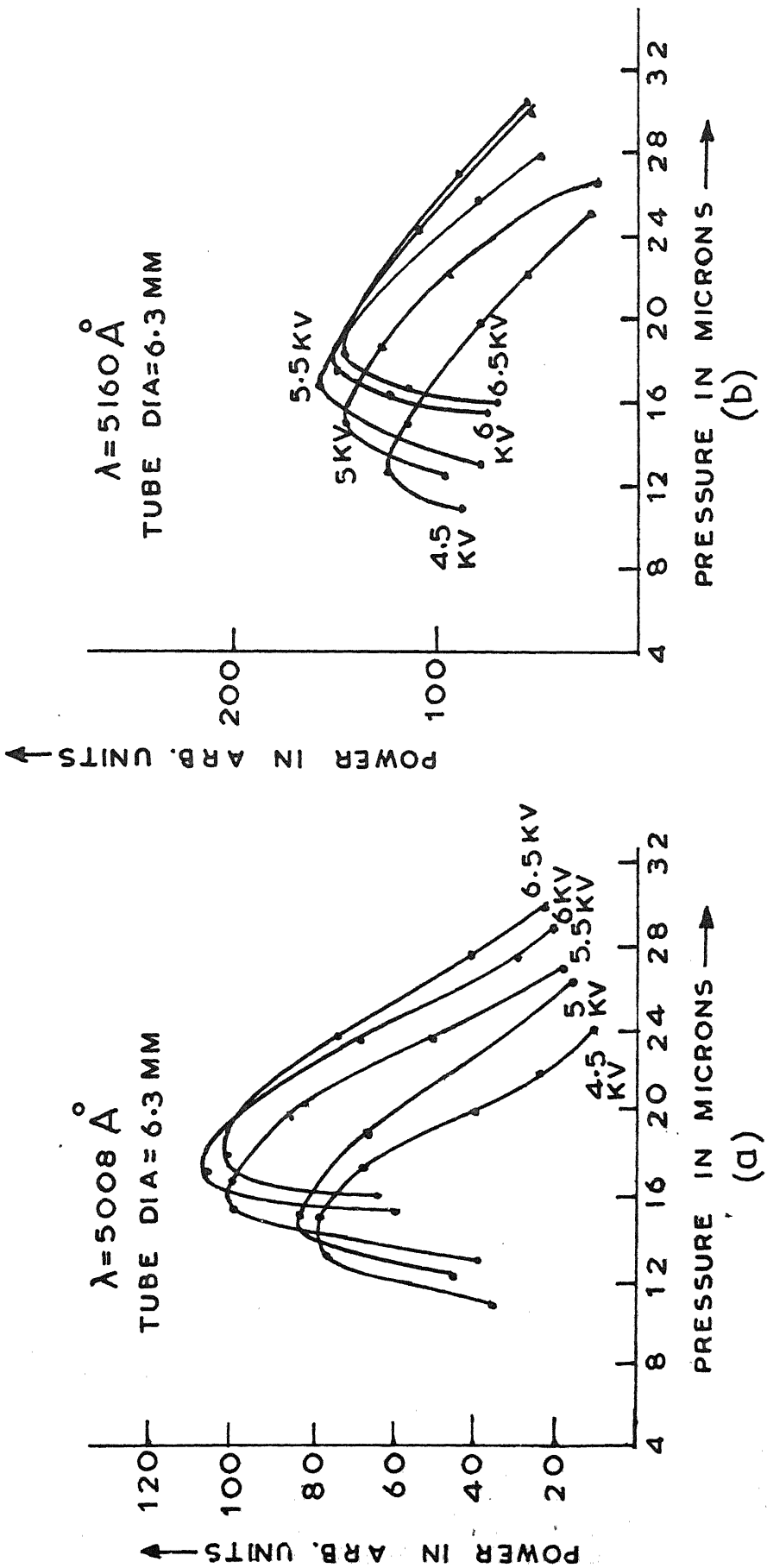

FIG. 3.4 POWER OUTPUT IN DIFFERENT WAVELENGTHS Vs PRESSURE, FOR DIFFERENT EXCITATION VOLTAGES.

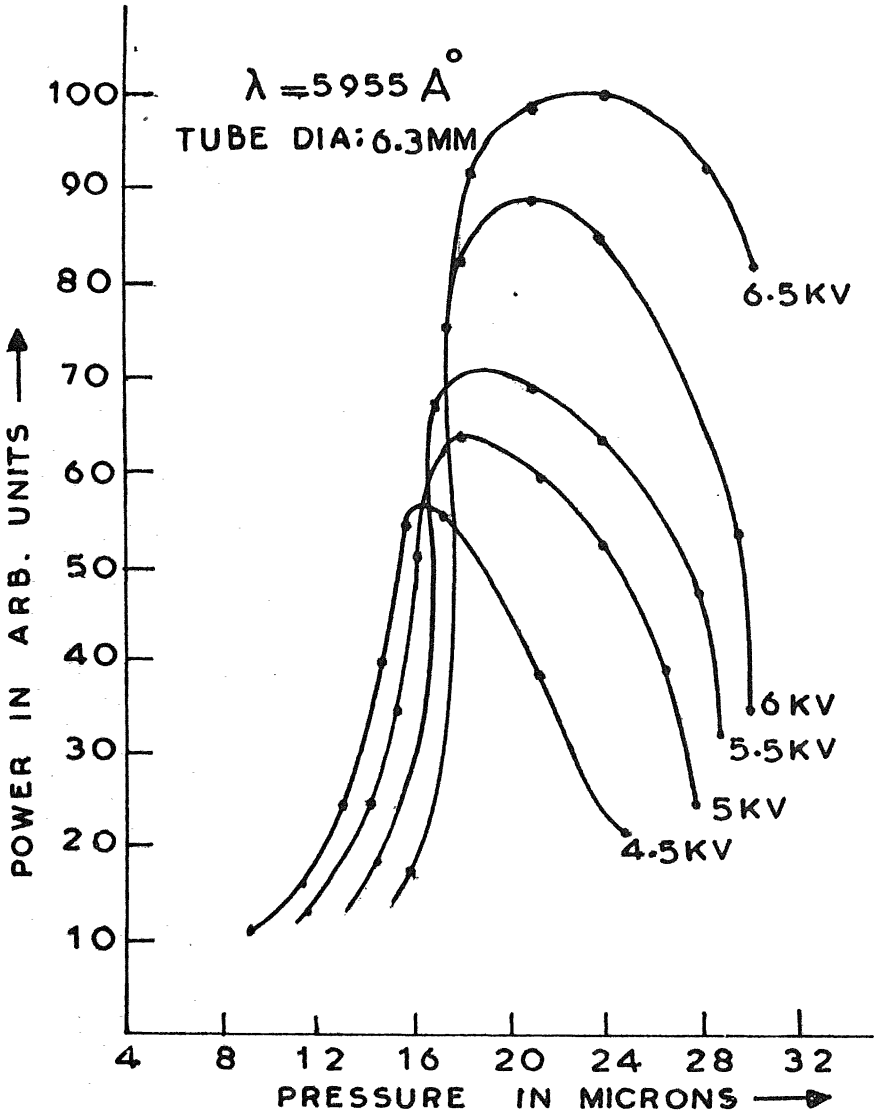

FIG. 3.5 POWER OUTPUT Vs PRESSURE, FOR DIFFERENT EXCITATION VOLTAGES

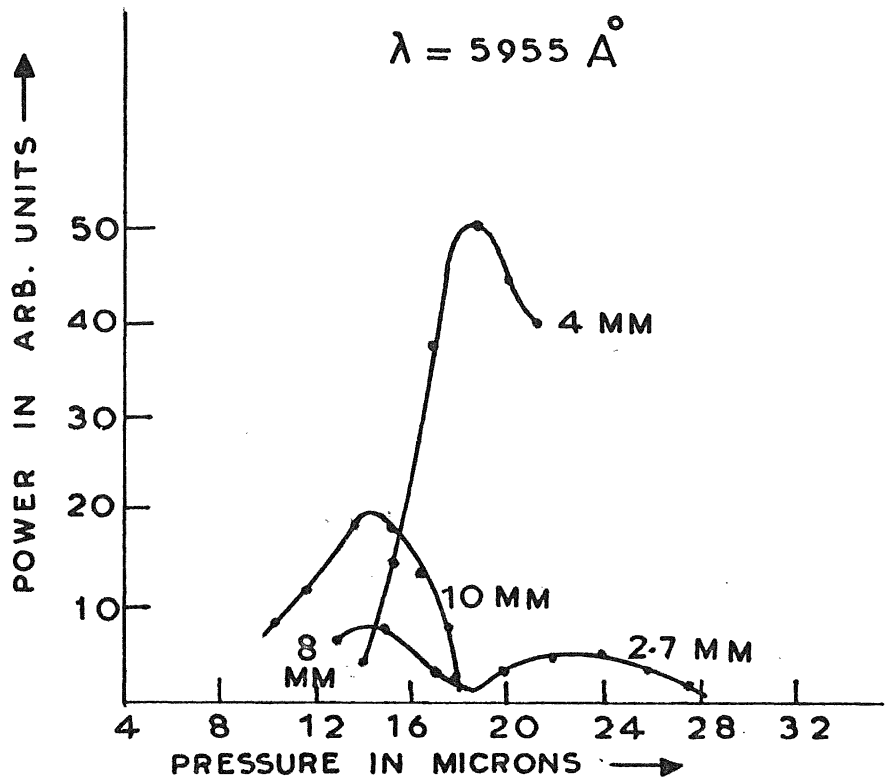

FIG. 3.6 POWER OUTPUT Vs PRESSURE, FOR DIFFERENT TUBE DIAMETERS

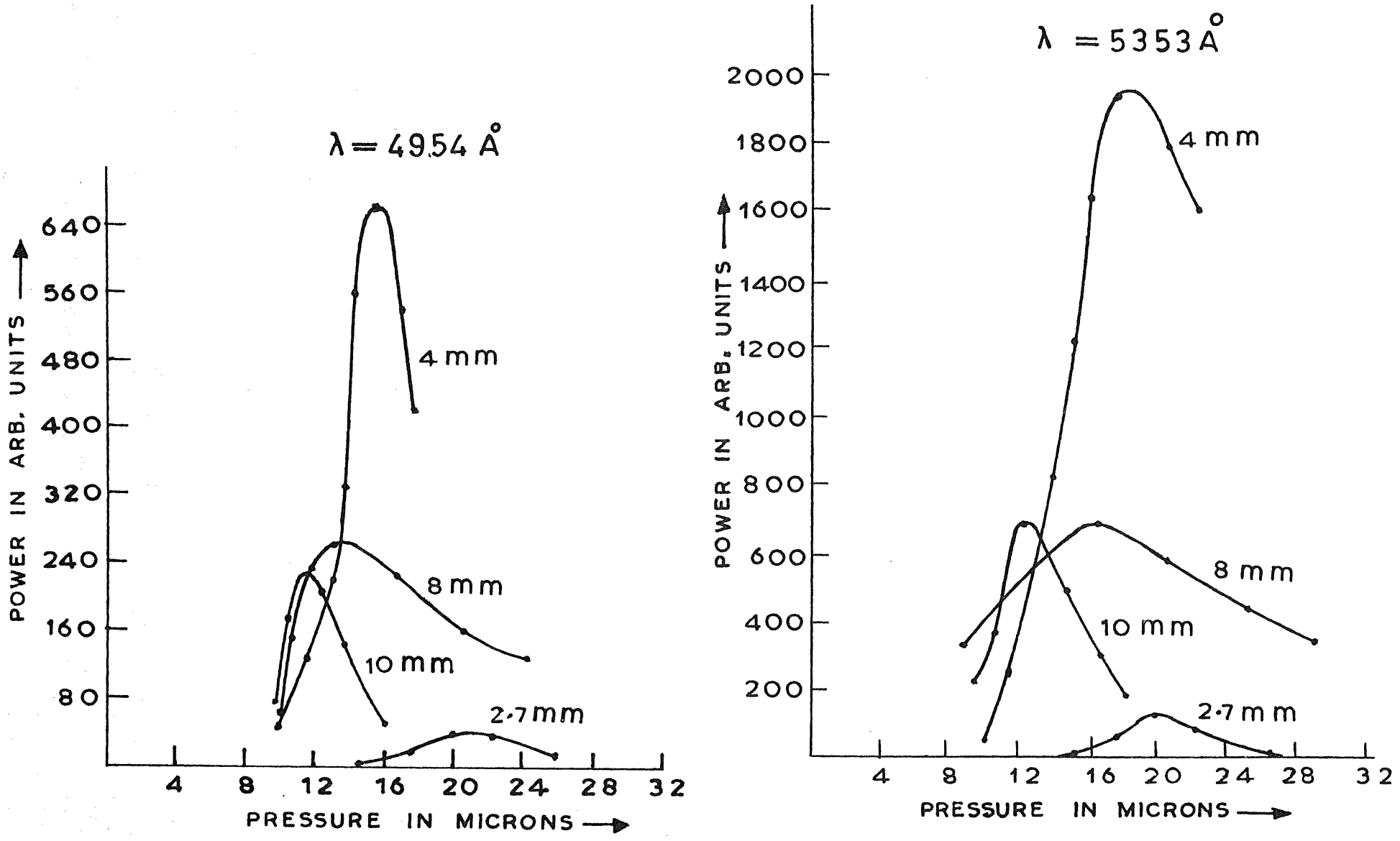

FIG.3.7 OUTPUT POWER vs PRESSURE FOR DIFFERENT DIAMETERS

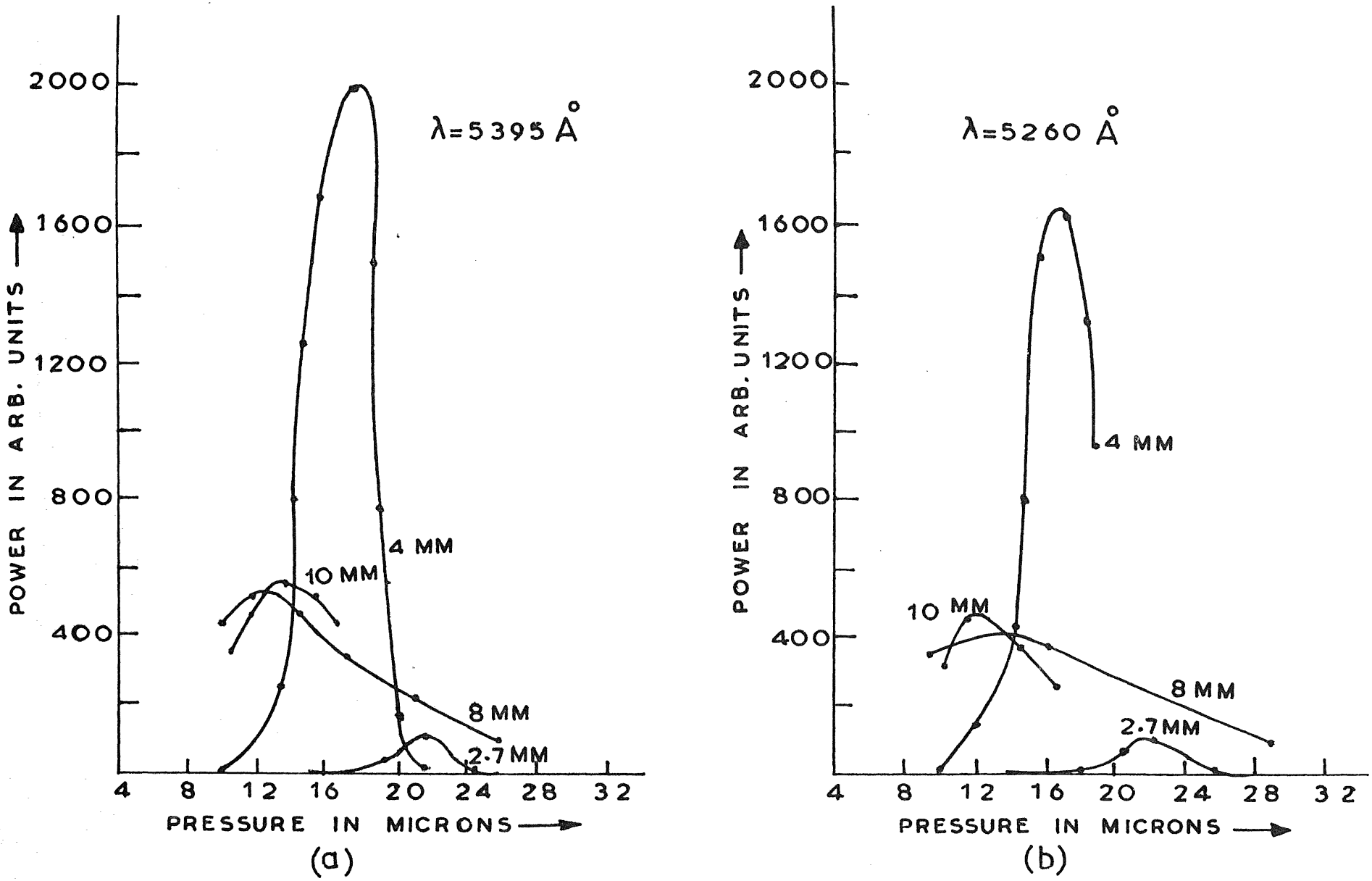

FIG.3.8 POWER OUTPUT IN DIFFERENT WAVELENGTHS Vs PRESSURE, FOR DIFFERENT TUBE DIAMETERS.

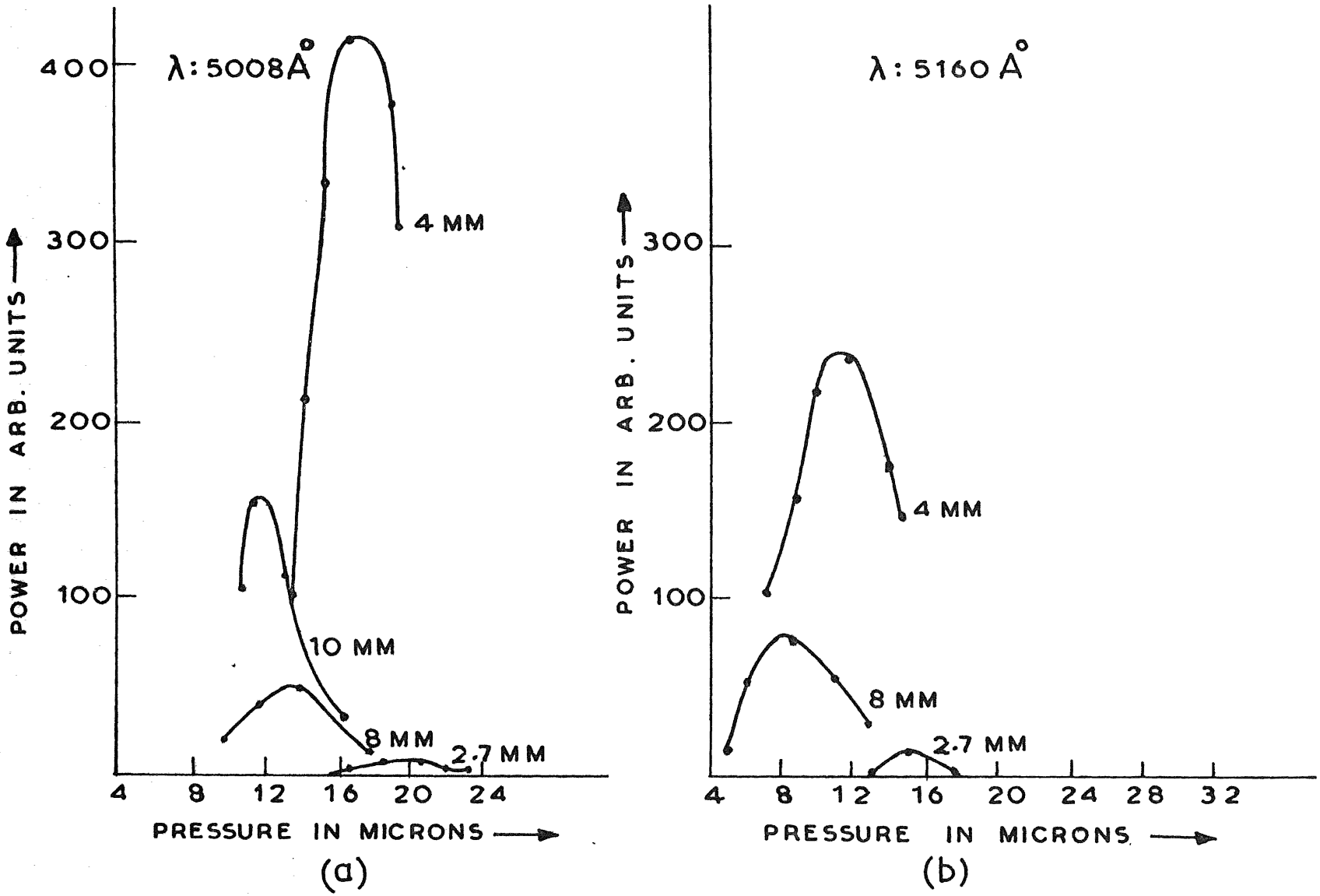

FIG.3.9 OUTPUT POWER Vs PRESSURE FOR DIFFERENT TUBE DIAMETERS

Table 3.1 : Distribution of Total Output Power at all-line Optimum Pressure.

Tube dia.: 6.3 mm, Excitation Voltage: 4.5 kV
Energy Storage Capacitor: 1μF

Wavelength in Å	Peak Output Power in watts
5394.62	131
5352.92	213
5260.19	147
5159.08	4
5007.8	36
4954.13	69

strongest and that nearly 80 percent of the total power is contributed by the four 'green' lines viz., 5395Å, 5353Å, 5260Å and 5160Å. This is in accordance with the observations of Simmons and Witte [43].

However, we have observed in addition that there is a marked change in the power distribution as the pressure is changed from its optimum value. At very high pressures, only the line at 5395Å lases and is quite powerful. This has been reported by Simmons and Witte also. Further, we have observed that as the pressure is reduced from this value, the line at 5260Å also starts lasing. The total laser output is then shared by these two lines with 5395Å being the stronger one. As the pressure is further reduced, 5353Å also starts lasing though being much weaker in comparison with the other two. On further reduction of pressure rest of the lines appear and 5353Å ultimately becomes the strongest. This behaviour is shown in Table 3.2.

The behaviour of the other lines is as follows. At higher pressures, the line at 5008Å becomes stronger than the one at 4954Å which lases strongly at lower pressures. The line at 5160Å is found to be more sensitive to pressure changes compared to other lines and lases in the narrowest pressure range. This line also favours lower pressures where it is stronger than 5008Å, though weaker than 4954Å. This variation is shown in Table 3.3. The 'orange' line at 5955Å is

Table 3.2 : Variation in Relative Power Distribution with Pressure

Power Output in arb. units
Tube dia.: 6.3 mm, Excitation Voltage: 4 kV
Energy Storage Capacitor: 1μF

Pressure in microns	Wavelength in Å			
	5394.62	5352.92	5260.19	Others
28	320	-	-	-
24	400	5	42.5	-
21	420	30	270	-
15.5	136	290	164	262.5

Table 3.3 : Variation in Relative Power Distribution with Pressure

Power Output in arb. units
Tube dia.: 6.3 mm, Excitation Voltage: 5 kV

Pressure in microns	Wavelength in Å			
	4954.13	5007.8	5159.08	Others
27	-	135	-	392
21.5	142	74	9.3	1200
15.5	142	50	71	590

observed to favour higher pressures and with He-Ne mirrors has continued to lase at pressures higher than those where even 5395Å stops lasing.

Thus we have observed that different lines have different optimum pressures which in turn differ from the all-line optimum pressure. Further, all the lines show maximum small-signal gain at their respective optimum pressures. For each line the optimum pressure varies with the tube diameter. Based on the available experimental data, Papayoanou et al. [49] gave the following empirical relation, relating the all-line optimum pressure to the tube diameter

$$P_{opt} = P_o + C(D_o - D) \qquad (3.1)$$

The slope of the line C was reported to be 0.6 μ/mm. Our results show that the all-line optimum pressure further depends upon the excitation voltage and to some extent on mirror transmission also. With increasing excitation voltage, the optimum pressure increases linearly. However, for a given excitation voltage, the all-line optimum pressure does vary linearly with tube diameter as shown in Figure 3.10. This variation can be represented by the following equation

$$P_{opt} = P_o - CD \qquad (3.2)$$

Fitting equation (3.2) to our data we have found that irrespective of the excitation voltage or the mirror set used, all the straight lines shown in Figure 3.10 have the same slope

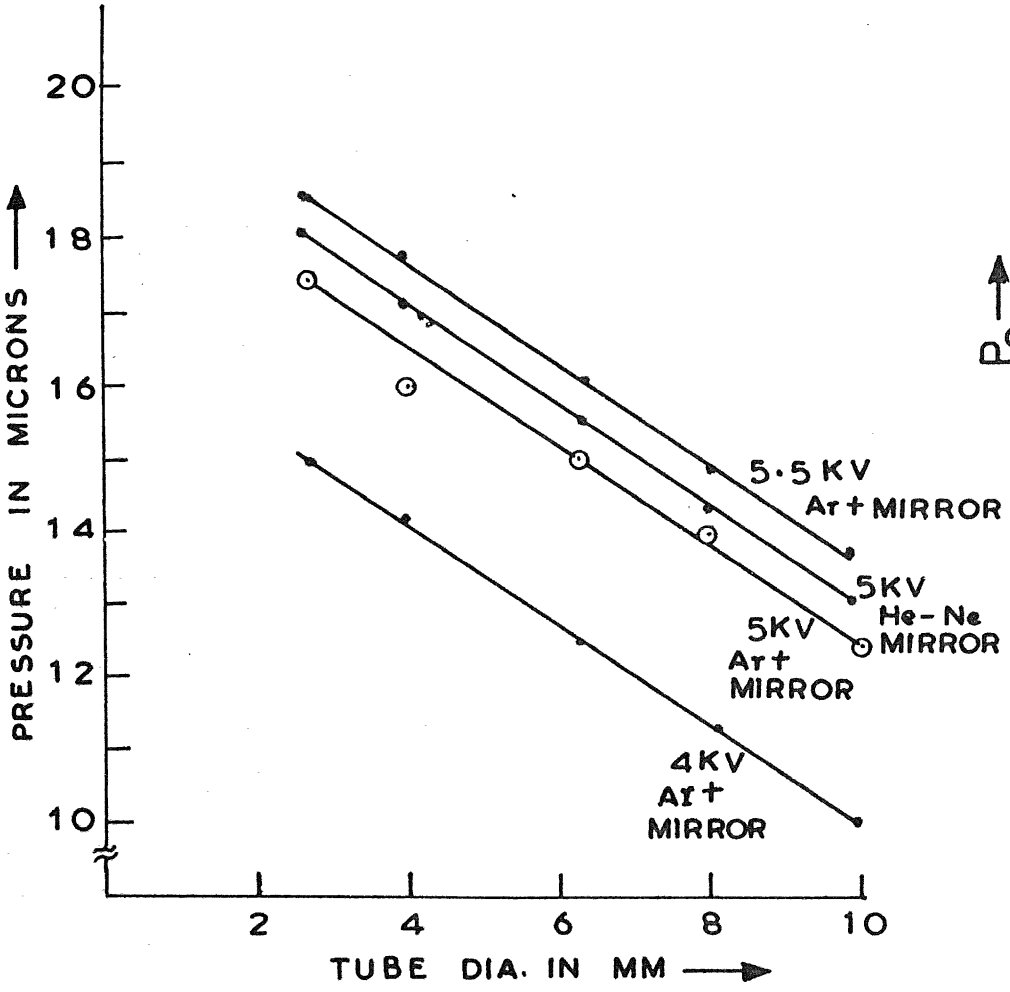

FIG.3.10 ALL LINE OPTIMUM PRESSURE Vs TUBE DIA. FOR DIFFERENT EXCITATION VOLTAGES.

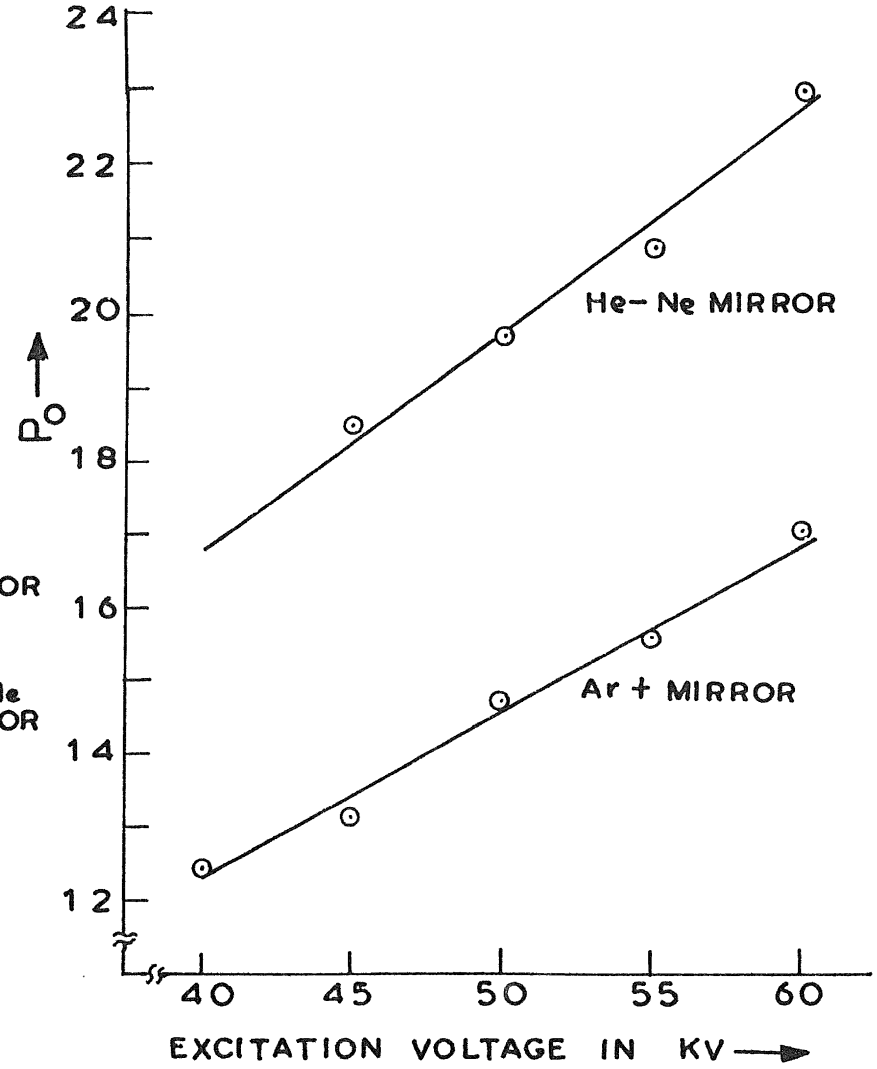

FIG.3.11 P_o Vs EXCITATION VOLTAGE FOR THE TWO MIRROR SETS.

of 0.7 μ/mm. The value of P_o however differs in each case and is a linear function of the excitation voltage as shown in Figure 3.11. This variation of P_o with excitation voltage is given by the following equation

$$P_o = a + bV \qquad (3.3)$$

where both a and b in turn depend on mirror transmission and the charging capacitance. In the present work a and b have the values 2.98 μ and 2.34 μ/KV respectively for Ar^+ mirrors and 5.09 μ and 2.94 μ/KV for He-Ne mirrors.

The dependence of the all-line optimum pressure can be understood from the fact that the various lines have different optimum pressures and depending on the mirror transmission, different lines will dominate the output spectrum. In the present case, with He-Ne mirrors the green lines are favoured over the blue lines. Hence, the all-line optimum pressure with He-Ne mirrors is higher than that with Ar^+ mirrors.

Although the all-line optimum pressure has shown a linear dependence on tube diameter, the optimum pressure variation for individual lines is markedly different as shown in Figures 3.12 to 3.15. Since the optimum pressures of individual lines do not show a linear dependence on tube diameter, we have attempted to fit this dependence into an equation of the following form

$$P_{opt} d^n = \text{constant} \qquad (3.4)$$

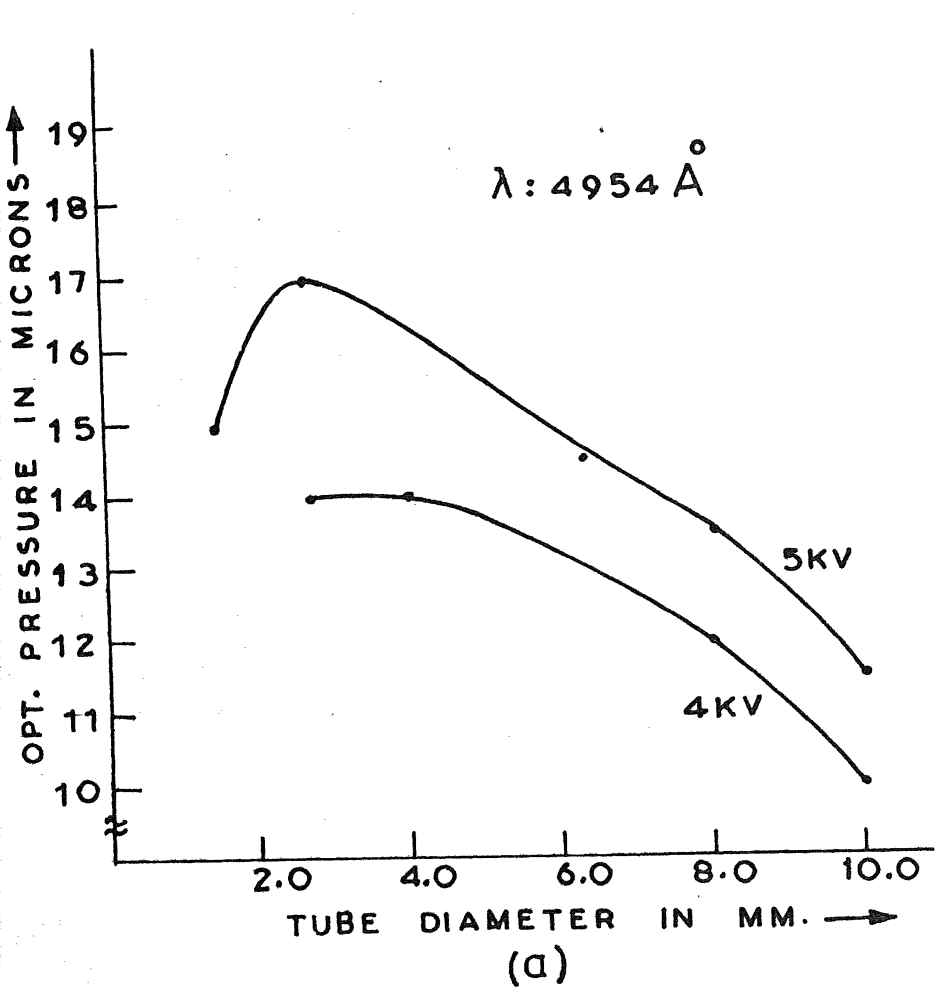

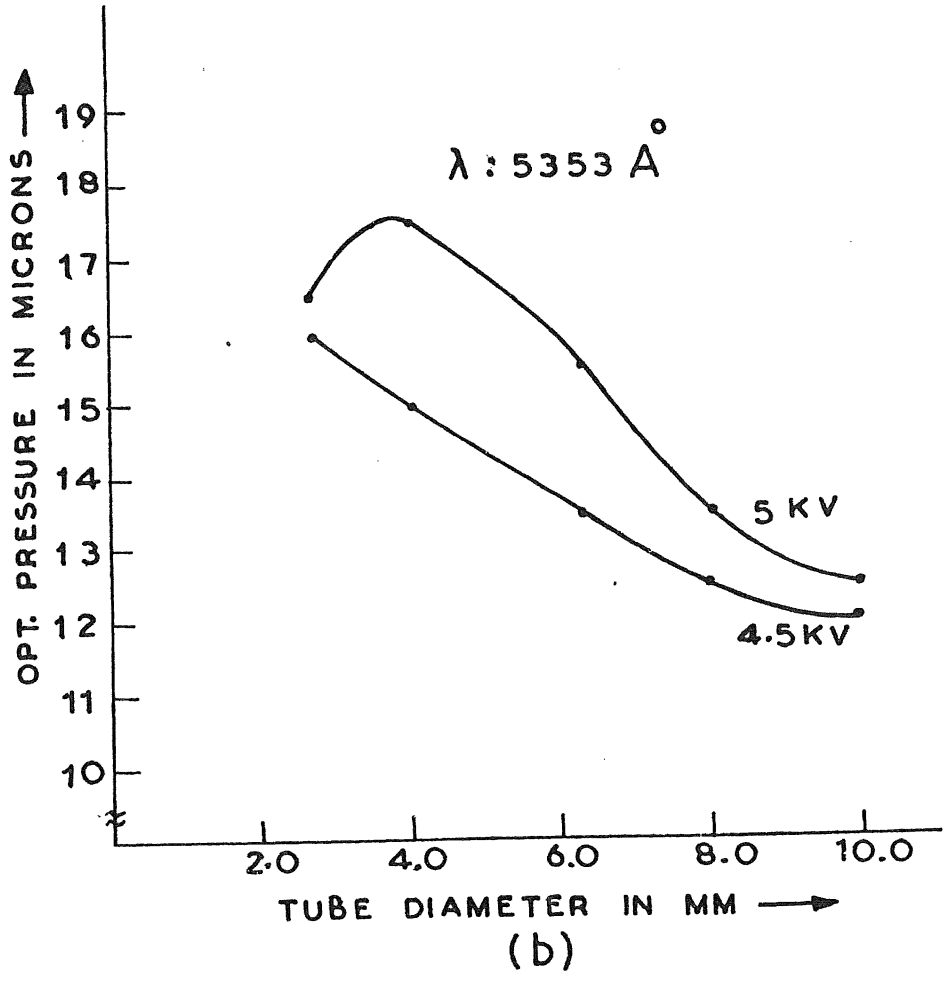

FIG.3.12 INDIVIDUAL LINE OPT. PRESSURE Vs TUBE DIAMETER FOR DIFFERENT EXCITATION VOLTAGES.

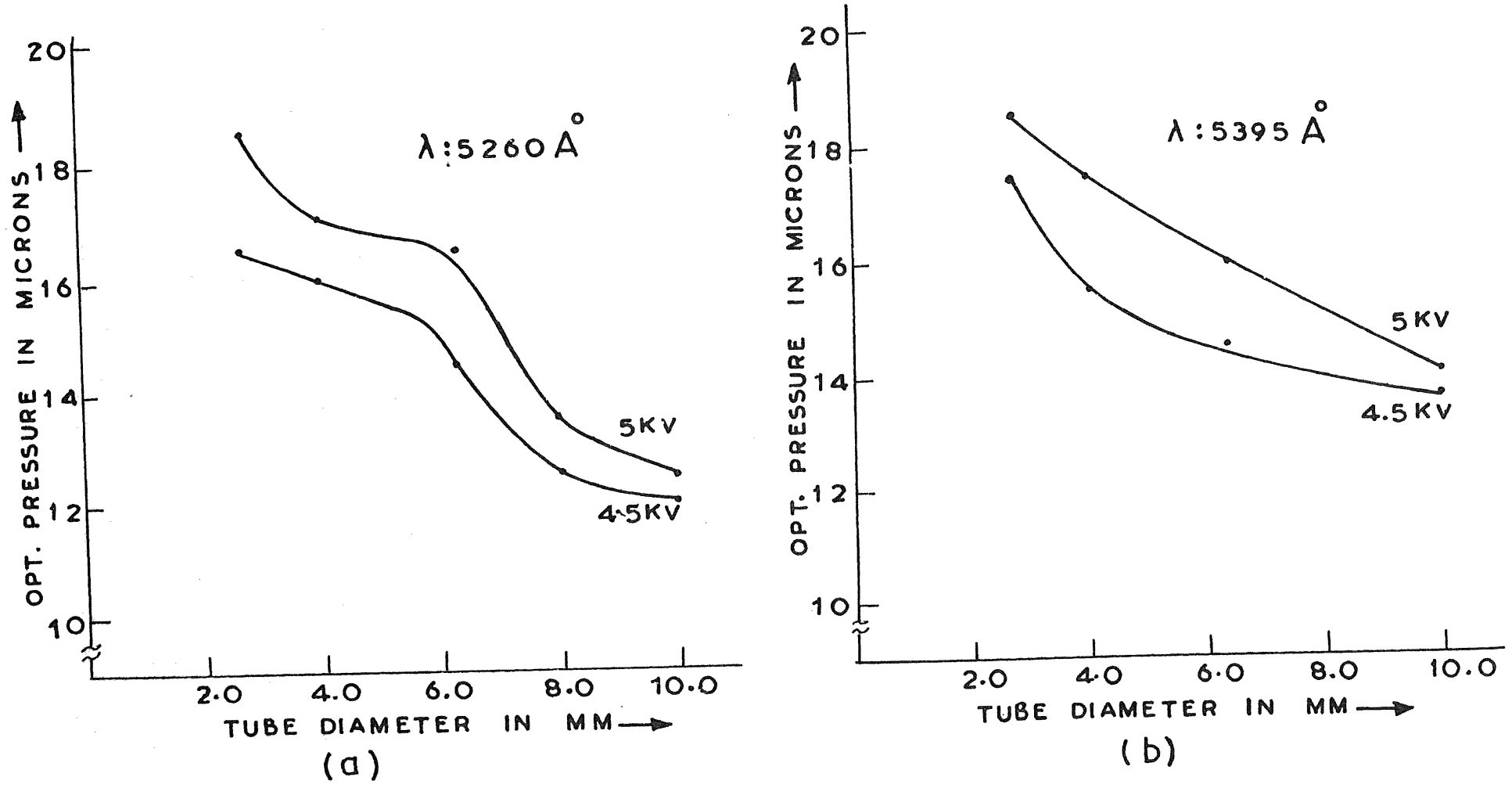

FIG.3.13 INDIVIDUAL LINE OPT. PRESSURE Vs TUBE DIAMETER FOR DIFFERENT EXCITATION VOLTAGES.

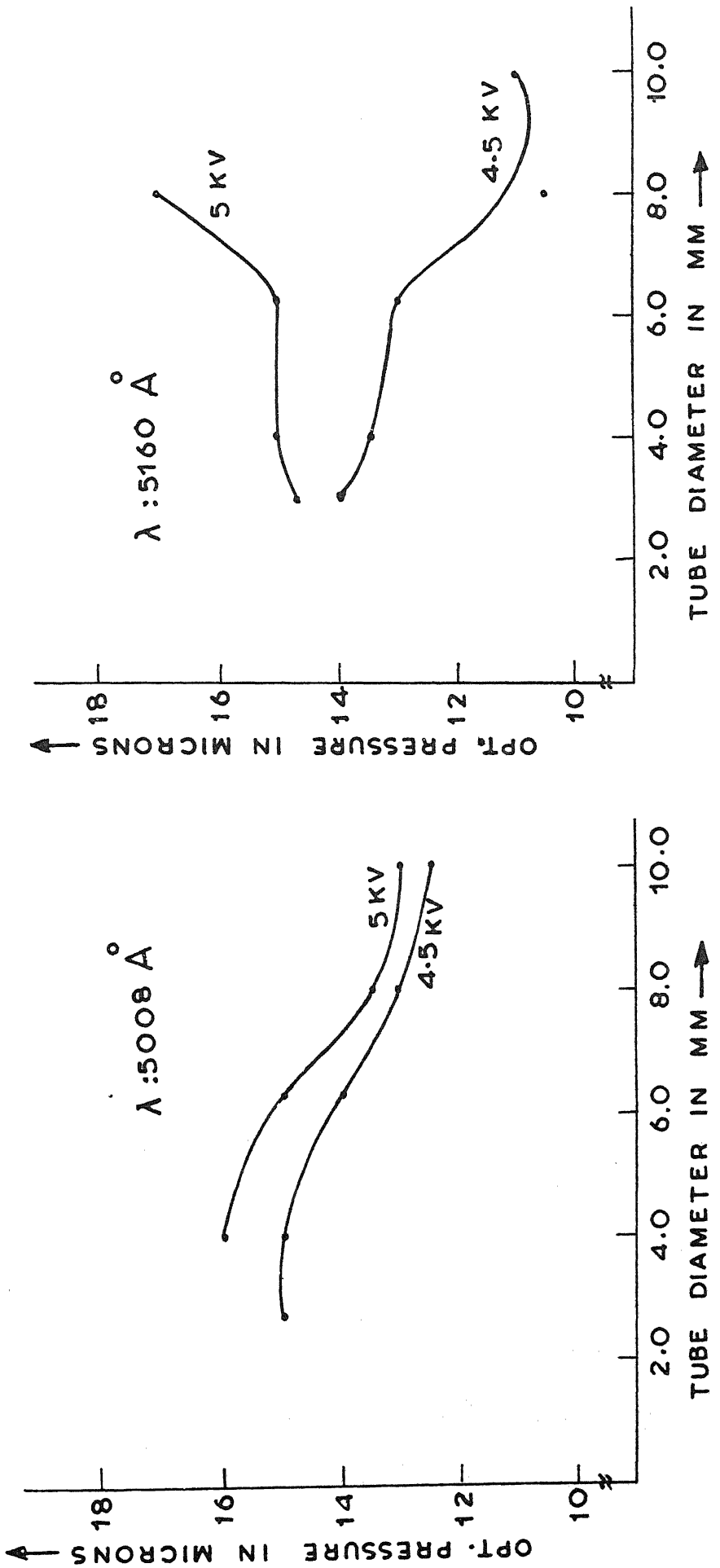

FIG. 3.14 INDIVIDUAL LINE OPT. PRESSURE Vs TUBE DIAMETER, FOR DIFFERENT EXCITATION VOLTAGES.

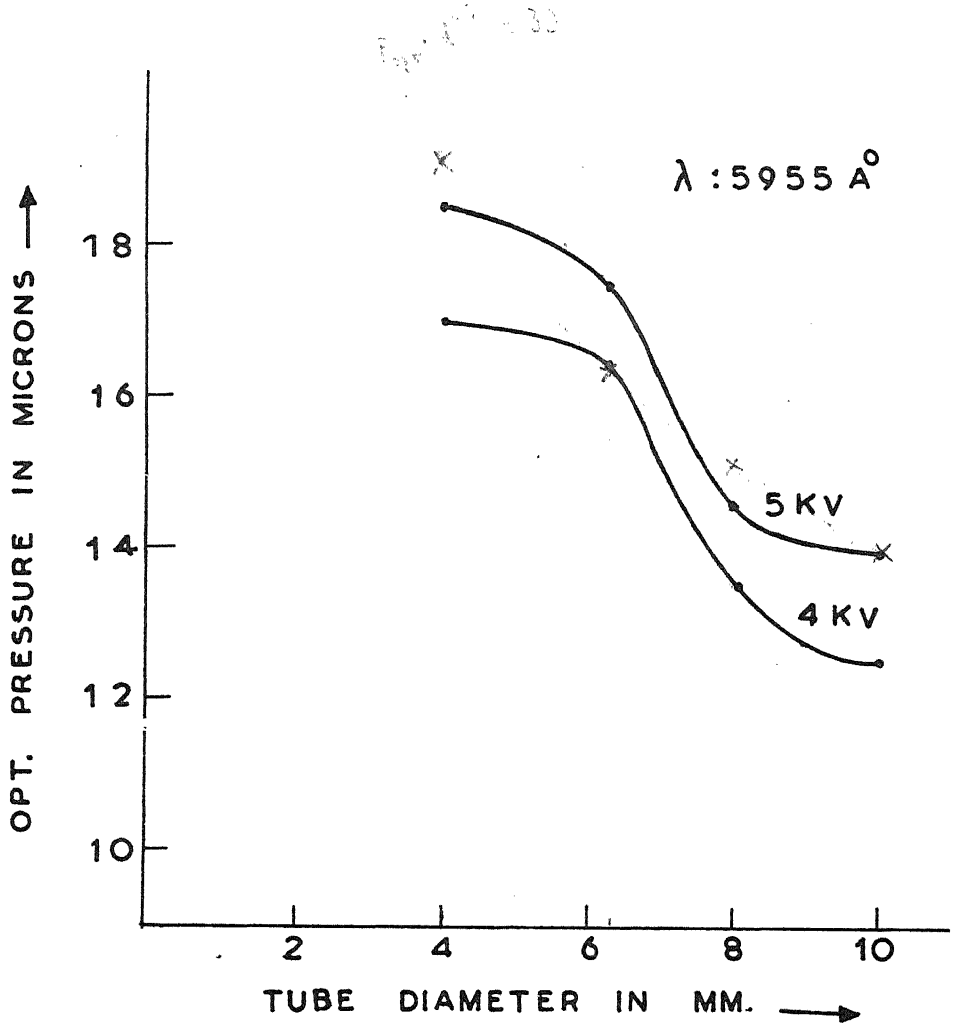

FIG. 3.15 OPT. PRESSURE Vs TUBE DIAMETER FOR DIFFERENT EXCITATION VOLTAGES.

Similar relationship has been given for the Ar^+ laser by Goldsborough [68] with a value of n equal to 1, and for the 3.5 μ Xe I laser transition by Clark [69] with a value of n equal to 3.2. The values of n obtained for different transitions in the present work are given in Table 3.4. It is seen that in all cases n is less than 1.0 and does not depend significantly on the excitation voltage, though it is too early to attach any physical significance to this behaviour.

The laser operation has been studied for two lengths of the plasma tube viz., 100 cm and 60 cm. It is observed that both the output power and the efficiency increase with increasing length. This is expected since the net gain (over loss) increases with increasing length. Further it is observed that the optimum pressure increases with increasing length which is consistent with the behaviour of the other ion lasers. The data for the two lengths are given in Table 3.5. The output power is seen to increase much faster than the ratio of lengths indicating that the gain in the laser is not fully saturated.

3.2 Power Output Variation with Other Parameters

The effect of varying the (initial) electric field on the laser output has been studied at different pressures. The threshold electric field variation with pressure for all

Table 3.4 : n Values for the Different Transitions

Wavelength in Å	Excitation Voltage	
	4.5 kV	5 kV
4954.13	.35	.36
5007.8	.2	.2
5159.08	.26	.2
5260.19	.34	.36
5352.92	.25	.38
5394.62	.16	.25
5955.67	.36	.33

Table 3.5 : Power Output and Optimum Pressure vs Plasma Tube Length

Wavelength in Å	Power Output in arb. units for Plasma Tube Length =		Opt. Pressure in Microns for Plasma Tube Length =	
	100 cm	60 cm	100 cm	60 cm
4954.13	400	154	15.5	12.5
5007.8	210	25	16	12.5
5159.08	40	20	15	14
5260.19	680	160	17	15
5352.92	1120	100	17	15
5394.62	640	100	17.5	15
5955.67	35	4	20	19

the seven lines is shown in Figures 3.16 to 3.18. Simmons and Witte [43] have reported variation of threshold current with pressure and their data are reproduced in Figure 3.19. As the excitation voltage is increased from the threshold value the output power increases sharply, saturates and then decreases. Typical data for all the seven lines at various pressures is given in Figures 3.20 to 3.23. This data is taken with the 4 mm tube. Other tubes have shown similar behaviour. For each line the E/p value at the peak output power, $(E/p)_{pk}$ has been calculated at several pressures. This $(E/p)_{pk}$ is found to be the same for each line and is independent of pressure for a particular tube diameter. Further, the closeness of the $(E/p)_{pk}$ values for all the seven lines is an indication of the fact that all these transitions belong to the same ionization species. However, the $(E/p)_{pk}$ value for each line shows a monotonic increase with increasing tube diameter, as shown in Table 3.6. It is to be noted that with increasing tube diameter proportionately larger charging voltages are needed for keeping the input energy density constant.

The efficiency of the laser is found to increase as the energy storage capacitance is decreased as shown in Table 3.7. With a smaller capacitance the rise-time of the current is shorter and electrons with higher average energy are produced. This increases the degree of multiple ionization

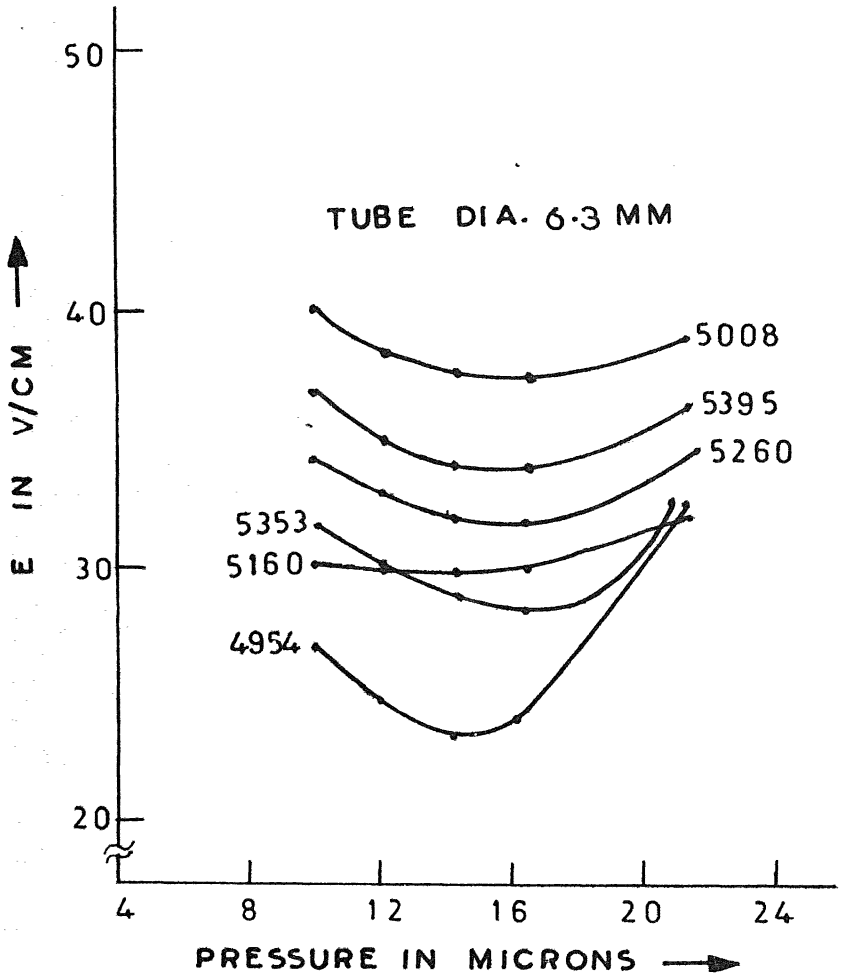

FIG.3.18 THRESHOLD E Vs PRESSURE

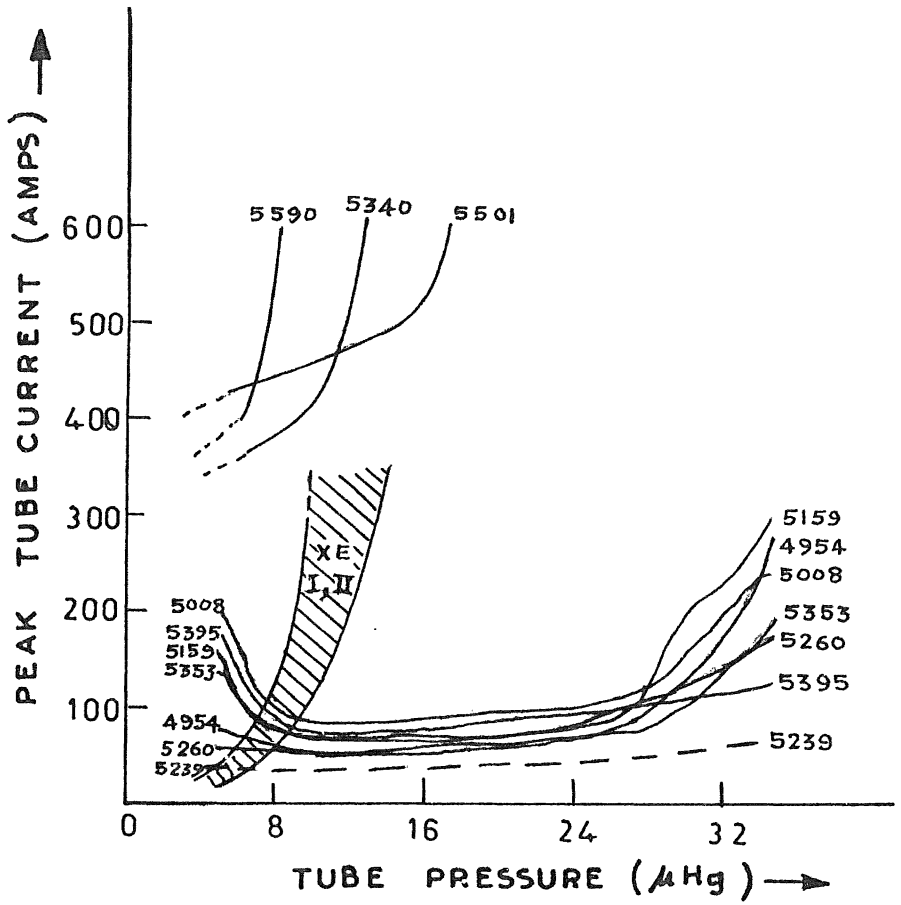

FIG.3.19 THRESHOLD CURRENT Vs PRESSURE. REPRODUCED FROM SIMMONS AND WITTE [43]

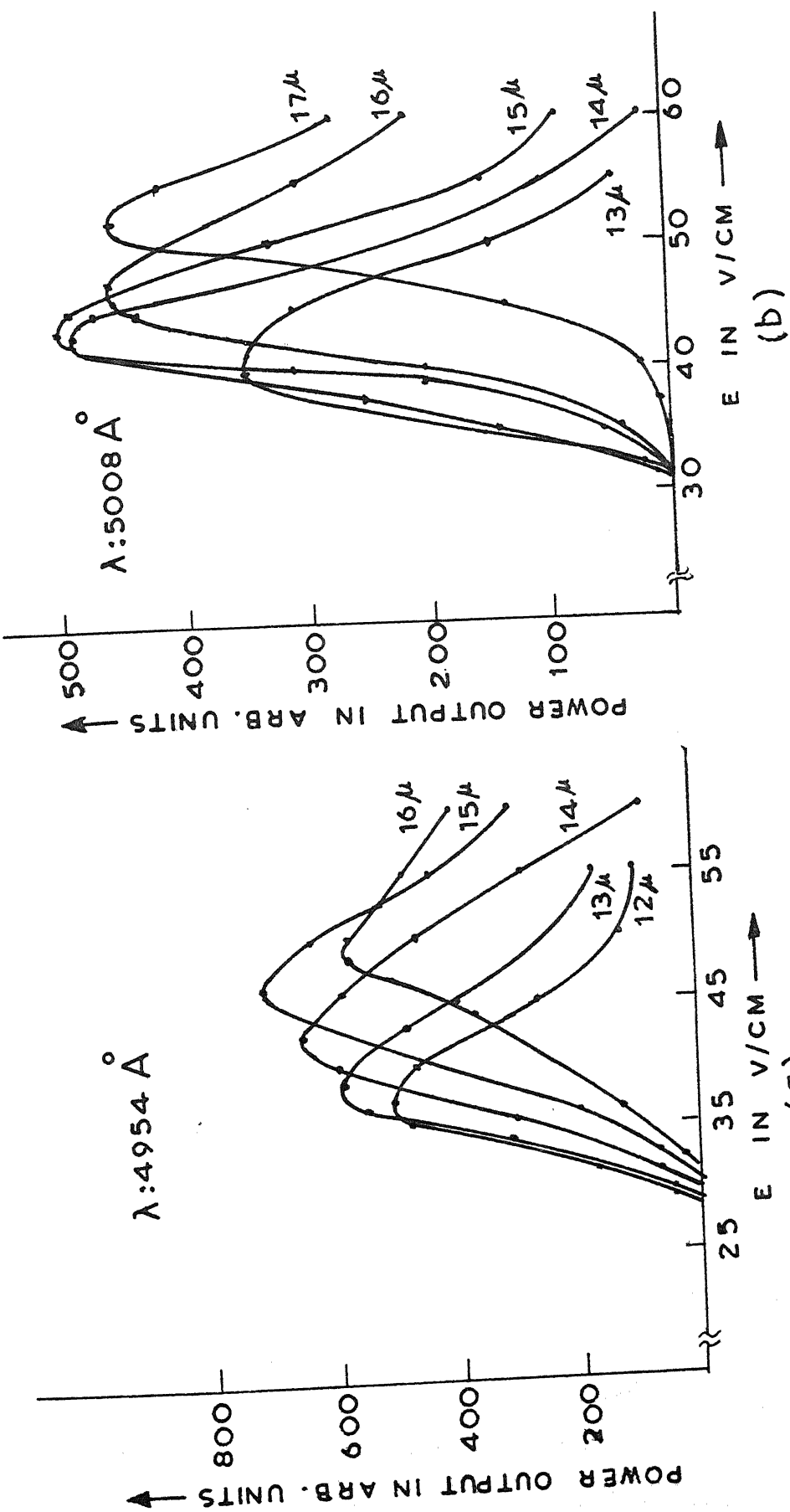

FIG. 3.20 OUTPUT POWER Vs INITIAL ELECTRIC FIELD AT VARIOUS PRESSURES BORE DIA : 4 mm

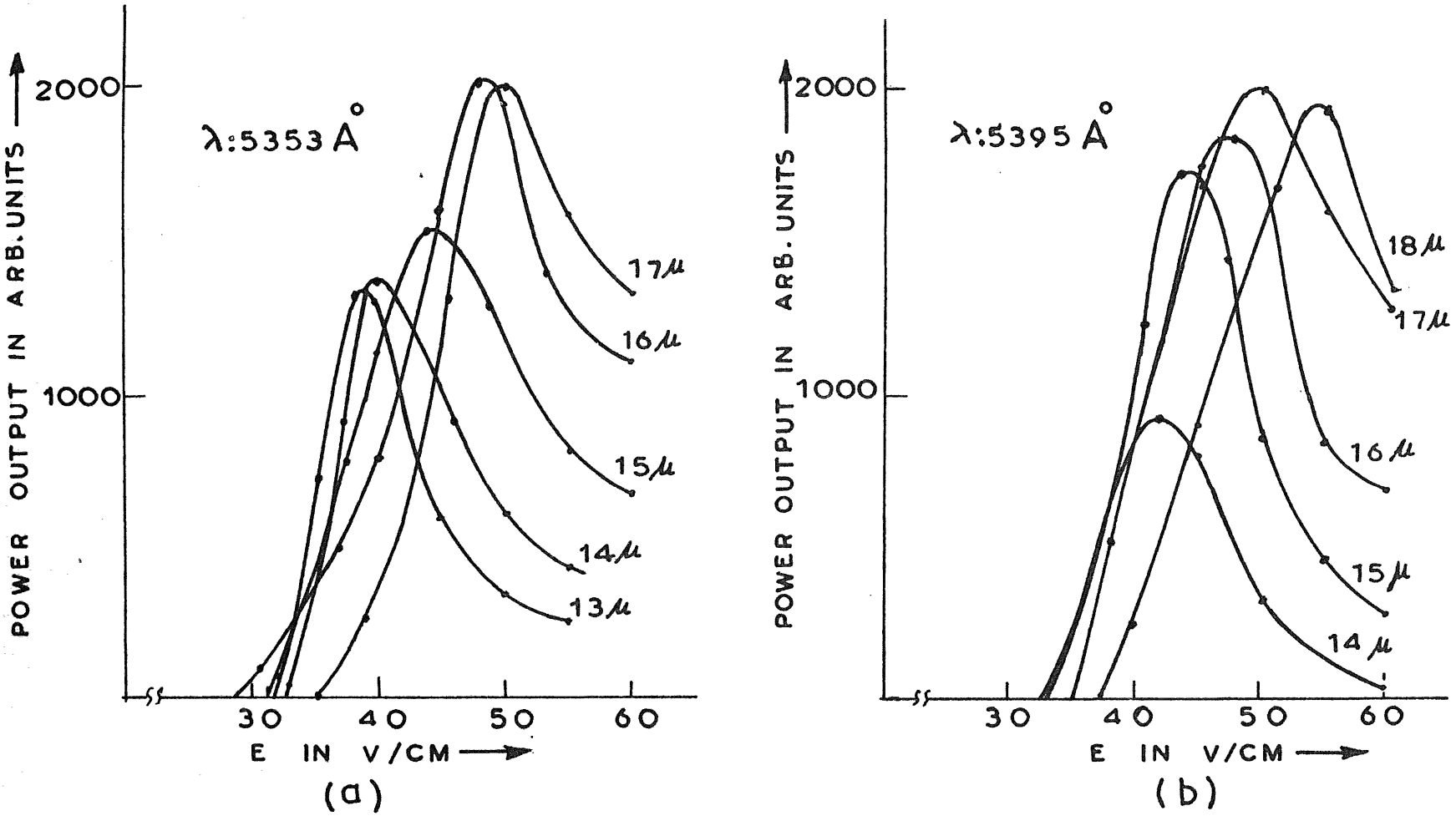

FIG. 3.21 OUTPUT POWER Vs INITIAL ELECTRIC FIELD AT DIFFERENT PRESSURES. BORE DIA : 4 mm.

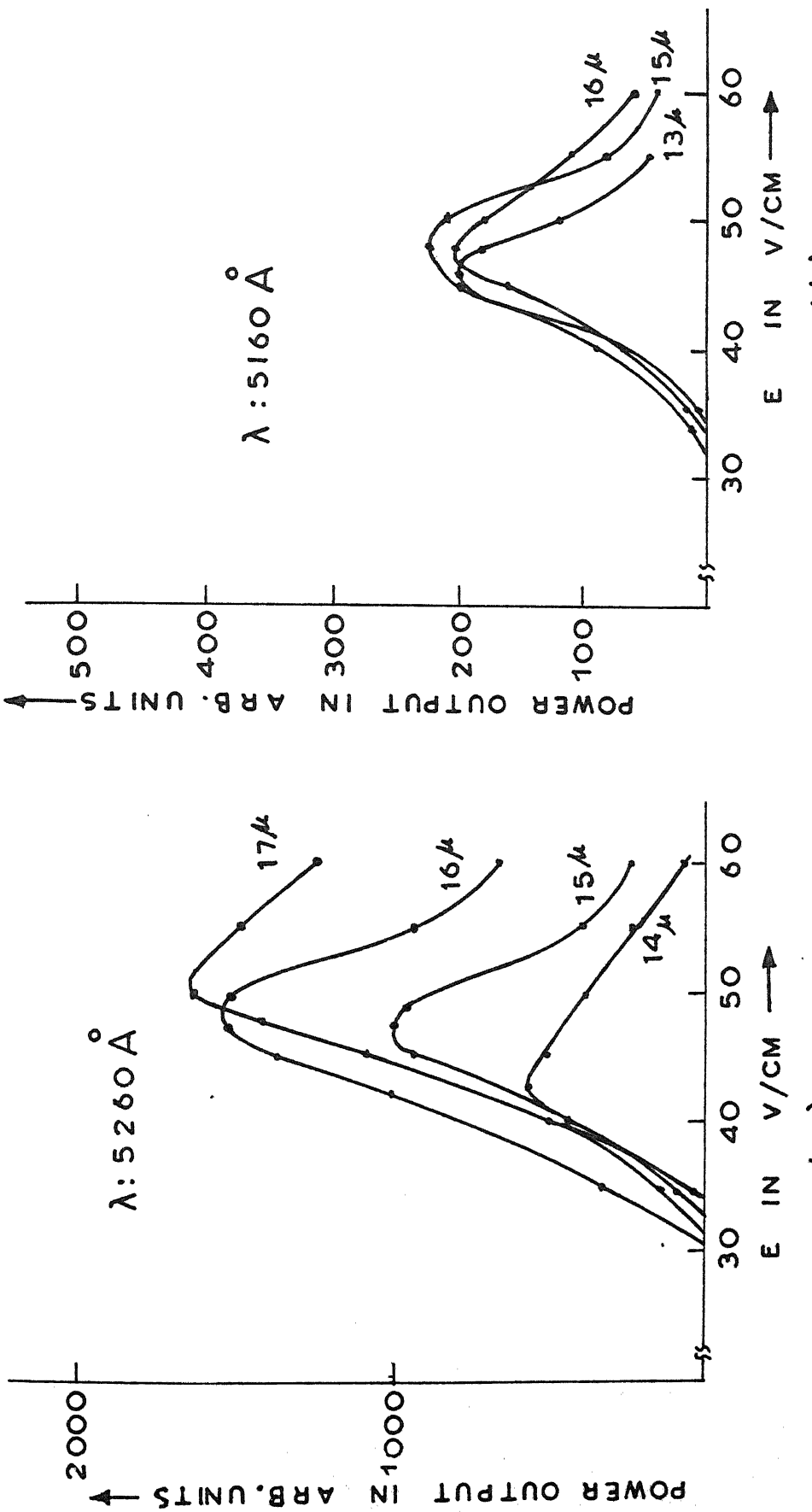

FIG. 3.22 OUTPUT POWER Vs INITIAL ELECTRIC FIELD AT VARIOUS PRESSURES. BORE DIA.: 4 mm.

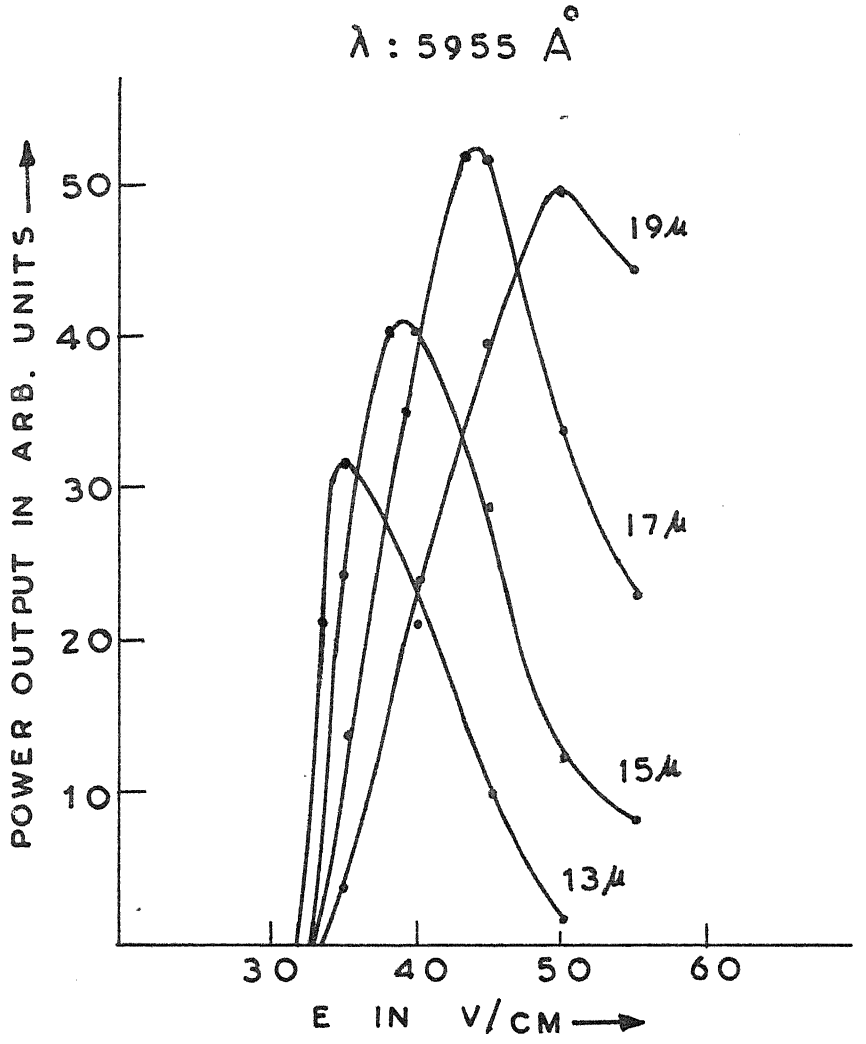

FIG. 3.23 OUTPUT POWER Vs INITIAL ELECTRIC FIELD FOR VARIOUS PRESSURES. BORE DIA. 4 mm

Table 3.6 : $(E/p)_{pk}$ for Different Wavelengths, in Volts/cm-micron

Wavelength in Å	Tube Diameter in mm			
	10	6.3	4	2.7
4954.13	4.5	3.5	3.3	2.4
5007.8	4.5	3.6	3.1	2.4
5159.08	4.3	3.3	3.6	2.5
5260.19	3.2	3.2	3.1	2.24
5352.92	4.0	3.3	3.1	2.4
5394.62	4.5	3.1	2.9	2.24
5955.67	3.6	3.0	2.7	2.37

Table 3.7 : Laser Efficiency, η, vs Capacitance

Wavelength in Å	Capacitance in μF	
	0.1	1
4954.13	$.9 \times 10^{-4}$	$.2 \times 10^{-4}$
5007.8	$.3 \times 10^{-4}$	$.1 \times 10^{-4}$
5159.08	$.1 \times 10^{-4}$	$.02 \times 10^{-4}$
5260.19	1.7×10^{-4}	$.4 \times 10^{-4}$
5352.92	3.7×10^{-4}	$.6 \times 10^{-4}$
5394.62	1.5×10^{-4}	$.4 \times 10^{-4}$

in the plasma and probably the efficiency. For the same reason, the optimum pressure decreases with decreasing capacitance and this has been verified in our work.

At the discharge currents used in our experiments it is expected that the plasma will be pinched to some degree. This will reduce the effective diameter of the discharge by constricting the current flow radially. Also near the tube walls, the wall collision effects are more predominant and these decrease the degree of multiple ionization but favour electron-ion recombination. In the ultraviolet transitions in ion lasers it has been observed [13] that lines belonging to higher ionization species do not lase in tubes of smaller diameter, while for lines belonging to lower ionization species laser power has been observed to increase with decreasing diameter [30].

We have observed that the Xe IV transitions do not lase strongly in smaller diameter tubes. In the 1.5 mm tube, only the two transitions which have the highest gain viz., 5353Å and 4954Å lase strongly. This indicates that wall collisions play a major role in discouraging the excitation process to higher ionization states thereby reducing the inversion density near the tube walls. To confirm this fact, a variable aperture has been inserted in the laser cavity and the multimode output power has been recorded as a function of the aperture diameter. The 6.3 mm tube has been used for

this experiment and the observed variation in power output is shown in Figure 3.24. It is clearly seen that increasing the aperture diameter beyond 3.75 mm does not result in any change in the output power, confirming that no inverted population exists near the tube walls. This point is further discussed in Chapter 5.

Finally, the effect of tube bore diameter on the maximum laser efficiency at each wavelength has been studied. For this, two efficiency parameters are defined. One parameter, η_1, is the ratio of output power at each wavelength to the total input energy under optimum operating conditions of the laser. Figure 3.25 shows the variation of η_1 with tube diameter for all the seven wavelengths.

The other parameter, η_2, is a ratio of the output power in each wavelength to the input energy density. This parameter has been calculated to obtain a better comparison of tube bore diameters normalised to the same input energy density. This data is presented in Figure 3.26. While plotting both Figures 3.25 and 3.26, suitable multiplicative scale factors have been used for η_1 and η_2 for a better representation of the data. However, the actual efficiencies at the seven wavelengths are given in Table 3.7 for the 4 mm tube.

The following observations can be made from this study.

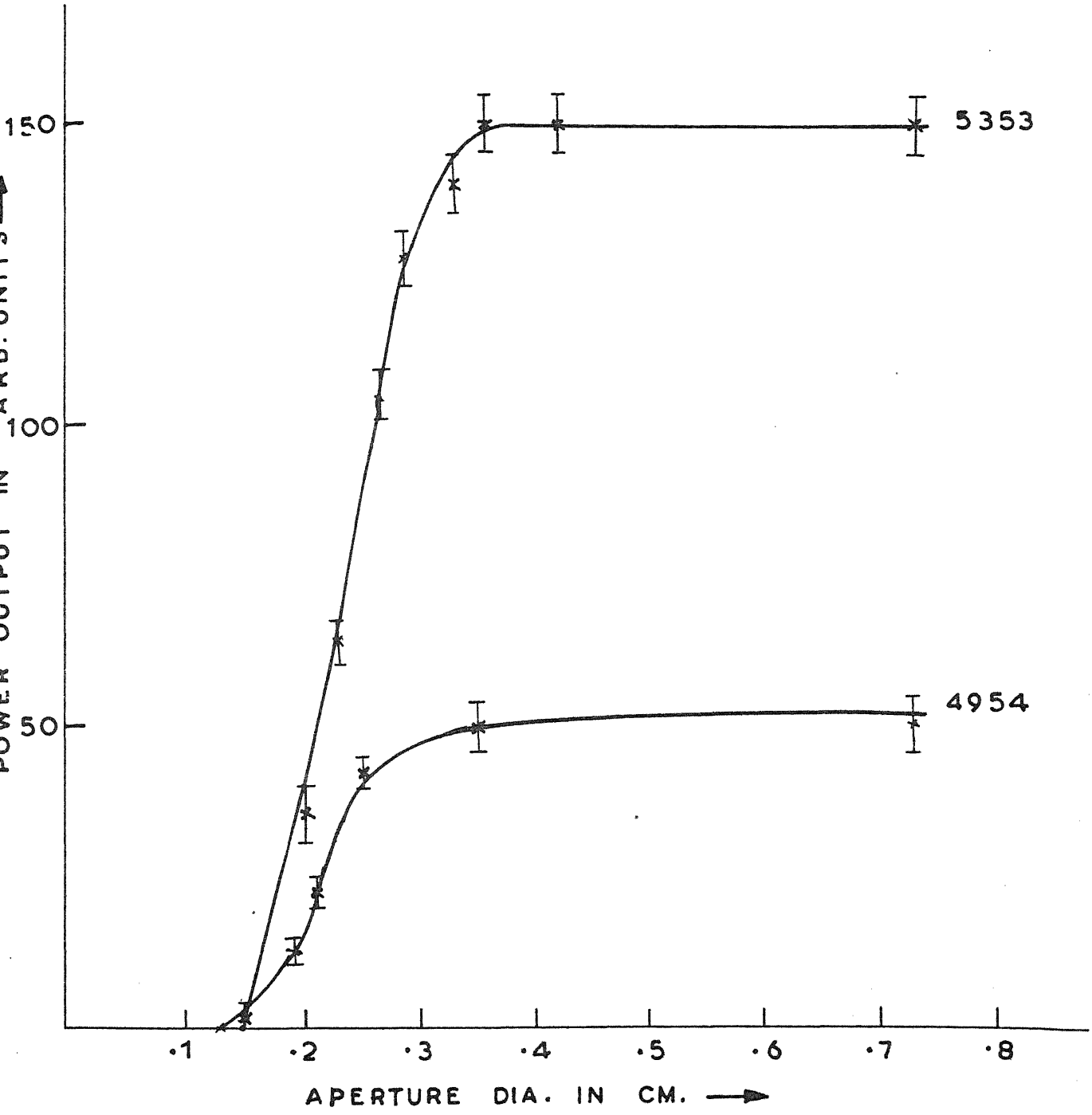

FIG.3.24 POWER OUTPUT Vs APERTURE DIAMETER.
TUBE BORE DIA. 6.3 mm.

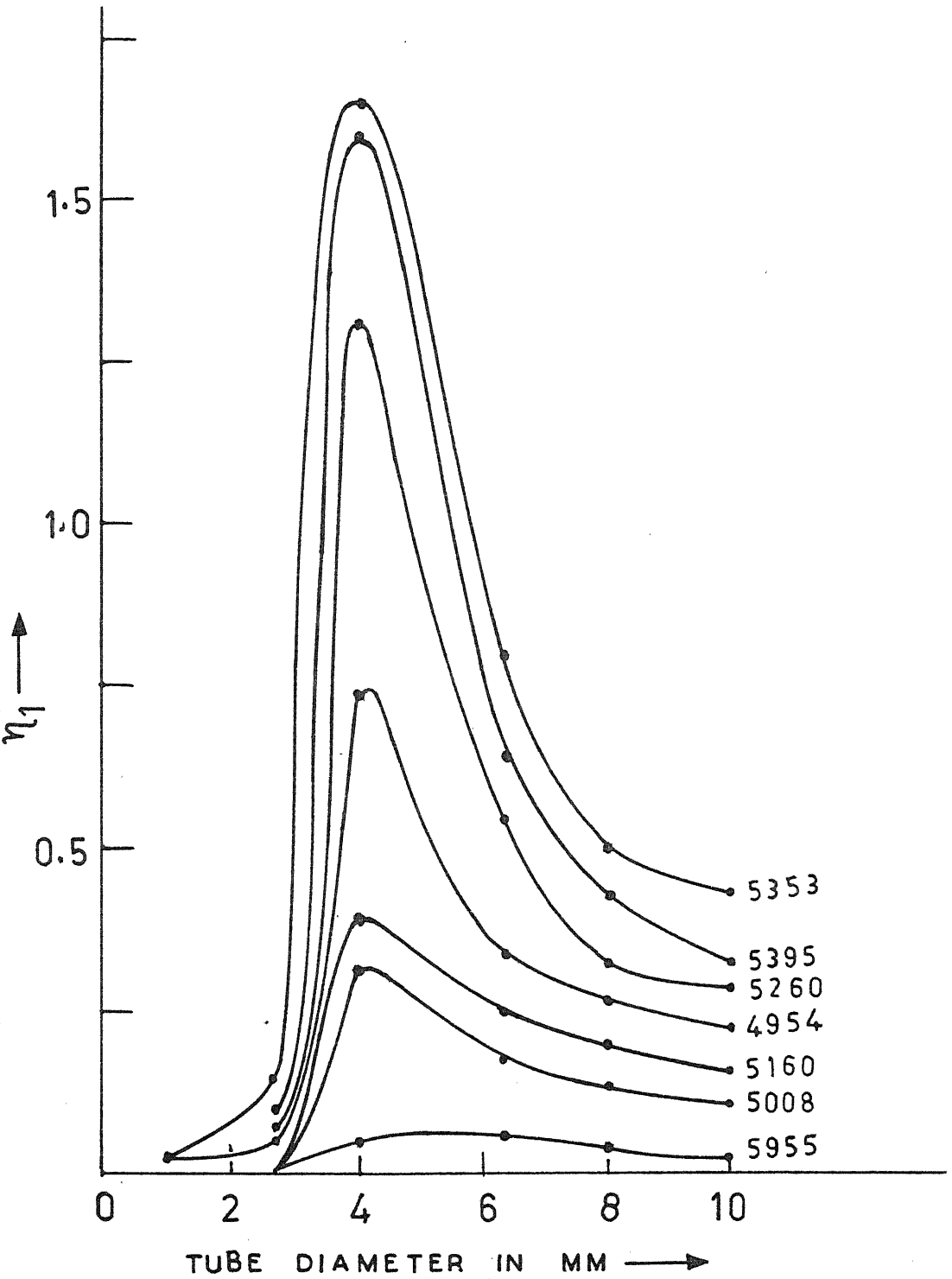

FIG.3.25 η_1 Vs TUBE DIAMETER. VALUES OF η_1 MULTIPLIED BY APPROPRIATE SCALE CONSTANT.

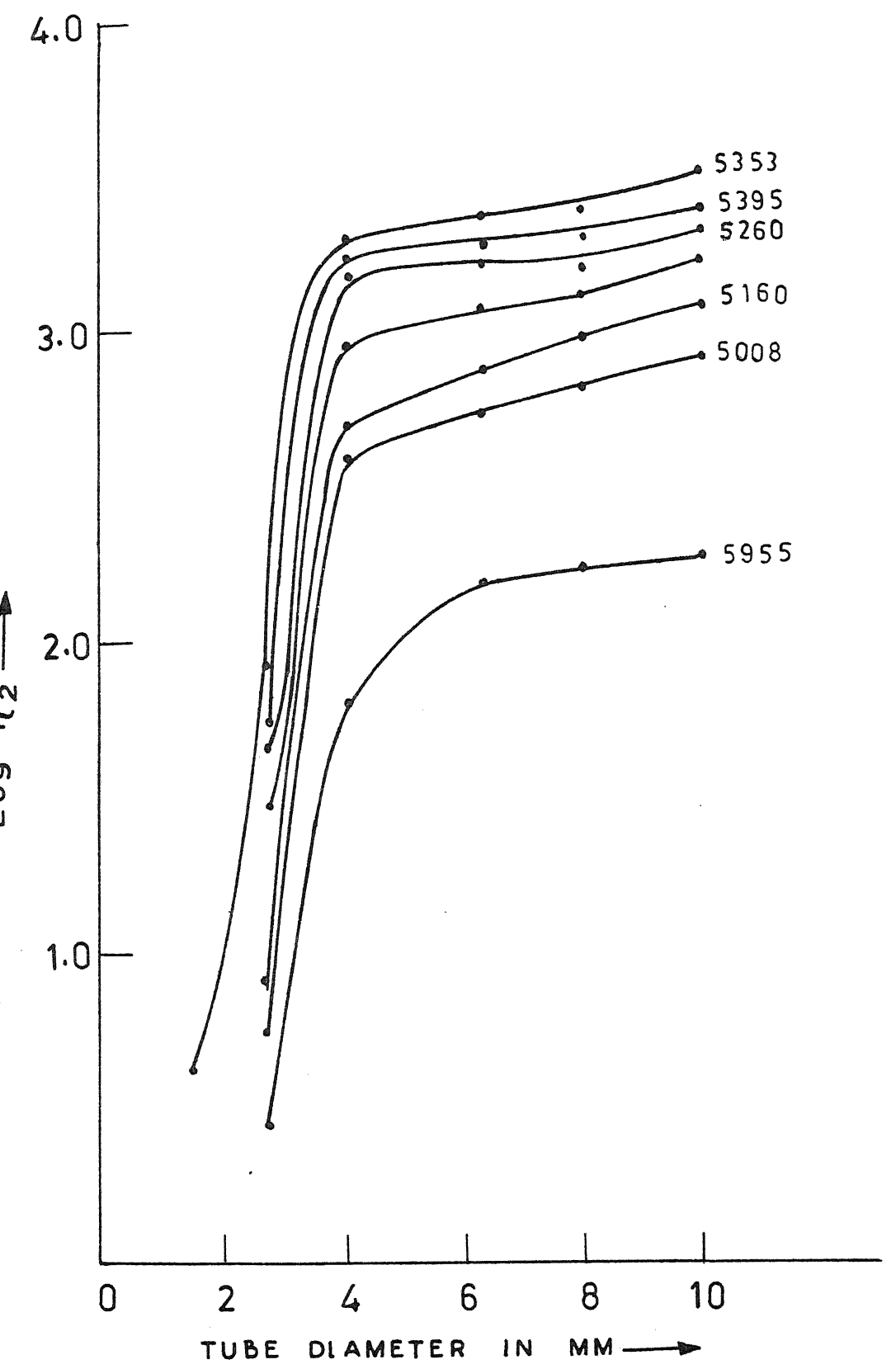

FIG.3.26 Log η_2 Vs TUBE DIAMETER. η_2 VALUES HAVE BEEN MULTIPLIED WITH APPROPRIATE SCALE CONSTANTS.

The optimum tube diameter is slightly more than 4 mm for the given excitation source.

For a given input energy density the efficiency increases with increasing tube diameter. This increase is very marked for diameters up to 4 mm. Beyond this diameter, there is a slow but distinct increase in the efficiency with tube diameter. This is also in accordance with the earlier conclusion that wall collisions discourage the excitation to multiply ionized species and thereby reduce the inversion density for the transitions from these states.

CHAPTER 4

GAIN MEASUREMENTS

In this chapter we present the results of small-signal gain measurements on the seven visible transitions in the pulsed Xe IV laser. No such detailed gain measurements have so far been reported for these transitions. An attempt is made, though qualitatively, to study the gain saturation behaviour of this laser.

In a medium exhibiting gain through inverted population density the change in the intensity of electromagnetic radiation, ΔI, as it propogates through it is given by

$$\Delta I = \alpha I \Delta Z \qquad (4.1)$$

α is the (small-signal) gain coefficient; it is independent of the radiation field intensity but depends on the properties of the transition and the inversion density, as

given by

$$\alpha(\nu) = \sigma(\nu) \Delta N \qquad (4.2)$$

Now as the inversion density and hence the gain of the active medium increase with pumping, laser oscillations build up from noise level provided that the inherent cavity losses are overcome by the gain present in the medium. The condition for these oscillations to sustain is given by

Gain per pass = Total loss per pass

This is true under all conditions and is independent of the radiation intensity circulating in the cavity. However, as the intensity of the field increases, the gain coefficient is no longer independent of the field and equation (4.1) is to be suitably modified to account for this non-linearity [70] as

$$\Delta I_\nu = [\alpha(\nu) I_\nu - \beta(\nu) I_\nu^2] \qquad (4.3)$$

Here $\beta(\nu)$ accounts for the saturation behaviour. Once again equating the saturated gain to the total cavity losses one can obtain the steady state intensity of the field in the laser.

The gain saturation behaviour of any laser further depends on the type of broadening mechanism operative in the active medium. For a four-level gas laser Rigrod [71], White et al. [72] and Smith [73] analysed the gain saturation behaviour, with both homogeneous and inhomogeneous broadening

mechanisms as limiting cases. Gaseous ion lasers fall under this category.

In these lasers, as the atom/ion undergoes a transition between the intermediate levels 2 and 3, the resulting radiation exhibits a Doppler-broadened profile centered at the transition frequency, ν_o, with a FWHM of $\Delta\nu_D$. The actual frequency, ν', emitted by the individual atom lies somewhere within the natural profile of the transition centered at ν' with FWHM of $\Delta\nu_N$. ν' in turn depends on the velocity of the atom undergoing the transition.

Assuming such an active medium, the gain coefficient is given by [70]

$$\alpha = \frac{1}{I'}\,\frac{dI'}{dz} = \frac{K_o}{\pi} \int_{-\infty}^{\infty} \frac{\exp(-\varepsilon x^2)\,dx}{(1 + x^2 + I')} \qquad (4.4)$$

where

$I' = I/I_o$ is the normalised radiation intensity

I_o is the intensity saturation parameter

$x = 2(\nu' - \nu_o)/\Delta\nu_N$

$\varepsilon = (\ln 2)^{\frac{1}{2}}\,\Delta\nu_N/\Delta\nu_D$

and K_o is a constant depending on the pumping rates and rate coefficients of levels 2 and 3.

The parameter ε contains the information about the broadening. Equation (4.4) when solved for the two limiting

cases reduces to one of the following two expressions:

For pure inhomogeneous broadening

$$\alpha_i = \alpha_{oi}/(1 + I/I_o)^{\frac{1}{2}}$$

For pure homogeneous broadening

$$\alpha_h = \alpha_{oh}/(1 + I/I_o)$$

The α_o's are the small-signal gain coefficients.

In general, noble gas ion lasers (singly ionised) show a broadening intermediate to these two limiting cases. These transitions have a large natural line width because of the short lifetimes of the lower laser levels and the line-shape shows a Voigt profile rather than a pure Doppler one. The ratio of the inhomogeneous to the homogeneous linewidth for a typical transition in these lasers is around 10 [18]. Further, in CW and pulsed noble gas ion lasers operating at high current densities the Stark broadening can be quite significant [18].

Thus the large homogeneous linewidth in noble gas ion lasers makes them behave in many ways as if they are homogeneously broadened. Measurements by several workers have shown that the Ar II laser transitions are inhomogeneously broadened just above threshold while well above threshold their behaviour is more like that of a homogeneously broadened transition.

4.1 Experimental Procedure

The experimental set-up for measuring the gain has already been described in Chapter 3. The small-signal gain has been obtained by measuring the loss in the cavity at which the laser just stops oscillating. Under these conditions the gain available in the medium just balances the total losses in the cavity. This criterion leads to the following expression for the small-signal gain, G, per pass

$$G = \exp(\alpha_o l) = \frac{1}{\sqrt{R_1 R_2}\ T_B^2 (1-L)} \qquad (4.7)$$

where α_o is the small-signal gain coefficient of interest, l is the length of the active medium, R_1, R_2 are the mirror reflectivities, T_B is the transmission through each of the Brewster windows and L is the value of the variable loss introduced to achieve the threshold oscillation condition; the scattering losses at the mirror surfaces are neglected as they are small and difficult to measure.

To study the saturation behaviour of this laser, its power output has been measured for different losses introduced in the cavity. Assuming that the oscillations stabilise where the losses balance the (saturated) gain, we have obtained the dependence of laser power output on the saturated gain [73].

4.2 Results and Discussion

A. Small-signal Gain Measurements

The variation of small-signal gain coefficient with input energy density has been studied for tubes of different diameters. The plots for the various wavelengths are given in Figures 4.1 to 4.7. These data have been collected mainly with a 1μF capacitor in the discharge circuit. However, for the 6.3 mm and the 4 mm tubes, additional data have been obtained with a 0.1μF capacitor; these results are also presented in the same figures.

From these figures it can be seen that in all cases as the input energy density increases the gain coefficient first increases, saturates and then decreases above a certain value of this energy density. This behaviour is consistently observed for all the tubes and the two capacitors used. The efficiency of laser operation also shows a similar dependence on the input energy density.

This can be explained to be mainly due to the fact that for a given tube and capacitance increase of input energy density implies increase of the electric field inside the plasma discharge. The laser will operate with maximum efficiency for an optimum value of this field. At too low an electric field, the excitation to the laser levels will not be efficient as these levels lie more than 65 eV above the

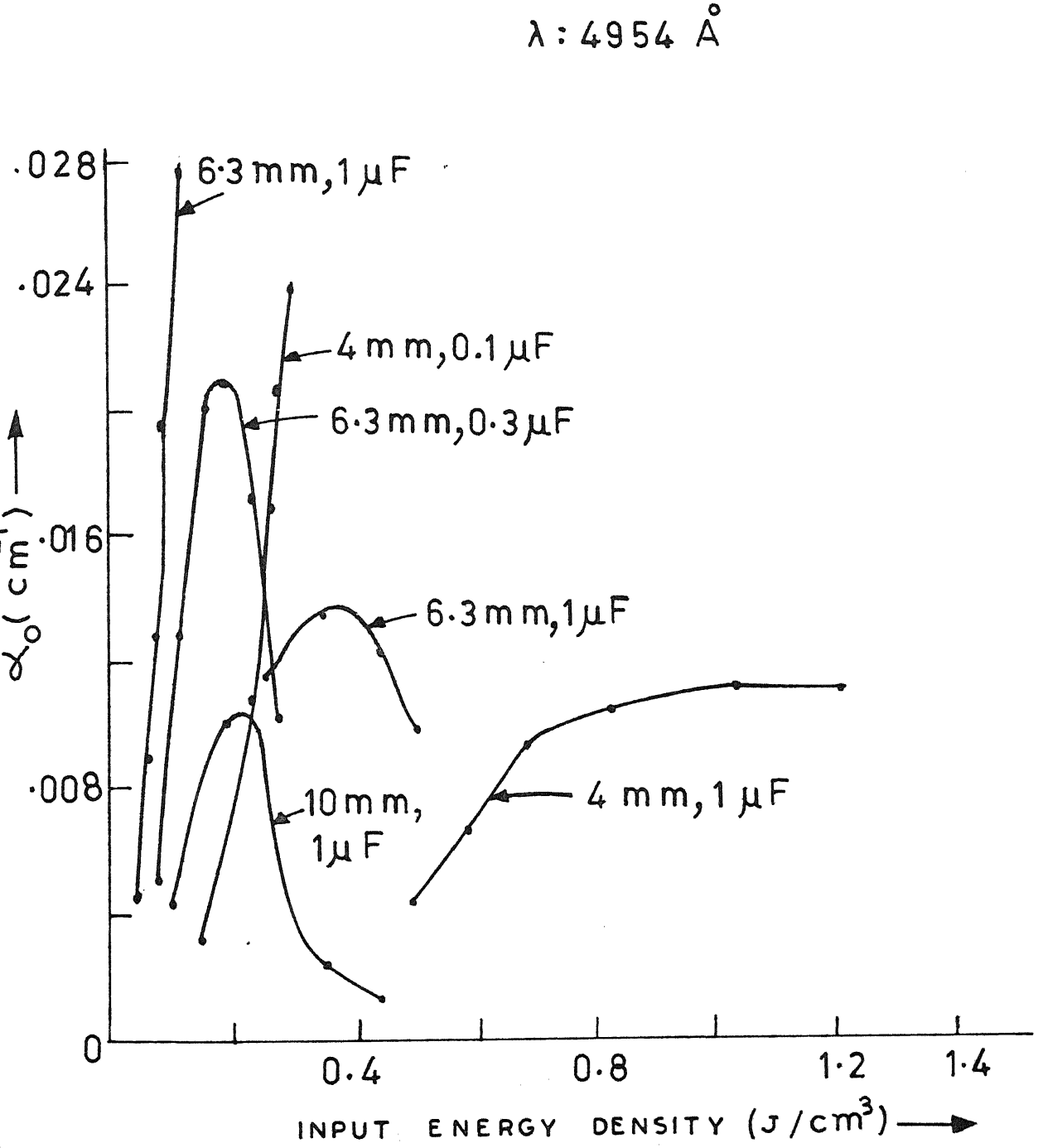

FIG. 4.1 α_o Vs INPUT ENERGY DENSITY

λ : 5008 Å

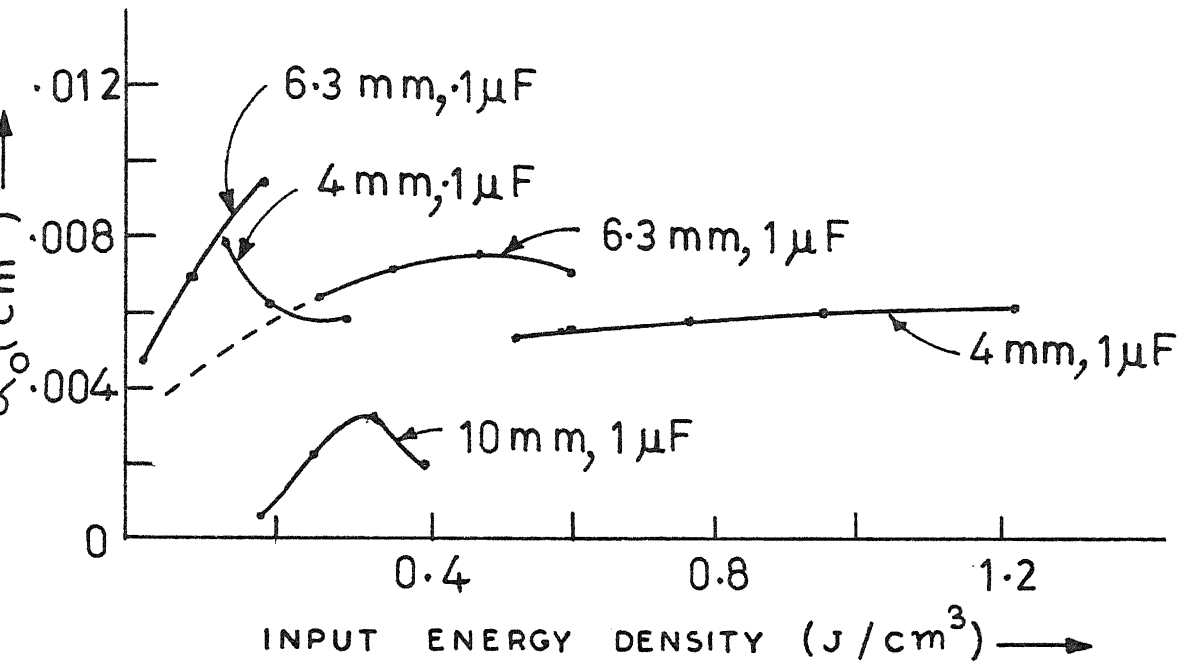

FIG. 4.2 α_o Vs INPUT ENERGY DENSITY

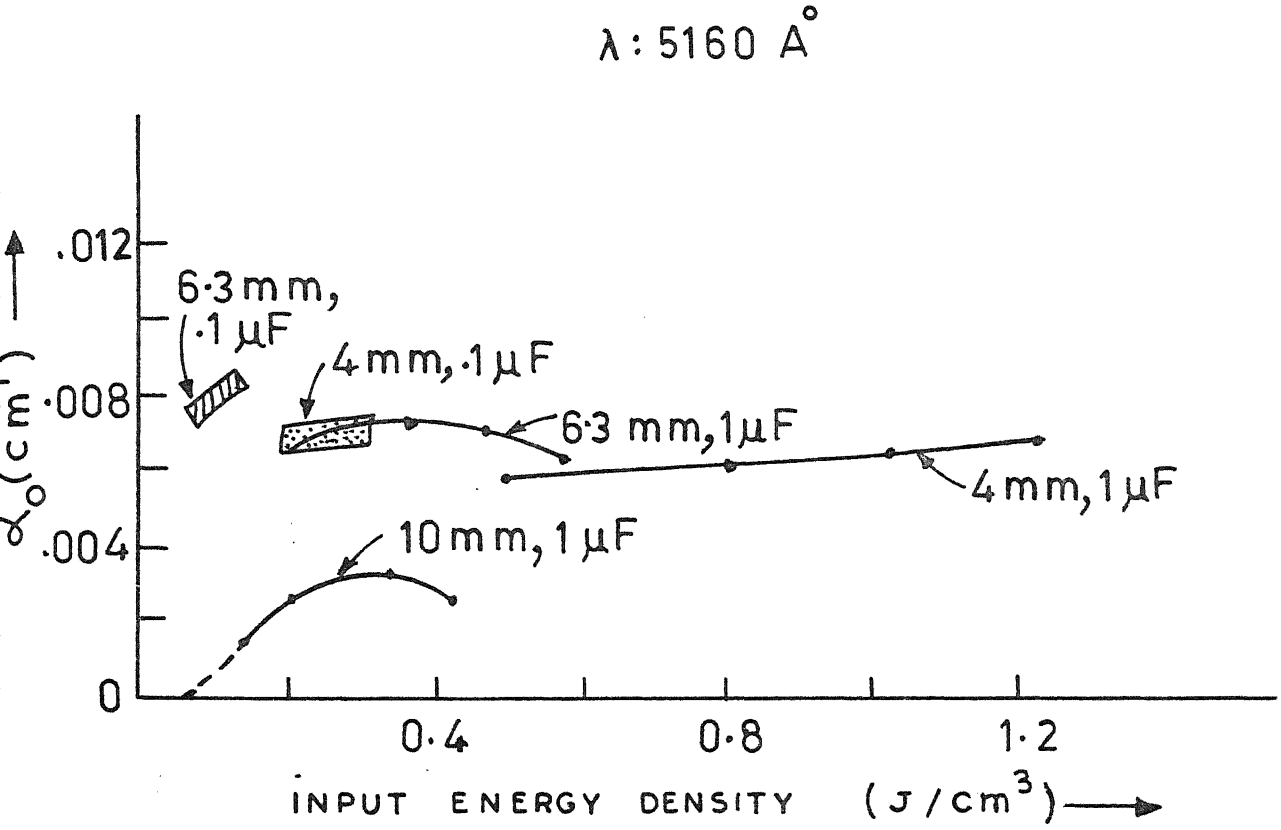

FIG. 4.3 α_o Vs INPUT ENERGY DENSITY.

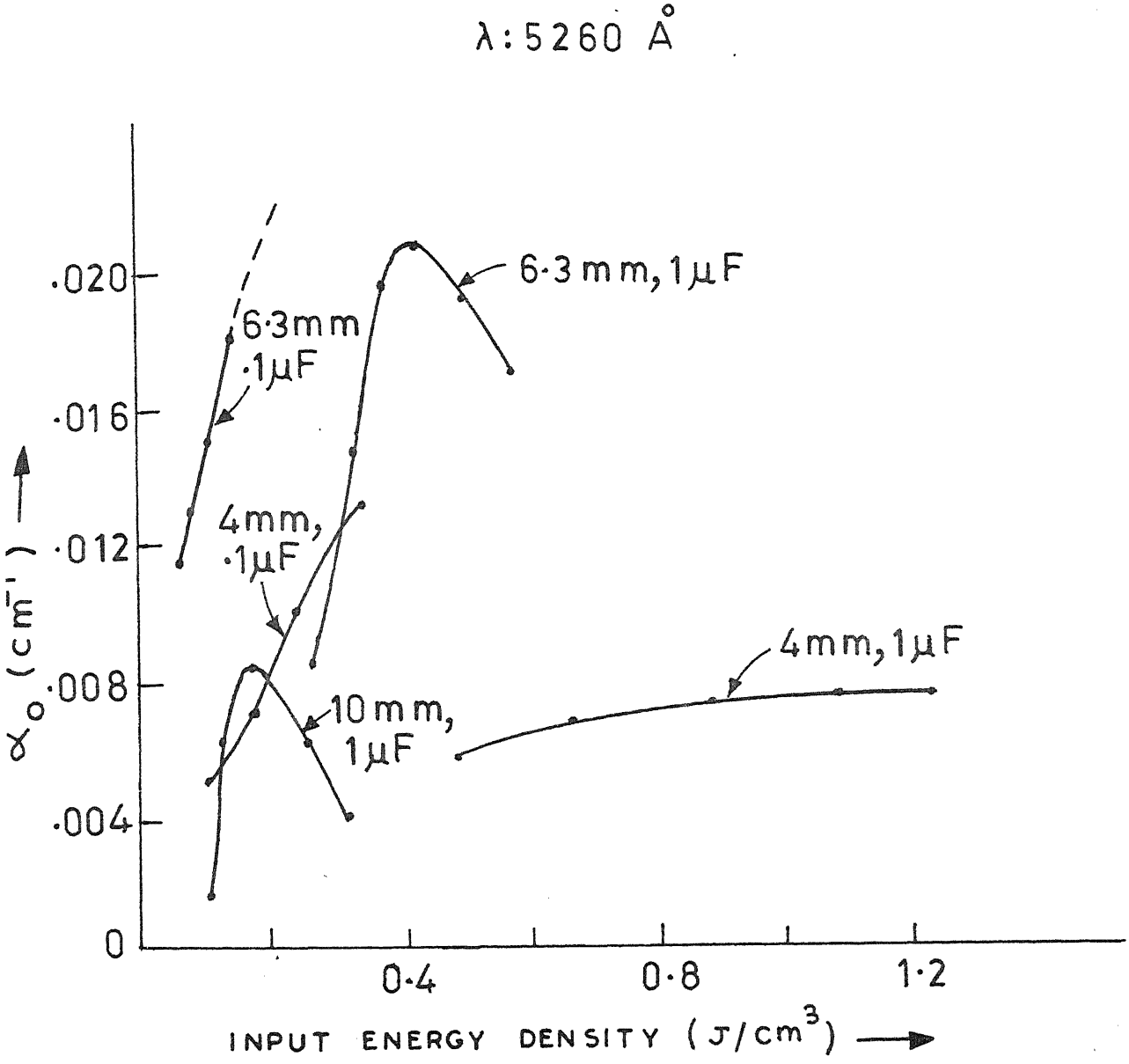

FIG.4.4 α_o Vs INPUT ENERGY DENSITY.

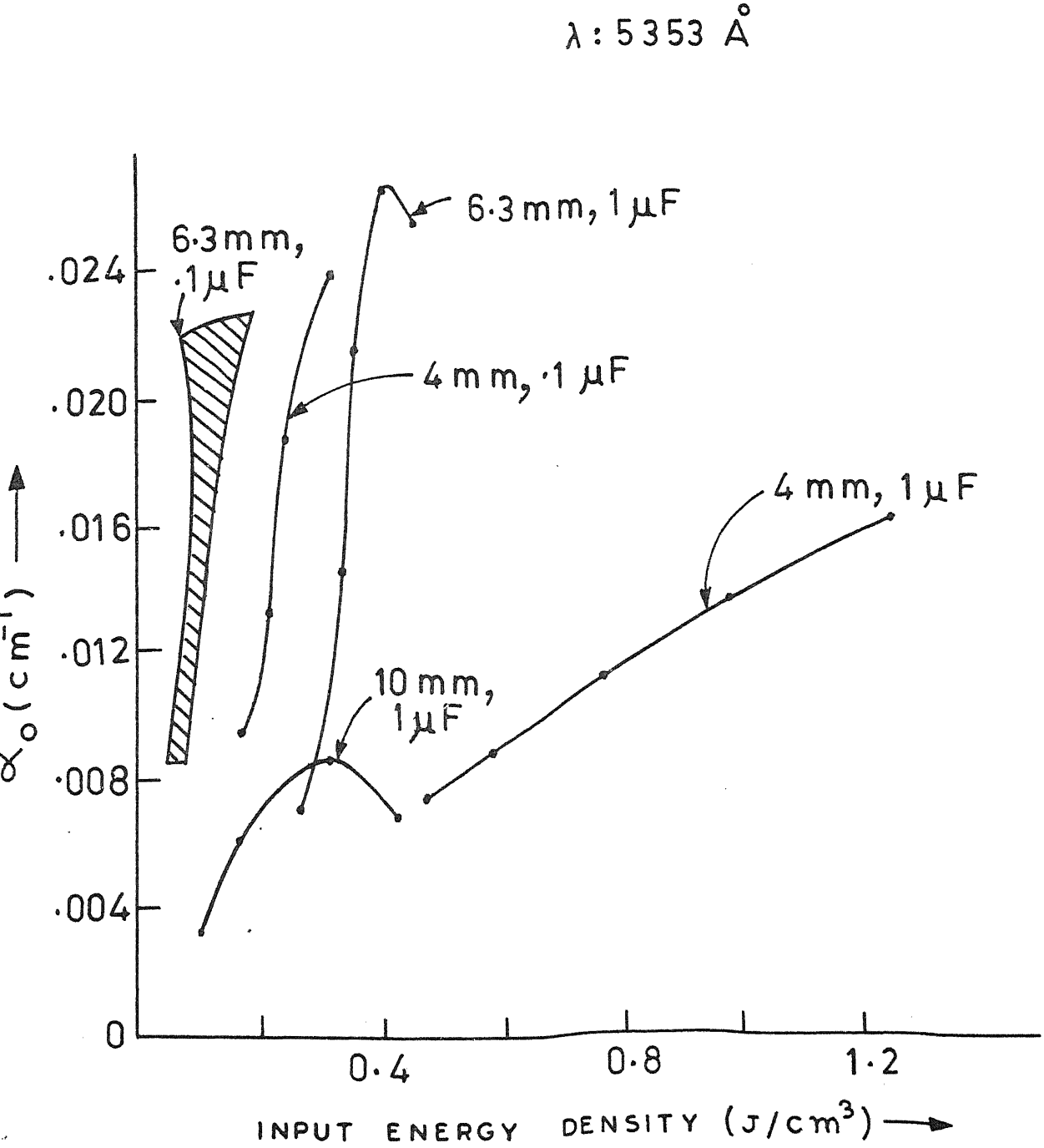

FIG. 4.5 α_o Vs INPUT ENERGY DENSITY.

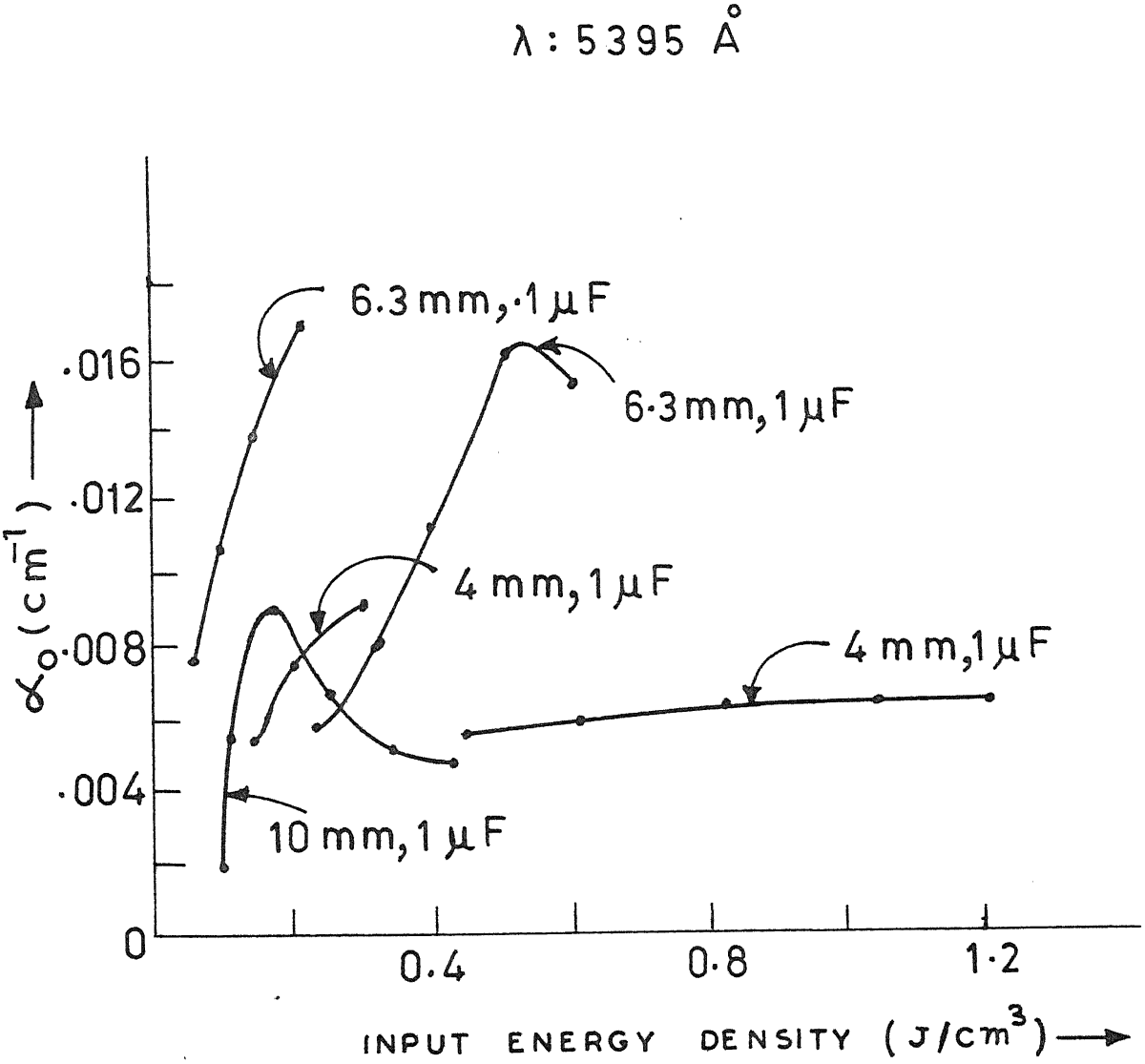

FIG. 4.6 α_o Vs INPUT ENERGY DENSITY.

λ:5955 Å

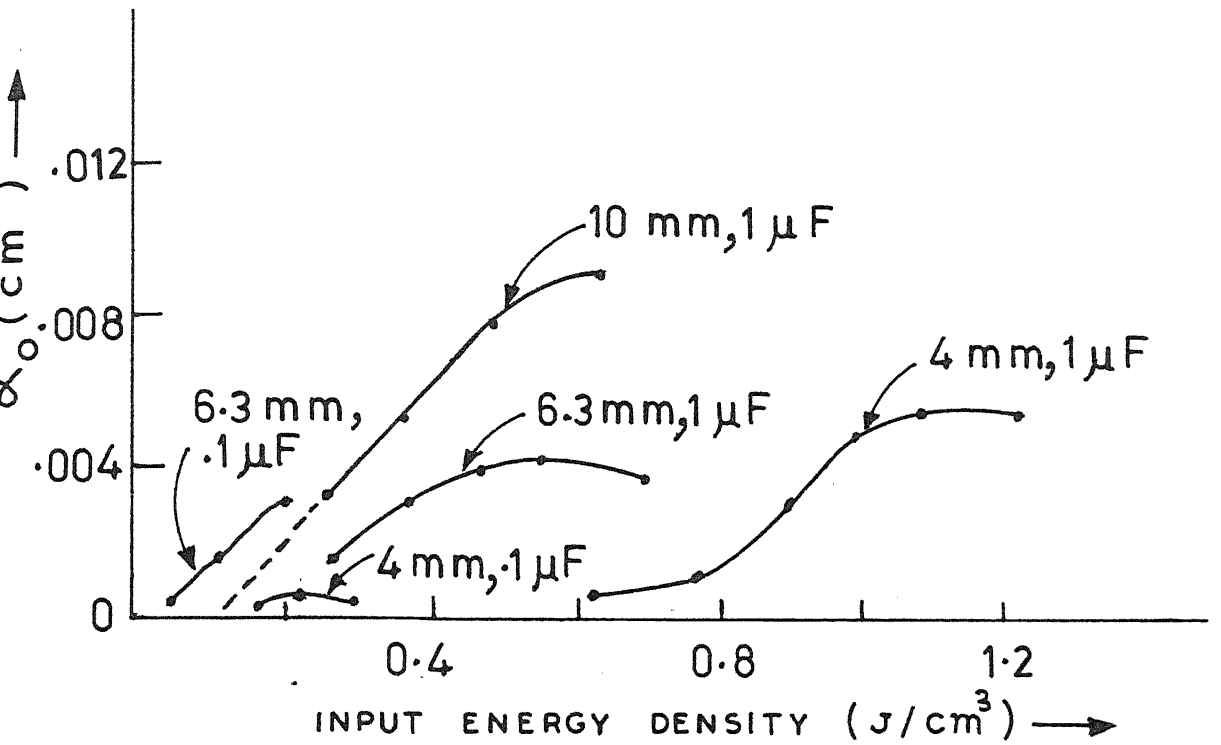

FIG. 4.7 α_o Vs INPUT ENERGY DENSITY.

ground state of the atom. However, if the field is too high, still higher-lying levels are preferentially excited at the expense of pumping into the desired levels. This will reduce the laser efficiency markedly unless cascade processes are prominent in inverting the population on these transitions. It is to be recalled that the gain coefficient is a direct measure of the population inversion present in the active medium.

These facts are substantiated by the observed variation of the laser output with electric field as shown in Figures 3.20-3.23. The same phenomenon can explain the observation that with smaller capacitors optimum gains are produced at lower values of input energy densities while smaller bore diameters require larger input energy density to reach their optimum operating condition. The latter behaviour, however, is also due to the fact that wall collisions play a significant role in quenching the excitation processes in this laser.

Finally, the observation that the smaller capacitance produces higher gains finds explanation in the fact that electrons with higher kinetic energy on the average are produced with these capacitors. For the same reason, the output efficiency of the laser will be higher for smaller capacitors as has already been discussed in Chapter 3.

With the 6.3 mm tube the variation of gain coefficient with pressure has also been studied and the data are presented

in Figures 4.8 and 4.9. As the pressure is increased beyond the optimum value the gain decreases. This can be due to the reduction in the cross-section for multiple ionisation at higher pressures. Further quantification of this behaviour is not possible at this stage for want of information on the spectroscopic properties of these transitions.

Table 4.1 lists the maximum unsaturated gains observed with different tubes. In each case these data have been obtained after optimising the operation of the laser with respect to the tube operating pressure and the excitation voltage. These results are consistent with the observed characteristics of the laser namely that the excitation processes are more efficient in larger bore diameter tubes while the operating pressures are lower and that electrons with appropriate kinetic temperature aid the excitation processes. The gain values observed in the present work are higher than those reported earlier in literature [43, 49], probably due to the optimisation of all the relevant parameters of the laser. Also, to our knowledge this is the only attempt to study the gain behaviour of the laser with respect to the different parameters of the discharge.

B. Saturation Behaviour

Equation (4.6) gives the dependence of the gain coefficient on intensity for the two limiting cases of (homogeneous and inhomogeneous) broadening. The data obtained

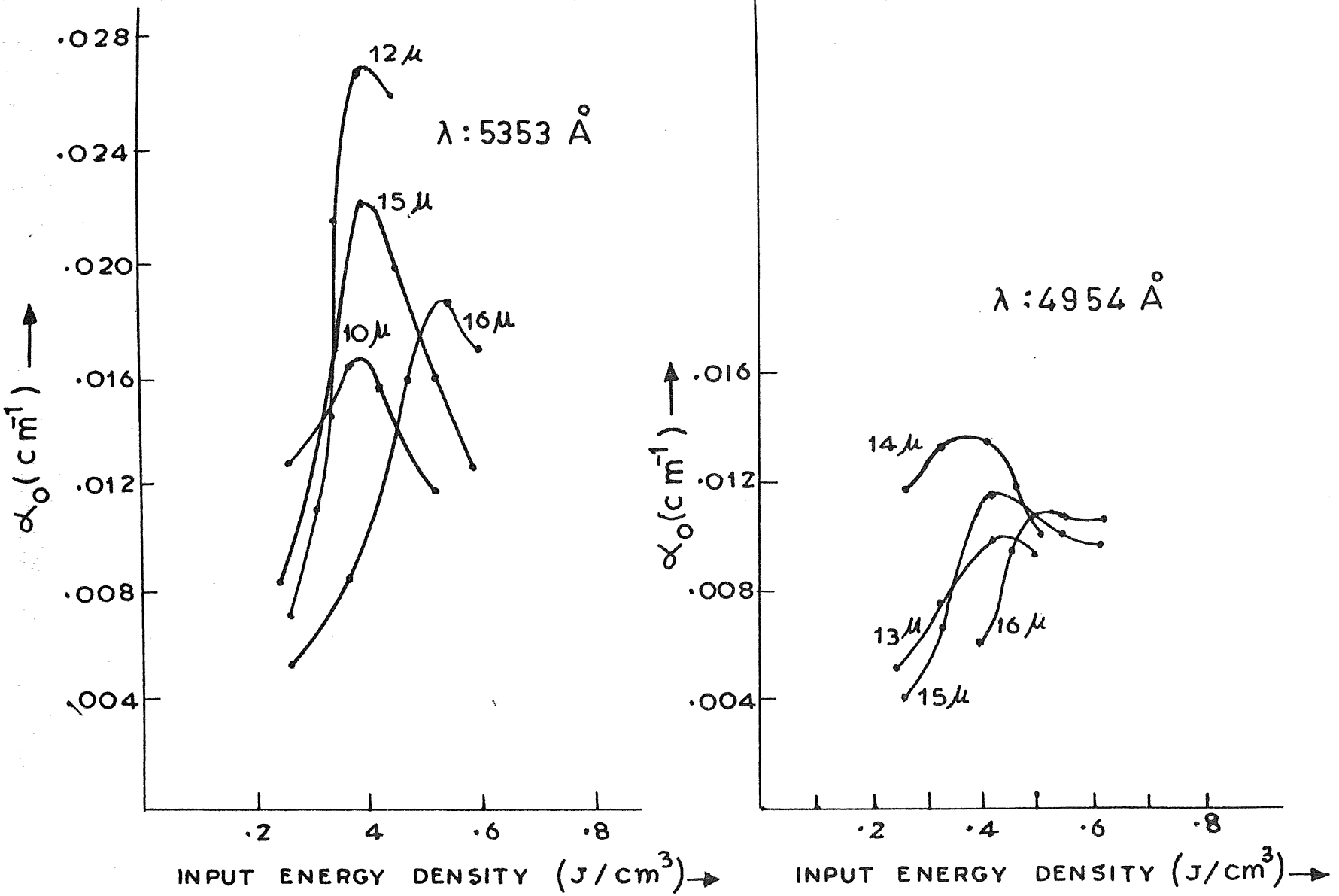

FIG. 4.8 α_o Vs INPUT ENERGY DENSITY.

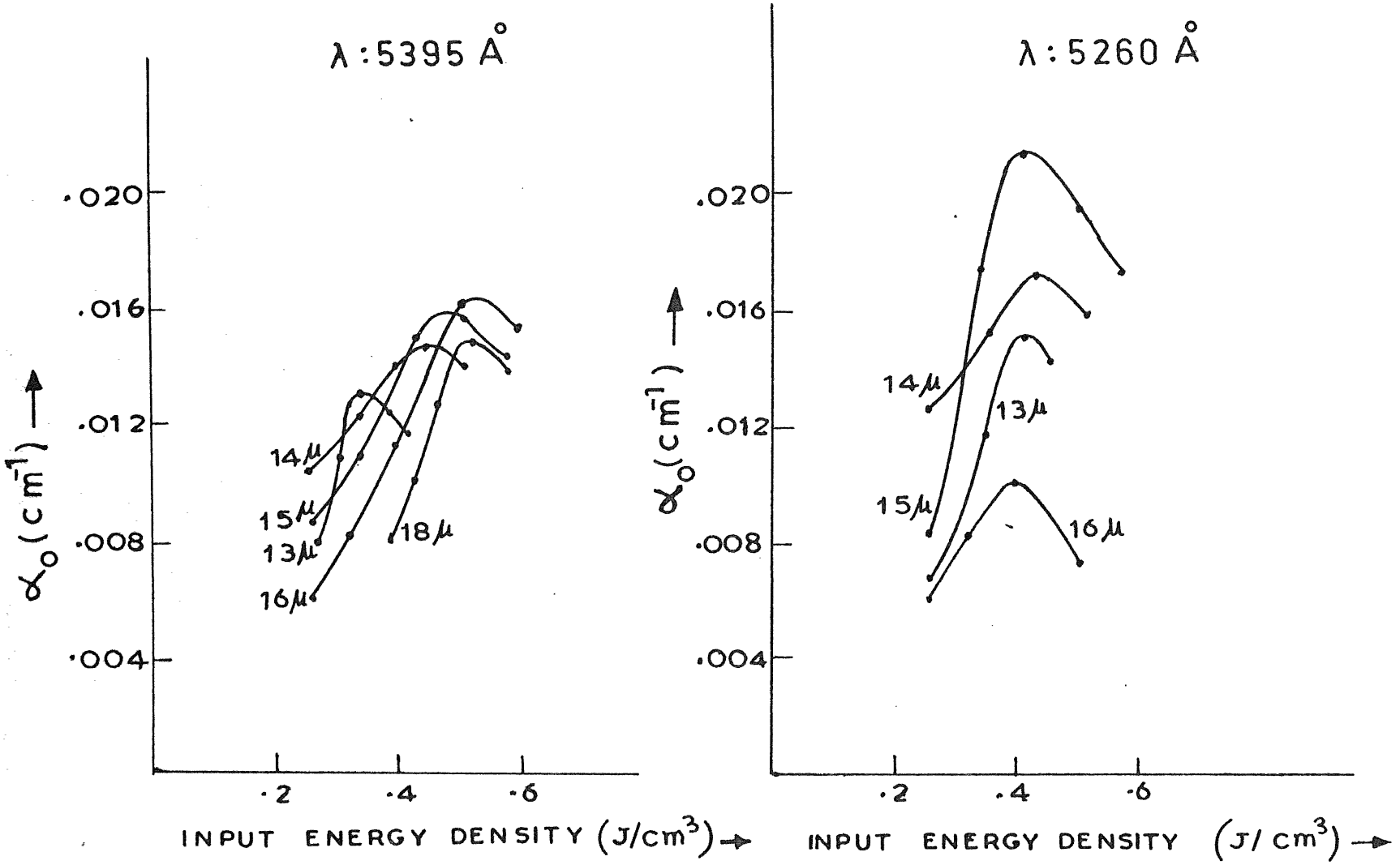

FIG. 4.9 α_o Vs INPUT ENERGY DENSITY AT DIFFERENT PRESSURES.

Table 4.1 : Maximum Threshold Gains at Different Wavelengths, in dB/m

Wavelength in Å	Tube Diameter, Capacitance					
	10 mm, 1μF	6.3 mm, 1μF	4 mm, 1μF	6.3 mm, .3μF	6.3 mm, .1μF	4 mm .1μF
4954.13	6.3	6.6	5.5	9.8	11.8	11.2
5007.8	2.0	3.8	3.8	3.8	4.0	4.0
5159.08	1.4	4.1	3.8	4.1	4.6	4.2
5260.19	4.0	9.6	3.7	5.8	9.3	6.9
5352.92	5.2	12.8	8.3	9.0	10.6	12.5
5394.62	5.1	8.0	6.9	7.4	6.9	5.5
5955.67	4.1	2.7	2.7	1.9	1.6	1.0

in the present work show a markedly different behaviour and attempts to fit into either of the two equations (4.6) or any other similar relation [74] have failed.

Figures 4.10 and 4.11 show the output power vs the excitation parameter η and the output power vs $\ln(\alpha_o/\alpha)$ plots for the 6.3 mm and the 10 mm tubes respectively. η is defined to be the ratio of the maximum unsaturated gain to the saturated gain while α_o and α are the corresponding gain coefficients. On comparing the output power vs η curves with the theoretical curves given in [73] it is seen that the behaviour is somewhat similar to that predicted for a single-mode laser, though in the present work the laser has not been operated single-mode.

One limitation in our data is the lack of sufficient information on the saturation behaviour at high intensities. Further, in the calculation of saturated gain coefficients it has been implicitly assumed that for these high gain transitions the laser intensity stabilises during the pulse to a value where the saturated gain just balances the cavity losses. The accuracy in the estimation of the saturated gain coefficient thus depends on how far this assumption is valid in short-pulse ($\lesssim 5\mu S$) lasers. However, it is seen that the output power at each wavelength is linearly dependent on the small-signal gain coefficient, as shown in Figure 4.12. This implies both a certain degree of saturation

compare remark on homogeneous broadening

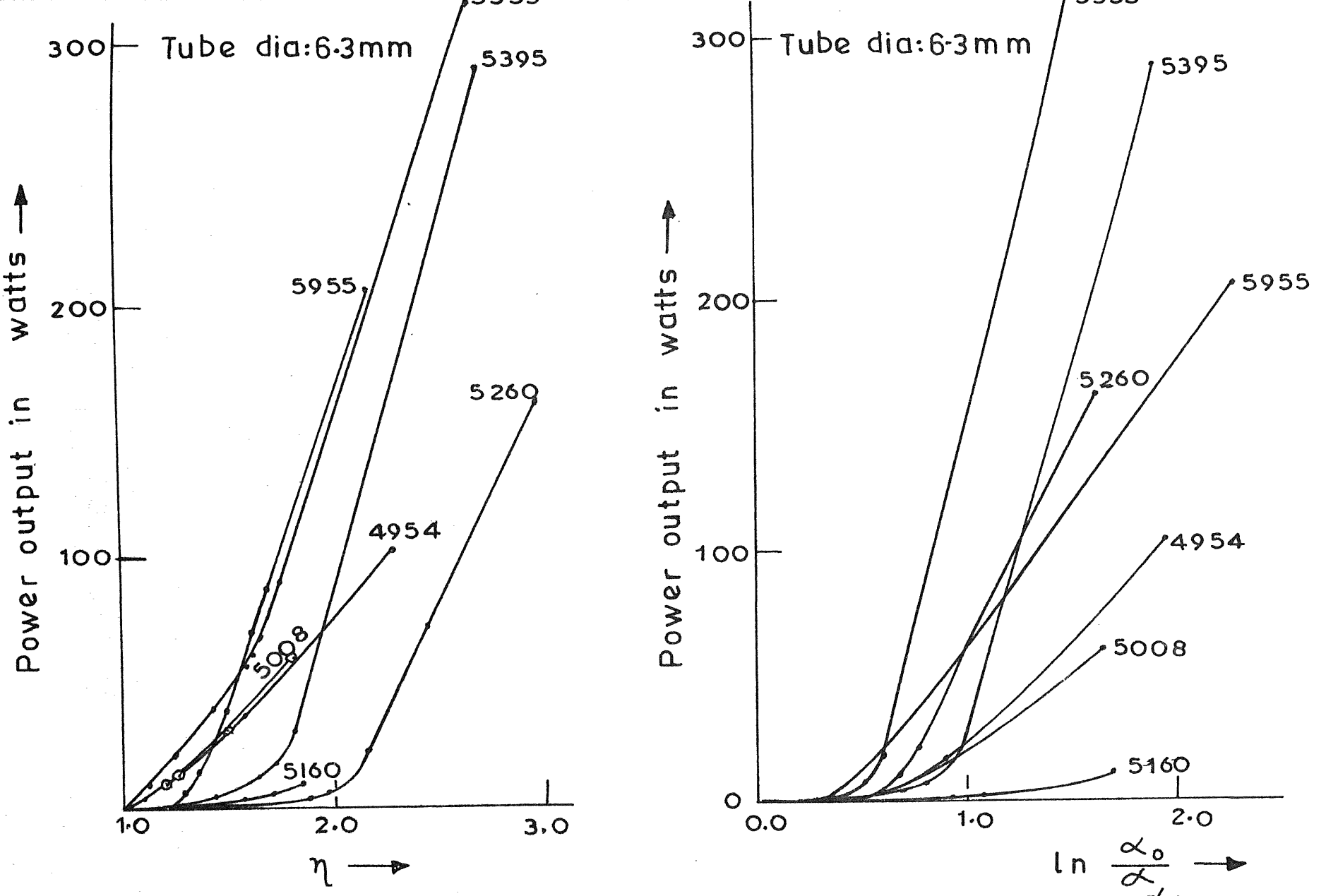

FIG. 4.10 a) Power output Vs η , b) Power output Vs $\ln \frac{\alpha_0}{\alpha}$

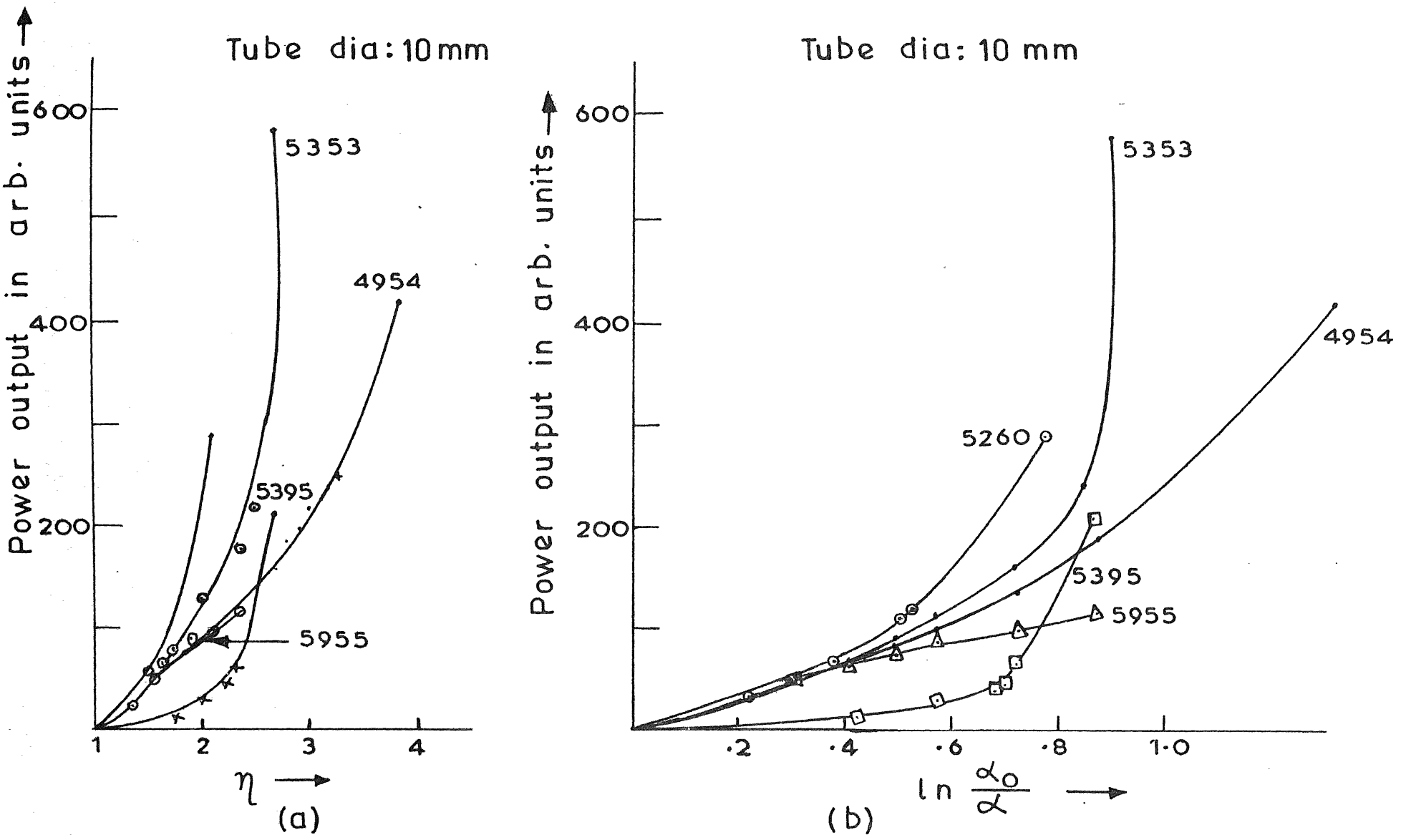

FIG. 4.11 a) Power output Vs η , b) Power output Vs $\ln \frac{\alpha_0}{\alpha}$

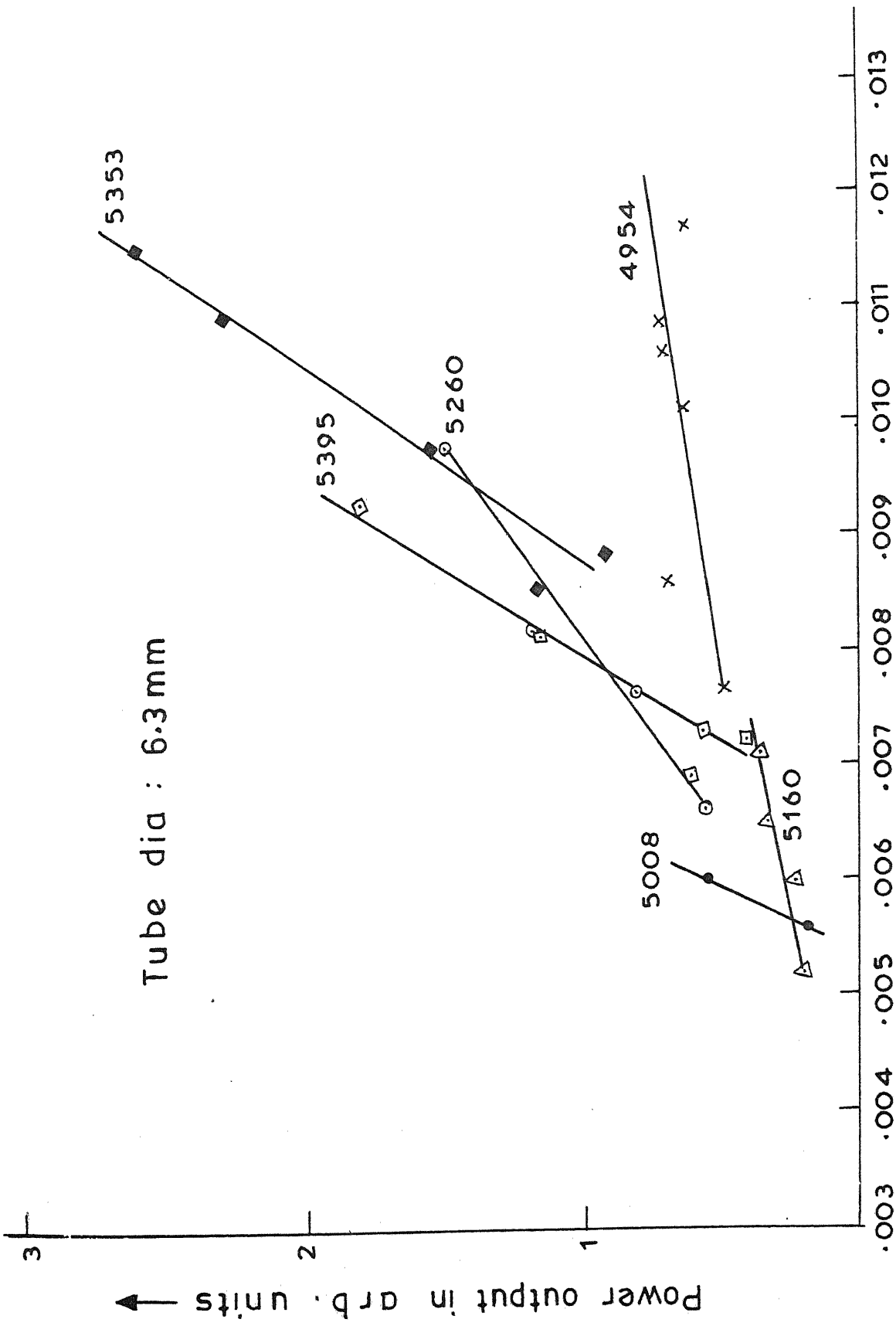

FIG. 4.12 POWER OUTPUT Vs α_o

as well as homogeneous broadening being operative in the gain medium [71, 31]. In addition, as this laser operates at extremely high current densities ($>5{,}000$ amps/cm^2), Stark effect can contribute significantly to the broadening of these transitions. The saturation behaviour of ion lasers under these conditions has not been analysed to our knowledge. This additional broadening mechanism might also be a reason why our data could not be fitted into a simple relation connecting the saturated gain and the power output. We are initiating experiments (as the follow-up programme to this work) to carry out the linewidth and lineshape measurements on these transitions with a view to understand the broadening mechanisms operative in this laser.

CHAPTER 5

EXCITATION MECHANISM

An attempt is made in this chapter to qualitatively discuss the excitation processes for the seven visible lasing transitions in the pulsed Xe IV laser mentioned in the earlier chapters.

The excitation mechanism of gaseous ion lasers in general involves various electron impact processes. The relative importance of any process in a particular case is decided by the different characteristic parameters of the discharge plasma like the electron energy distribution, the number densities and temperatures of neutral atoms, electrons and the various kinds of ions, the relevant cross-sections and the populations of the energy states involved etc.

Determination of these quantities requires exhaustive plasma diagnostic experiments which are difficult to perform and, in many cases, require in addition a suitable theoretical modelling of the plasma discharge to deduce the required parameters from the experimental observations. However, usually the populations of the upper and lower laser levels due to the different electron impact processes are determined by rate equations which results in a simple relation between the current density and the inversion produced in the medium [18,30,35]. Thus a knowledge of the variation of power output of the laser with current density coupled with some information on the plasma parameters can give a good idea of the excitation processes involved.

For transitions belonging to highly ionised species complications arise due to the fact that the populations of different kinds of ions do not show a simple dependence on current. Also, due to the large number of intermediate states present many competing processes are possible and the dominant excitation mechanism in a particular case is difficult to identify and is decided by the actual plasma conditions. Further, as these transitions usually lase in high current density discharges the resulting large self magnetic fields can be significant in determining the radial electron density distribution.

broadened, the authors attributed the excitation of the first pulse to a single-step process from the neutral atom ground state while that of the second pulse to a multi-step process. The cessation of the first pulse was tentatively attributed to radiation trapping but without any experimental evidence to support this.

Cheo and Cooper [44] have observed ring-shaped formation in the output beam at high currents for some of the transitions in Xe IV. Taking an analogy from the Argon transitions, the cause was attributed to resonance trapping of radiation from the lower laser level. However, later experiments by several workers have shown that even for Ar^+ laser transitions radiation trapping though present does not play the deciding role in quenching laser action either in pulsed or cw operation [76, 77,78]. At high current densities used in pulsed lasers the collisional effects are found to mask the radiation effects [77]. However, to our knowledge, no attempt has been made so far to understand the excitation mechanisms in short-pulse Xe IV lasers; these can be markedly different from the mechanisms operative in cw or quasi-cw operation.

In the present work an attempt has been made to understand the excitation processes in short-pulse Xe IV laser based on careful measurements of the output power dependence on current etc. We believe that our results are typical of a short-pulse laser. However, due to lack of spectroscopic data and other relevant information on the excitation cross-

sections for these transitions, the results could not be quantified further.

5.1 Experimental Details

At optimum conditions of pressure and current the laser pulse has shown a single peak for all wavelengths. At high pressure and current values (different for each transition) a second peak appears after the first. The laser operation under both the conditions has been investigated.

The laser pulse and the current pulse have been recorded using a boxcar integrator in the scan-gate mode with aperture time set at 10 nsec. The scan rate and the time base of the boxcar were adjusted to give a smooth curve at the output, which was recorded on a strip chart recorder.

As discussed in Chapter 3, the variation in multi-mode output power across the tube cross-section has shown that the inversion is present mainly near the centre of the tube. To investigate this further, a variable aperture was introduced in the cavity and for different experimental conditions the temporal variation of the laser output was recorded for different intracavity apertures.

The peak power output in each wavelength for different currents has been measured. For each case a polynomial of the following form has been fitted to the data using a least-squares fit computer program.

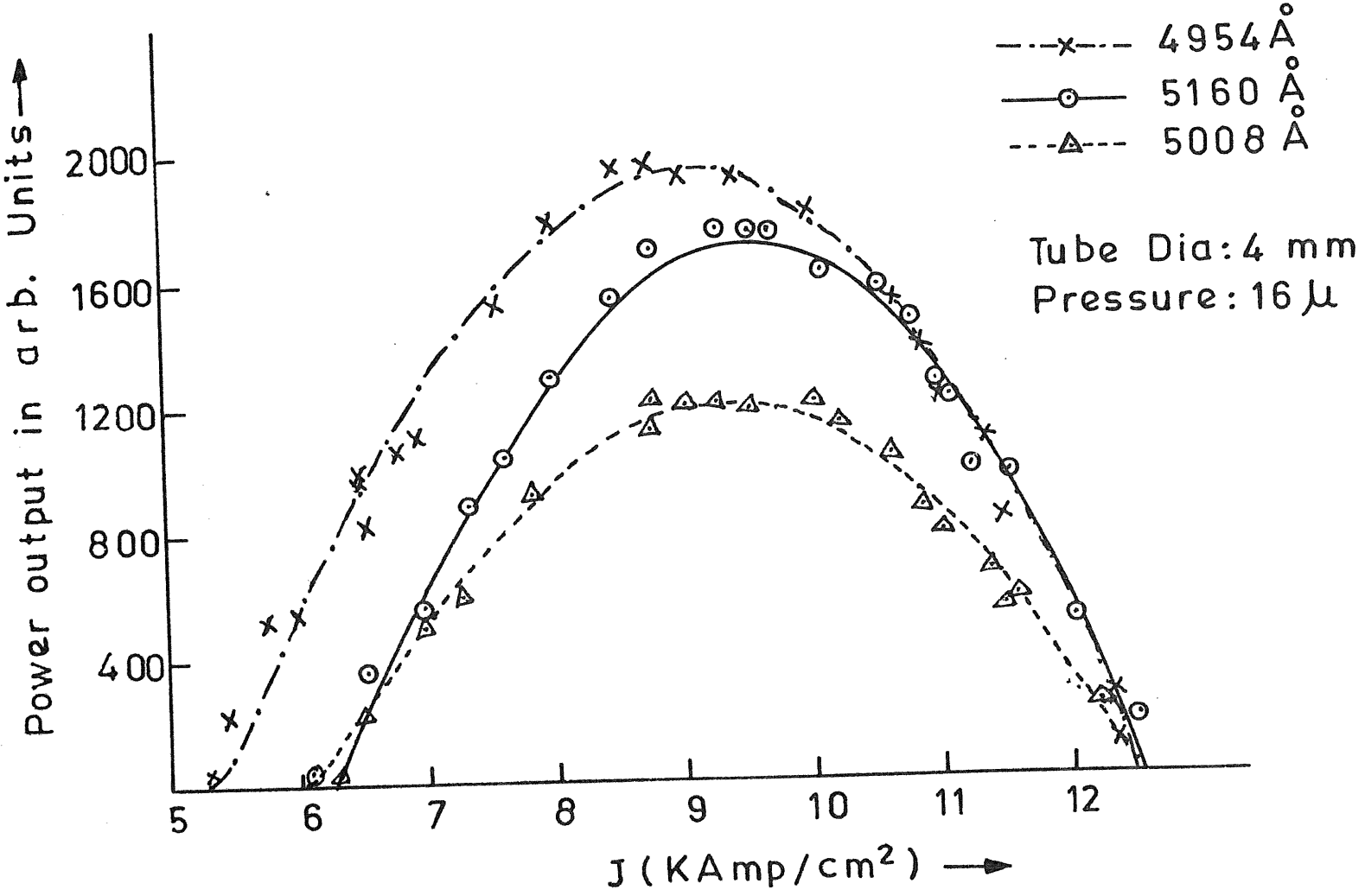

FIG.5.1 POWER OUTPUT Vs CURRENT DENSITY AT CONSTANT PRESSURE.

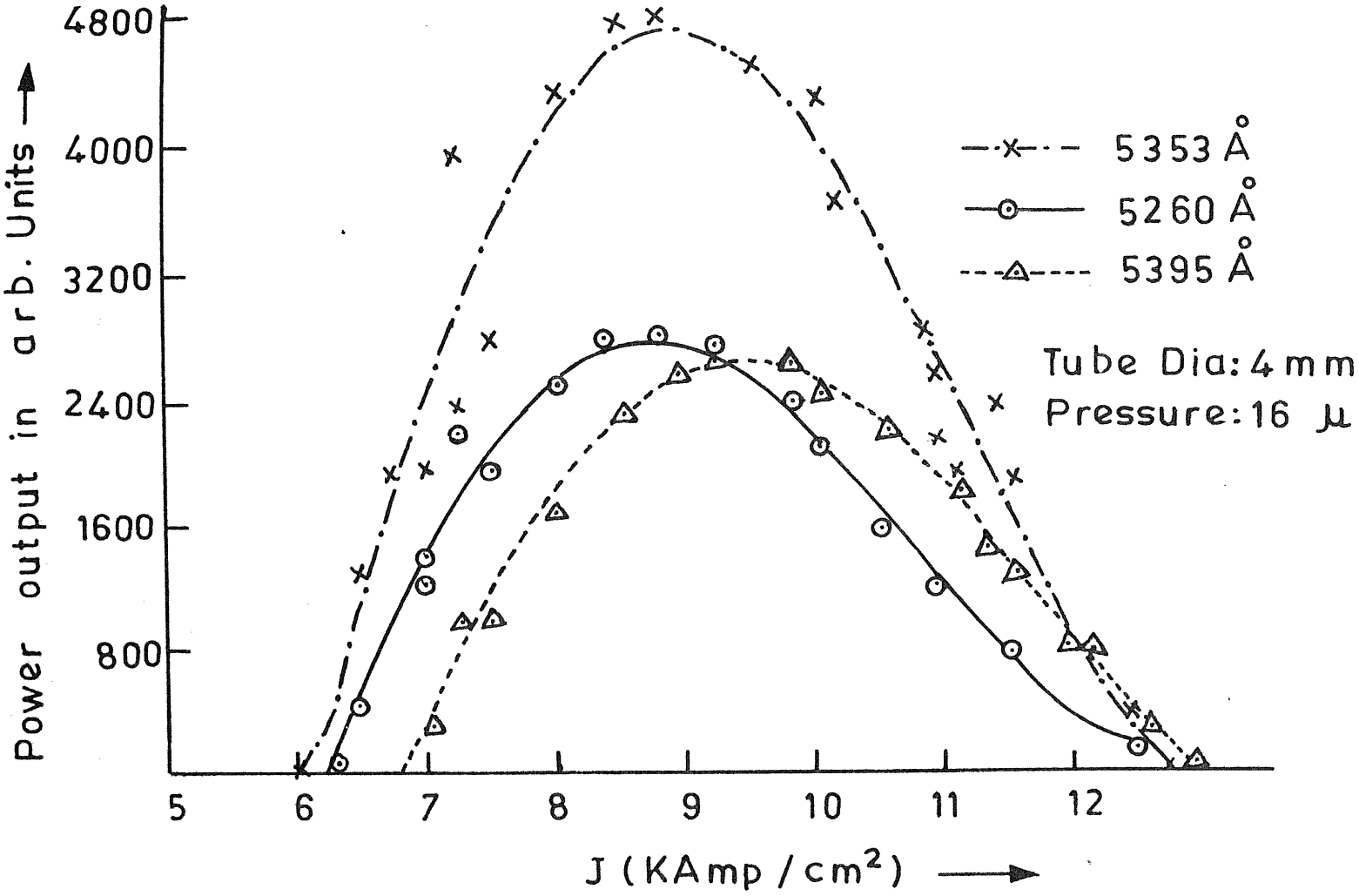

FIG.5.2 POWER OUTPUT Vs CURRENT DENSITY AT CONSTANT PRESSURE.

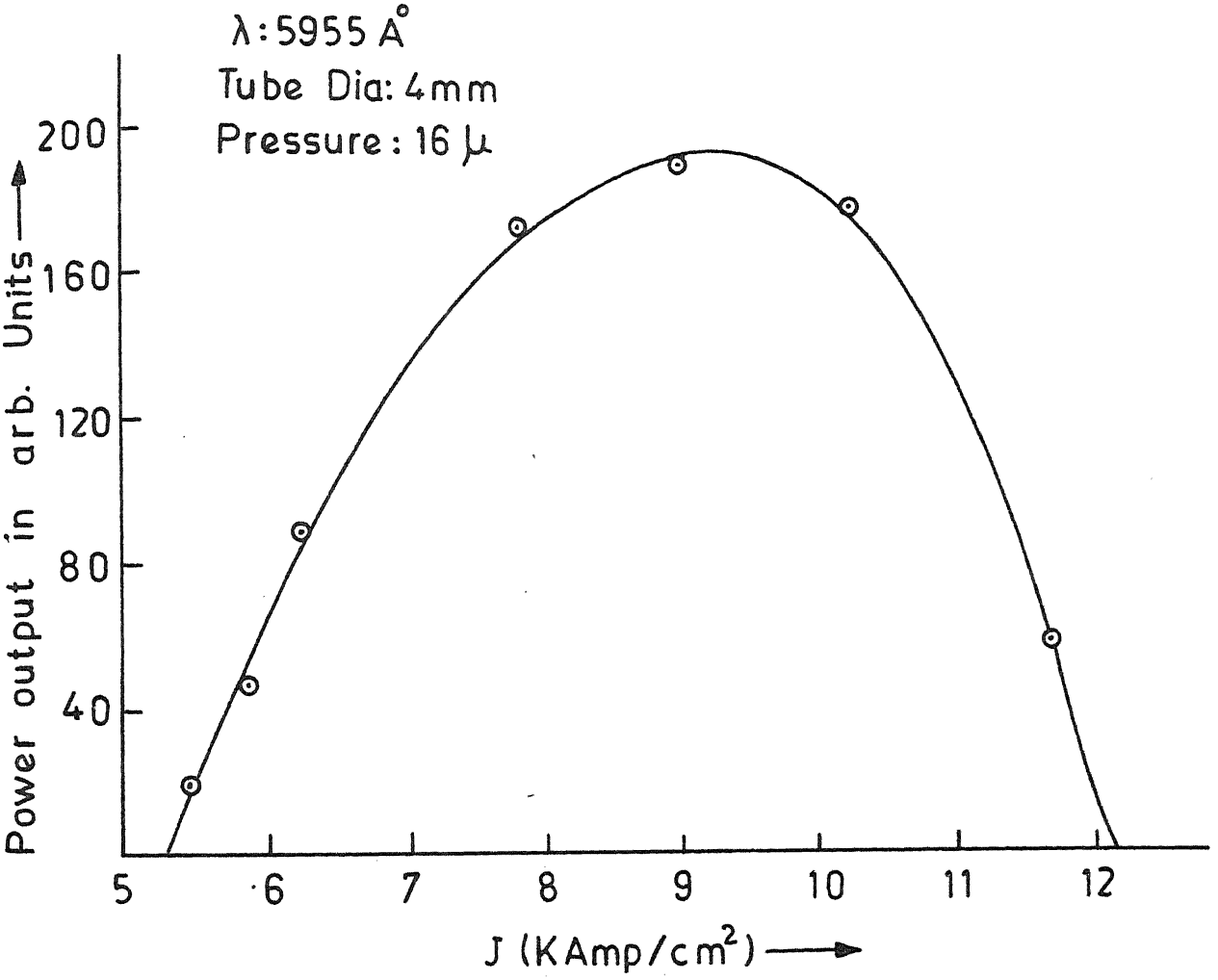

FIG.5.3 POWER OUTPUT Vs CURRENT DENSITY AT CONSTANT PRESSURE.

$$P_{out} = a_1 J + a_2 J^2 + \ldots + a_n J^n - a_{th}$$

where a_{th} is a threshold parameter, a's are multiplicative constants. n has been varied from 3 to 8 and the best fit polynomial selected. For all lines n = 4 has given the best fit. This data is reproduced in Figures 5.1 - 5.3. The lines indicate the best-fit computed curves while the points are the actual experimental data. The tube bore diameter is 4 mm, the energy storage capacitor used is 1 μF.

5.2 The Rate Equation Approach to the Problem

Let us consider a general energy level scheme as shown in Figure 5.4. Levels 5 and 4 are the upper and lower laser levels respectively, levels i with i = 1,2,3 are the intermediate levels participating in the excitation process and the level 0 is the neutral atom ground state, the reservoir level. The level j is representative of the high-lying levels from which levels 4 and 5 are populated through radiative cascade.

The main processes considered phenomenologically for excitation to any state are

a. electron collisions with the neutral atoms in ground state,

b. electron collisions with the atoms in excited or ionised states and

c. radiative cascade from higher excited states.

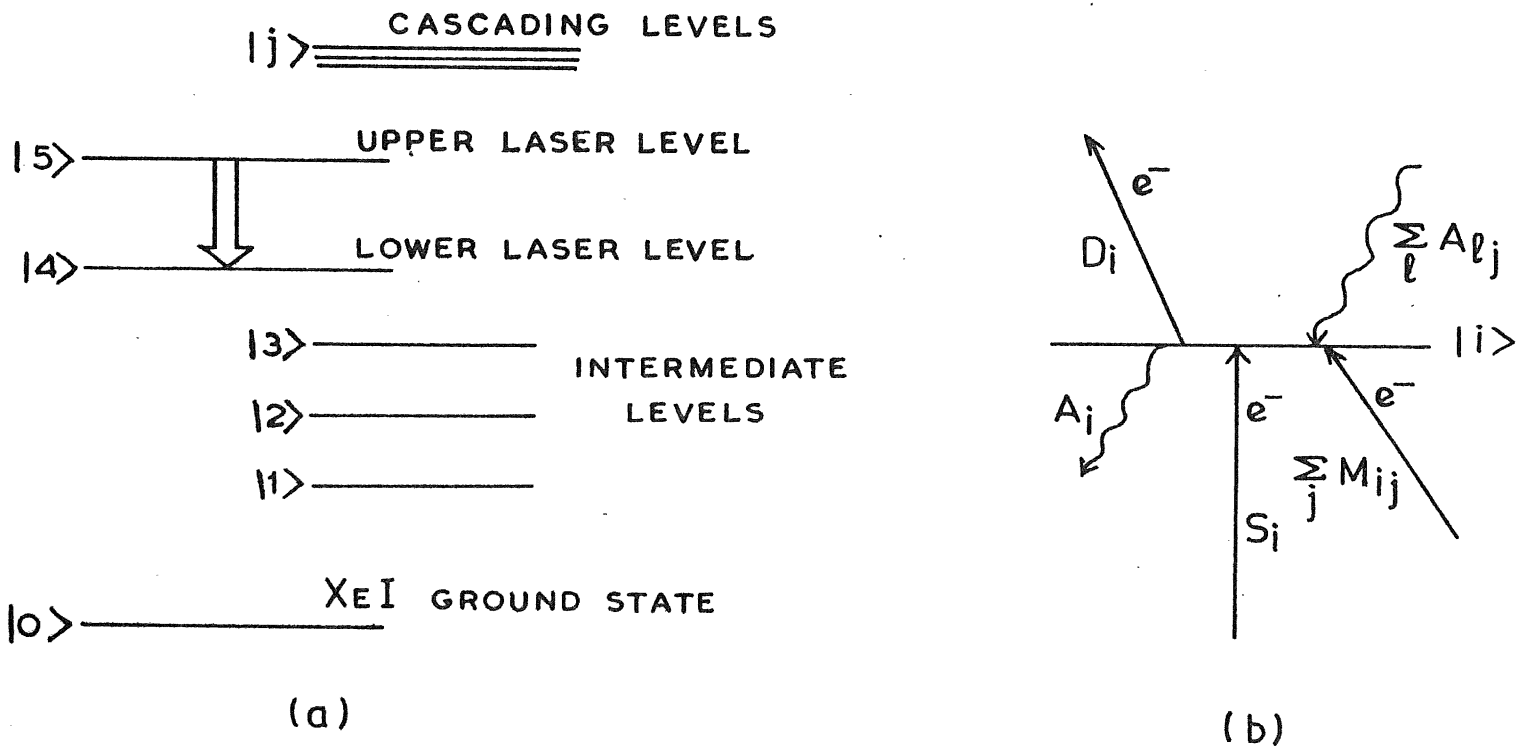

FIG. 5.4 GENERAL ENERGY LEVEL SCHEME FOR XENON

The deexcitation processes considered are radiative decay and electron collisions. Trapping of the radiation from the lower laser level is not considered important as we have not obtained any experimental evidence for it in our observations. This point has been discussed in a later section of this chapter.

Now, the rate equation for the population of any state i can be written as

$$\frac{dn_i}{dt} = - A_i n_i - D_i n_i n_e + S_i n_e n_o + \sum_k M_{ik} n_k n_e + \sum_j A_{ji} n_j \qquad (5.4)$$

where A_{ij} is the transition probability between levels i and j, $A_i = \sum_j A_{ij}$, D_i is the level destruction rate by electron collision, S_i and M_{ik} are the formation rates for the single-step and multi-step processes respectively. The term $\sum_j A_{ji} n_j$ represents the total contribution due to the radiative cascade from high-lying levels. For simplification, this term has been approximated to $r_i A_i n_i$, where r_i is the fraction of the total population of the ith level, in equilibrium, due to radiative cascade.

The rate equations have been solved to give the population inversion density present in the medium and the detailed solution is outlined in the appendix to this chapter. In obtaining the solution the following assumptions have been made:

i. In steady state, $dn_i/dt = 0$ for all i. This assumption is not rigorously true in the short-pulse case. However, for the transitions of our interest, it can be justified in the following manner. The gain exhibited by these transitions is high enough so that the oscillations in the cavity build up in a much shorter time compared to the duration of the laser pulse. In view of this the relevant matter-radiation interaction processes in the medium can be assumed to reach a quasi-equilibrium condition, justifying the assumption, $dn_i/dt \backsim 0$ in solving the rate equations.

ii. The population of the reservoir level has been assumed to be constant throughout, though it is not strictly justified in the present case. At high enough current density the depletion of the ground-state population can be quite significant, leading to a decrease in the excitation rate [37,79].

With these assumptions and some approximations as discussed in the appendix, the inversion density can be shown to be given by an equation of the form

$$\Delta n = C_1 n_e + C_2 n_e^2 + C_3 n_e^3 + C_4 n_e^4 \qquad (5.5)$$

The C's are defined in the appendix and depend on the rate coefficients.

The power output of the laser in the present case has been observed to be linearly proportional to the small-signal gain coefficient. This has been discussed in Chapter 4. In view of this, one can write

$$P_{out} \alpha \Delta n - (\Delta n)_{th} \qquad (5.6)$$

where Δn is the inversion present in the medium and $(\Delta n)_{th}$ is the threshold inversion density required to overcome the cavity etc. losses in the laser. Thus, if Δn is given by equation (5.5), the power output of the laser will be given by a polynomial of the form

$$P_{out} = K_1 n_e + K_2 n_e^2 + K_3 n_e^3 + K_4 n_e^4 - K_{th} \qquad (5.7)$$

where K's are multiplicative constants dependent on the constants C's in equation (5.5).

At the high current densities used in the present work, the self magnetic field produced can be significant. This field affects the plasma discharge properties by radially constricting (pinching) the current flowing through the discharge tube, thus increasing the current density near the tube axis. Thoneman and Cowhig [80] have shown that the self magnetic field of a high current discharge can reduce the radial electric field thus increasing the life of the positive ions and increasing the number of electron-ion collisions. To determine the presence of the pinch effect in a discharge, Gorog and Singer [81] have defined a dimensionless figure of merit K given by

$$K = 2.4 \times 10^4 \; t_o^2 \; J_o^2 / P_o A \qquad (5.8)$$

where P_o is the effective discharge pressure at 300^oK, t_o is the time taken for the current to reach its peak value I_o, $J_o = I_o/\pi R^2$ is the average current density at the peak of the current pulse and A is the atomic mass number.

For the discharge conditions used in the present work, the factor K turns out to be much less than 1 even at the lowest pressure and the highest current density used. According to Gorog and Singer a value of K less than 1 implies that the maximum compression of the discharge occurs after the first maximum of the magnetic field and the pinch effect becomes less signficant.

Papayoanou et al. [49] have studied laser action in a pinched Xe IV laser and have suggested that pinching occurs in a discharge when the value of $(I/R)^2$ exceeds 10^5 amp^2/mm^2 where R is the tube bore radius. The highest current values used in our experiments give the $(I/R)^2$ ratio around this value. From this we can conclude that though the pinch effect is present, it probably does not significantly affect the excitation process. Levinson et al. [37] have experimentally shown that the effect of the pinch in a multiply-ionised plasma is to make the electron density linearly proportional to the current density by smoothening out the step-wise variation in n_e due to successive ionisation.

Thus in the present case, n_e can be taken to be linearly dependent on J and the relation between the two can be written as

$$J = e \langle v \rangle n_e \tag{5.9}$$

Then the equation (5.7) can be rewritten in terms of the current density as

$$P_{out} = \alpha_1 J + \alpha_2 J^2 + \alpha_3 J^3 + \alpha_4 J^4 - \alpha_{th} \tag{5.10}$$

which is the final form of the equation used for curve fitting.

5.3 Results and Discussion

As shown in Figures 5.1 - 5.3 a fairly good fit has been obtained for the equation (5.10) with the experimental data. All lines show similar behaviour and the following general characteristics have been observed:

a. The coefficients of J and J^3 are negative while those of J^2 and J^4 are positive.

b. The relative contribution from the second term (αJ^2) is the largest, while that from the fourth term (αJ^4) is the smallest.

c. At low currents, the contribution from the first and the third terms are of nearly the same magnitude. At high currents the contribution from the third term increases till it becomes comparable to that from the second term.

d. The relative magnitude of the contribution from the fourth term increases with increasing current but even at the highest current it is only one-fourth of that from the second term.

The coefficient of the J term is seen from equations (A5.20) and (A5.24) to be proportional to $(\sigma_5 - \frac{g_5}{g_4}\sigma_4)$. This term will be negative if either $S_5 > S_4$ or $r_4 > r_5$, assuming $g_5 \backsim g_4$. That is, either the excitation rate through a single step excitation is higher for the lower laser level

or that the total cascade rate to the lower laser level is more. If the lower laser level is trapped it will decrease the effective A factor of the lower level and thus increase σ_4. However, our experimental observations have shown that radiation trapping is not significant in this case.

The coefficient of J^2 depends on two kinds of processes. One is a two-step excitation from the neutral atom ground state through an intermediate level. The second process depletes the level by electron collision. This coefficient has been experimentally observed to be positive and to play the major role in producing the inversion. This indicates that either the single-step excitation rates are much smaller than the multi-step excitation rates or that the collisional deexcitation rates are small. For the two-step excitation the intermediate states 1,2 and 3 can belong to any of the Xe I, Xe II, Xe III or Xe IV states. Considering the two mechanisms given by equations (5.1) and (5.2) it is more likely that the intermediate state is either a Xe III or a Xe IV state. However, the ionisation potentials of the different Xe species are 12.127, 21.1 and 32.1 eV respectively which means that the Xe III ground state is 33.327 eV above the neutral atom ground state while the Xe IV state is at 64.427 eV. For excitation to Xe IV states by a two-step process the intermediate state might be halfway in between the ground state and the laser levels. Thus it probably

belongs to Xe III though it need not necessarily be the Xe III ground state; thereby supporting the mechanism proposed by Bennett.

The J^3 term has a negative coefficient and becomes very prominent as the current increases, indicating that this is the main quenching process at high currents. The coefficient of J^3, as given by equations (A5.20) and (A5.24) depends on the three-step excitation rates and electron deexcitation rates of the two laser levels. The total coefficient will be negative if either the three-step process predominantly populates the lower laser level or if the electron deexcitation from the upper level is more significant. In the latter case, that is, if δ_p is large, σ_p must be small in order that the factor ($\delta_p^2\sigma_p$) is less than the negative terms.

The coefficient of J^4 depends again on rate coefficients for various processes. The different rate coefficients are such that the net effect is an increase in the inversion. However, this process is not as efficient in the short-pulse case as the main two-step excitation. As can be seen from equation (A5.20) both the four-step excitation and the two-step excitation coupled with collisional deexcitation of different levels contribute to the inversion process. The three-step excitation coupled with collisional deexcitation reduces the inversion. Increase in cascade transitions to

different levels can also increase the inversion. However, both the cascade transitions and the processes involving multiple collisions are 'delayed' processes and would be more effective only in the later part of the current pulse. An excitation process involving more number of collisions requires in addition, electrons of lower temperature. Thus, these secondary processes can produce inversion even when the excitation through the two-step process becomes less. We believe that these processes contribute to the double peak in the laser pulse, as discussed in the following section.

Double Peak Formation

It has been observed that as the pressure is increased from the optimum, the delay between the current pulse initiation and the laser pulse increases. This is shown in Figure 5.5. With the increase of pressure electron temperature decreases which reduces the rate of excitation by a two-step process. So it takes more time for the inversion to cross the threshold value. Equally well, the excitation is achieved by a multi-step process which is a delayed process; this explains the delay in the build-up of laser action.

At higher pressures as the current is increased, a second peak starts appearing after the main one. This peak increases in amplitude as the current/pressure are increased while the main peak decreases as the pressure is increased

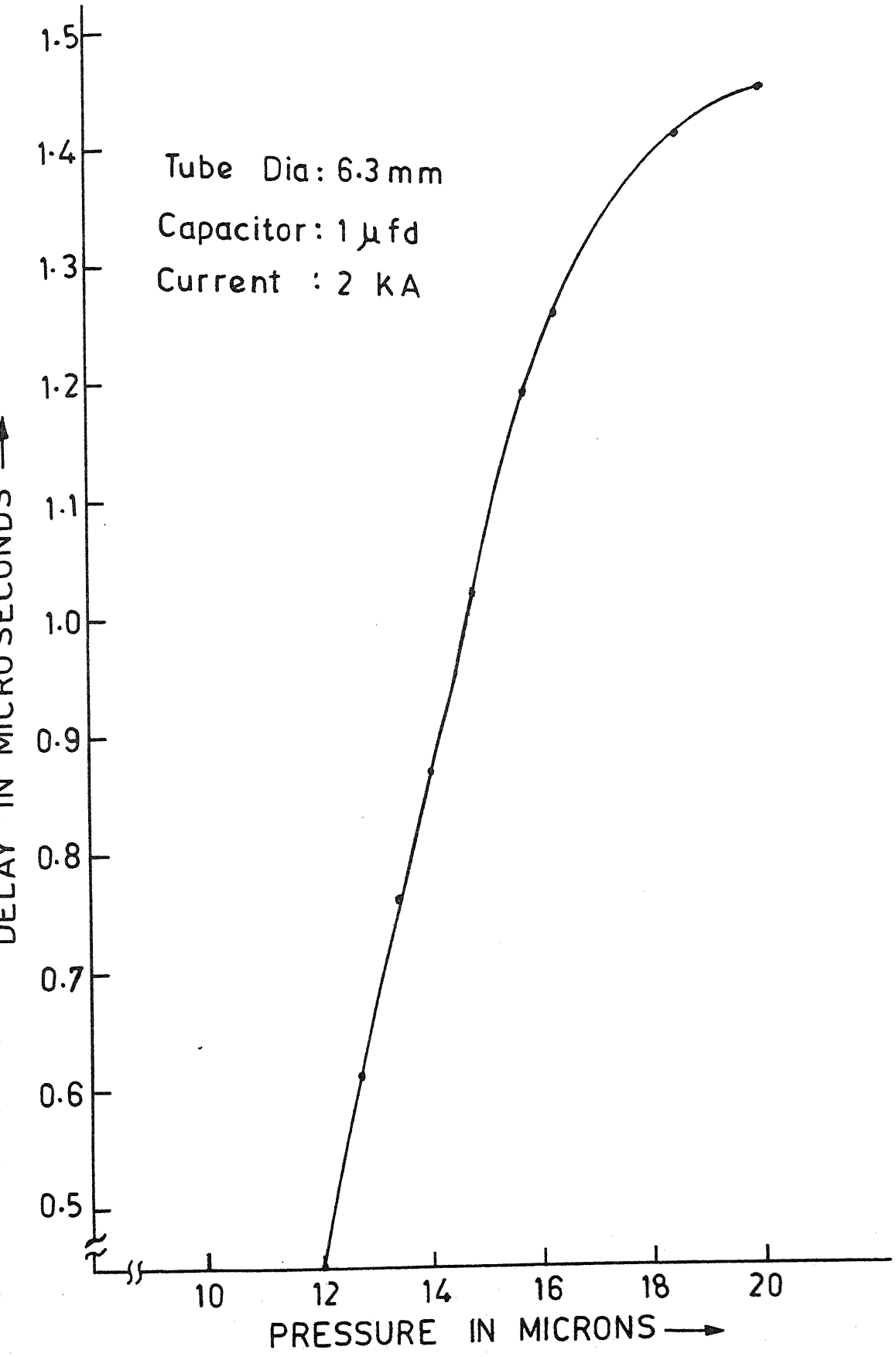

FIG.5.5 DELAY BETWEEN BEGINNING OF CURRENT AND LASER PULSES VS PRESSURE

from the optimum value. As discussed above, the inversion build-up for the main peak is mostly because of the J^2 term. At higher pressures, with the consequent lowering of the electron temperature, the efficiency of this two-step process will go down, resulting in the reduction of output power. However, other processes for example the process given by the J^4 term, might become more significant at lower electron temperatures and higher current densities. Since these mechanisms involve more number of collisions and cascade processes, the time taken for the inversion to build-up is longer than that needed for the two-step excitation. So the second peak is shifted and appears after the main peak. The cessation of the first peak is more probably due to quenching of the inversion by collisional deexcitation and not due to trapping of the radiation from the lower laser level.

These conclusions are further supported by the following observations:

(a) Figure 5.6 shows the variation in pulse shape with pressure for the transition at 5353Å. At the lowest pressure a faint peak is present in the rising edge of the current pulse, when the hottest electrons are present in the discharge. At lower pressures the electron temperature is higher. So this faint peak can be due to a single-step excitation from the neutral atom ground state. This mechanism is however, not very significant for the type of discharge excitation used in

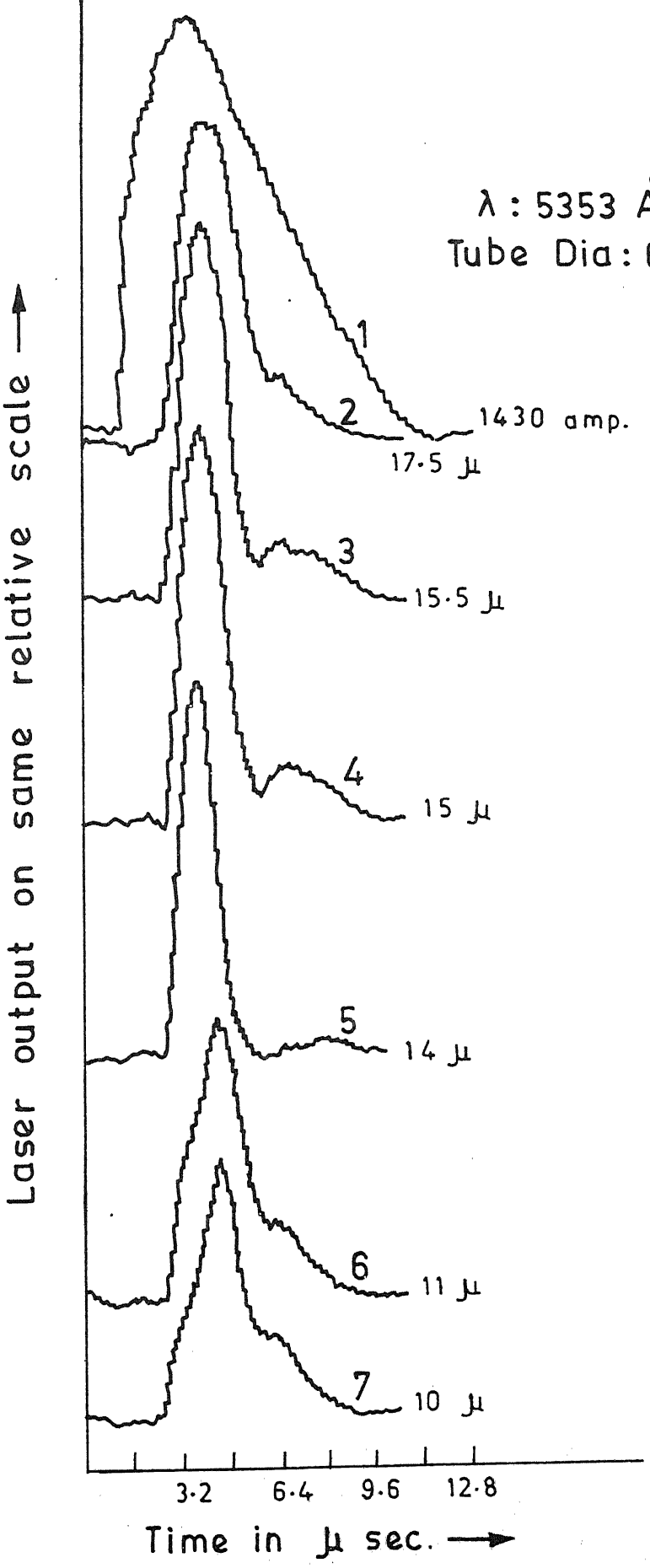

FIG.5.6 LASER PULSE SHAPE VARIATION WITH PRESSURE.
1 : Current pulse , 2-7 : Laser pulse.

the present work and this peak quenches as the pressure is increased slightly. The main peak increases as the pressure is increased towards the optimum and beyond that it starts decreasing. As the pressure is raised, another peak starts appearing in the falling edge of the current pulse. This peak first increases with increasing pressure and then decreases. The main peak is still present at the pressure where the third peak is quenched.

This indicates that radiation trapping cannot be the mechanism responsible for the double peak formation as in that case the main peak would be expected to continuously narrow down and the energy content in the third peak to increase as the pressure is increased. This has not been observed in the present case and the third peak is always observed to contain less energy than the main peak.

On the other hand, if the excitation in the third peak is ascribed to some cascade processes, the observed behaviour can be explained in the following way. At sufficiently low pressures, the number density may not be enough for the inversion produced inthis way to cross the threshold while at very high pressures the electron temperature may not be sufficient to excite the cascading levels efficiently. Obviously this mechanism is less efficient than that responsible for the main peak which explains the relative magnitude of the two peaks.

(b) For the transitions at 5395Å and 5260Å it was observed that at high pressures the laser pulse shows two peaks near the centre of the plasma tube. However, near the walls only the second peak is present. The magnitude of this second peak decreases as one moves away from the tube centre towards the walls. These observations can not be accounted for satisfactorily on the basis of radiation trapping. The observed behaviour can however be explained in the following manner. Near the walls the electron temperatures are lower and the direct (two-step) excitation process for producing the first peak is less efficient. However, some atoms which are excited to states higher than the upper laser level at the centre of the tube, can diffuse towards the walls and in time, either due to recombination at the walls or due to subsequent collisions, come down to the upper laser level, producing enough inversion for lasing to occur during the second peak.

(c) The radial variation for the double peak behaviour at high pressures and currents is very marked for the transition at 4954Å. To study this behaviour a variable aperture was inserted in the cavity and the laser pulse was recorded for different aperture diameters. This experiment was performed with the 6.3 mm tube and the results for two currents are shown in Figure 5.7. It is seen that at the higher current (Figure 5.7,a) the first peak does not lase at all with the minimum aperture and only the second peak is present.

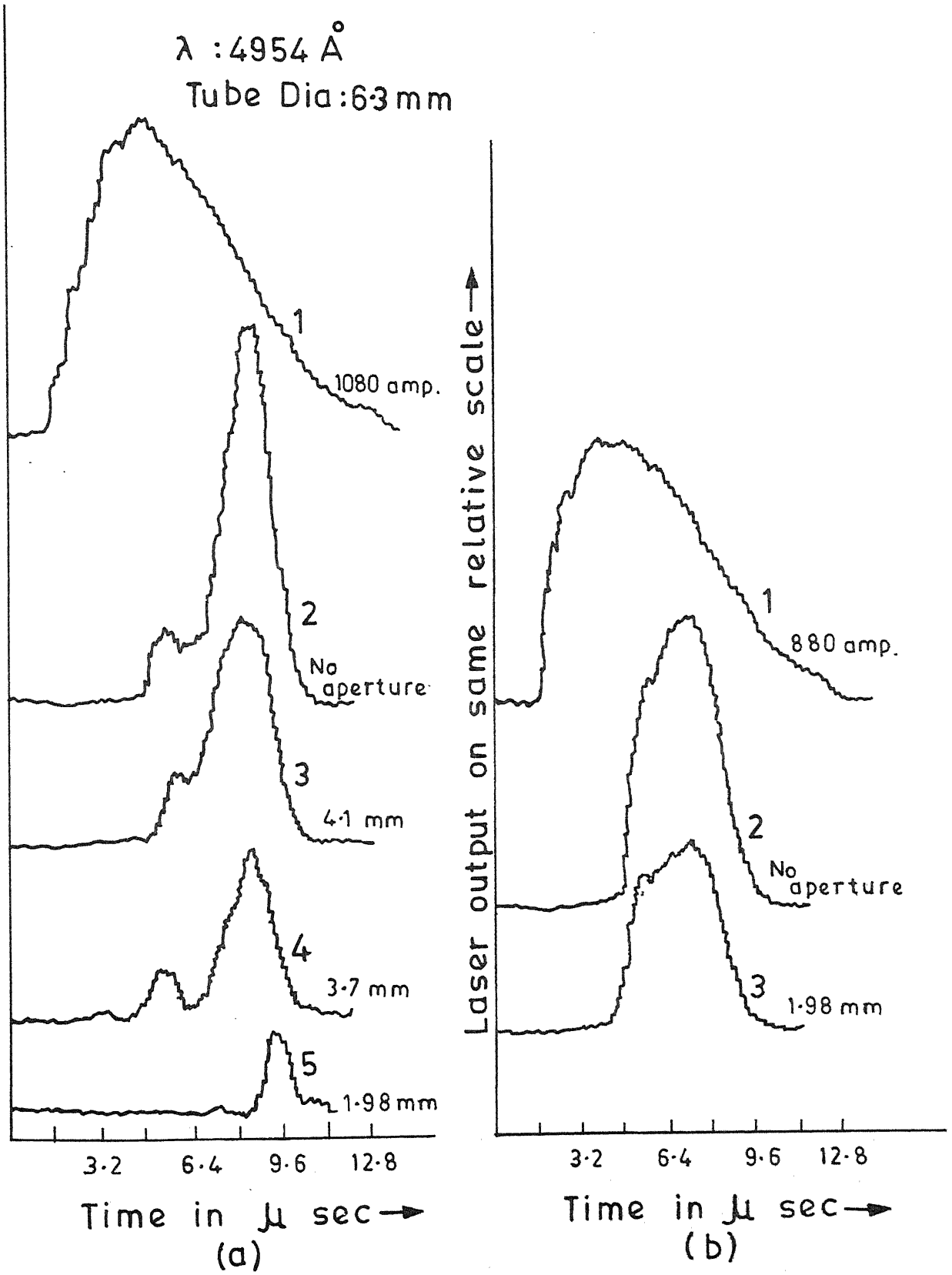

FIG. 5.7 EFFECT OF INTRA CAVITY APERTURE DIA ON LASER PULSE SHAPE
1: Current pulse, 2-5: Laser pulse

However, as the aperture is increased the first peak begins to appear though always smaller than the second one. This indicates that for this transition the radiative cascade processes are more significant than the direct excitation processes in producing inversion at high pressures and currents, at least during the initial phase and until after the peak of the current pulse. Under these conditions, at the centre of the tube, where the hottest electrons are present, the atoms are excited to high-lying levels during the initial part of the current pulse. In course of time, these atoms will cascade down to the upper laser level and thus produce inversion for lasing to occur. Away from the centre of the discharge tube the electron temperatures are lower and both the direct excitation and the cascade processes are possible, producing the two peaks as discussed earlier. It is to be noted that this transition has a markedly low excitation electric field threshold at lower pressures, (Figure 3.10) when direct excitation processes are more significant. Further, this line continues to lase even at very low pressures and input energy densities where other lines are quenched, indicating that it has the lowest inversion threshold/highest gain among this group of lines.

To summarise, the following conclusions have been arrived at regarding the excitation mechanism of the short pulse Xe IV laser:

i. The main excitation mechanism is a two-step electron collision process from the neutral atom ground-state to the upper laser level. The intermediate level probably belongs to Xe III though it is not necessarily the Xe III ground-state.

ii. At high pressures and currents, another excitation process becomes significant which involves a four-step excitation along with some cascade processes. This mechanism contributes to the double peak formation in the laser pulse.

iii. The quenching of the first peak in the laser pulse is probably due to collisional deexcitation of the upper laser level. Trapping of the radiation from the lower laser level does not necessarily play a significant role. On the other hand, collision and recombination at the walls of the plasma tube can quench the lasing.

iv. The effect of pinching in the discharge is not significant.

Further quantification of these results is not possible at this stage due to the lack of any relevant information about the transitions and the energy level scheme for this species (Xe IV).

APPENDIX

We consider the general energy level scheme shown in Figure 5.4(a). The different electron impact and radiative processes considered for population and depopulation of any level are shown in Figure 5.4(b). These are electron collisions with the atoms in the ground state, 0, electron collisions with the atoms in excited or ionised states shown by levels 1,2 and 3, radiative cascade from high lying levels like j, radiative decay and collisional deexcitation.

From equation (5.4) the rate equations for the populations of the three levels 1,2 and 3 can be written as,

$$\frac{dn_1}{dt} = - A_1 n_1 - D_1 n_1 n_e + S_1 n_o n_e + \sum_j A_{j1} n_j \qquad (A5.1)$$

$$\frac{dn_2}{dt} = - A_2 n_2 - D_2 n_2 n_e + S_2 n_o n_e + M_{21} n_1 n_e + \sum_j A_{j2} n_j \qquad (A5.2)$$

$$\frac{dn_3}{dt} = - A_3 n_3 - D_3 n_3 n_e + S_3 n_o n_e + \sum_{i=1}^{2} M_{3i} n_i n_e + \sum_j A_{j3} n_j \qquad (A5.3)$$

For any other level, p, which is populated from levels 0,1,2 and 3 through different processes, the rate equation is given by,

$$\frac{dn_p}{dt} = - A_p n_p - D_p n_p n_e + S_p n_o n_e + \sum_{i=1}^{3} M_{pi} n_i n_e + \sum_j A_{jp} n_j \qquad (A5.4)$$

The various coefficients A,D,S and M are defined in the text. As discussed there the term $\sum_j A_{ji} n_j$ can be approximated to $r_i A_i n_i$, hence the equations (A5.1)-(A5.4) reduce to the following:

$$\frac{dn_1}{dt} = -(1-r_1)A_1 n_1 - D_1 n_1 n_e + S_1 n_o n_e \qquad (A5.5)$$

$$\frac{dn_2}{dt} = -(1-r_2)A_2 n_2 - D_2 n_2 n_e + S_2 n_o n_e + M_{21} n_1 n_e \qquad (A5.6)$$

$$\frac{dn_3}{dt} = -(1-r_3)A_3 n_3 - D_3 n_3 n_e + S_3 n_o n_e + \sum_{i=1}^{2} M_{3i} n_i n_e \qquad (A5.7)$$

$$\frac{dn_p}{dt} = -(1-r_p)A_p n_p - D_p n_p n_e + S_p n_o n_e + \sum_{i=1}^{3} M_{pi} n_i n_e \qquad (A5.8)$$

Putting $dn_i/dt = 0$, justification for which has already been discussed in the text, the above equations give for different n_i,

$$n_1 = \frac{S_1 n_o n_e}{(1-r_1)A_1 + D_1 n_e} \qquad (A5.9)$$

$$n_2 = \frac{1}{A_2(1-r_2) + D_2 n_e}\left[S_2 n_o n_e + \frac{M_{21} S_1 n_o n_e^2}{A_1(1-r_1) + D_1 n_e}\right] \qquad (A5.10)$$

$$n_3 = \frac{1}{A_3(1-r_3) + D_3 n_e} \times$$

$$\left[S_3 n_o n_e + \frac{M_{31} S_1 n_o n_e^2}{A_1(1-r_1) + D_1 n_e} + \frac{M_{32} S_2 n_o n_e^2}{A_2(1-r_2) + D_2 n_e}\right.$$

$$\left. + \frac{M_{32} M_{21} S_1 n_o n_e^3}{(A_1\overline{1-r_1} + D_1 n_e)(A_2\overline{1-r_2} + D_2 n_e)}\right] \qquad \text{(A5.11)}$$

$$n_p = \frac{(S_p n_o + \sum_{i=1}^{3} M_{pi} n_i) n_e}{(1-r_p)A_p + D_p n_e} \qquad \text{(A5.12)}$$

Unless the electron number density is exceedingly large or the relevant level is metastable, one can assume for any level i,

$$D_i n_e < A_i(1-r_i)$$

Then using Binomial expansion one can write,

$$\frac{1}{D_i n_e + A_i(1-r_i)} = \frac{1}{A_i(1-r_i)}\left[1 + \frac{D_i n_e}{A_i(1-r_i)}\right]^{-1}$$

$$= \frac{1}{A_i(1-r_i)} \sum_{n=o}^{\infty} (-\delta_i n_e)^n \qquad \text{(A5.13)}$$

where $\delta_i = \dfrac{D_i}{A_i(1-r_i)}$

Through similar substitutions, viz.,

$$\frac{S_i}{A_i(1-r_i)} = \sigma_i \text{ and } \frac{M_{ij}}{A_i(1-r_i)} = \mu_{ij}$$

and using equation (A5.13), the expressions for the populations of the various levels can be written as,

$$n_1 = n_o\sigma_1\Big[\sum_n (-\delta_1 n_e)^n\Big]n_e \qquad \text{(A5.14)}$$

$$n_2 = n_o\sigma_2\Big[\sum_n (-\delta_2 n_e)^n\Big]n_e + \mu_{21}\sigma_1 n_o\Big[\sum_n (-\delta_2 n_e)^n\Big]\Big[\sum_n (-\delta_1 n_e)^n\Big]n_e^2 \qquad \text{(A5.15)}$$

$$n_3 = n_o\sigma_3\Big[\sum_n (-\delta_3 n_e)^n\Big]n_e + \sum_{i=1}^{2}\Big[\mu_{3i}\sigma_i n_o\Big(\sum_n - \overline{\delta_3 n_e}^n\Big)\Big(\sum_n - \overline{\delta_i n_e}^n\Big)\Big]n_e^2 + \mu_{32}\mu_{21}\sigma_1 n_o\Big[\sum_n (-\delta_3 n_e)^n\Big]\Big[\sum_n (-\delta_2 n_e)^n\Big]\times\Big[\sum_n (-\delta_1 n_e)^n\Big]n_e^3 \qquad \text{(A5.16)}$$

$$n_p = n_o\sigma_p\Big[\sum_n (-\delta_p n_e)^n\Big]n_e + \sum_{i=1}^{3}\mu_{pi} n_i\Big[\sum_n (-\delta_p n_e)^n\Big]n_e \qquad \text{(A5.17)}$$

Substituting in equation (A5.17) for n_1, n_2 and n_3 from equations (A5.14) - (A5.16) we get for the 'normalised' population density in level p,

$$\frac{n_p}{n_o} = \sigma_p n_e + (\mu_{p1}\sigma_1 - \delta_p\sigma_p)n_e^2 + [\mu_{p2}\mu_{21}\sigma_1 + \mu_{p3}\mu_{31}\sigma_1$$

$$+ \mu_{p3}\mu_{32}\sigma_2 - \sum_{i=1}^{3} (\mu_{pi}\sigma_i\delta_p) + \delta_p^2\sigma_p]n_e^3$$

$$+ [\mu_{p3}\mu_{32}\mu_{21}\sigma_1 - \sum_{i=2}^{3} \sum_{\substack{j=1 \\ i\neq j}}^{2} \mu_{pi}\mu_{ij}\sigma_j(\delta_p+\delta_i+\delta_j)$$

$$+ \sum_{i=1}^{3} \mu_{pi}\sigma_i(\delta_p^2 + \delta_i^2 + \delta_p\delta_i)]n_e^4$$

$$+ \text{----------} \qquad \text{(A5.18)}$$

The population inversion density present in the gain medium is given by

$$\Delta n = n_5 - \frac{g_5}{g_4} n_4 \qquad \text{(A5.19)}$$

Making p equal to 5 and 4 respectively in equation (A5.19) one can obtain the expression for the inversion density as follows,

$$\frac{\Delta n}{n_o} = (\sigma_5 - \frac{g_5}{g_4}\sigma_4)n_e + [(\mu_{51}\sigma_1 - \frac{g_5}{g_4}\mu_{41}\sigma_1) - (\delta_5\sigma_5 - \frac{g_5}{g_4}\delta_4\sigma_4)]n_e^2$$

$$+ [(\mu_{52}\mu_{21}\sigma_1 - \frac{g_5}{g_4}\mu_{42}\mu_{21}\sigma_1) + (\mu_{53}\mu_{31}\sigma_1 - \frac{g_5}{g_4}\mu_{43}\mu_{31}\sigma_1) + (\mu_{53}\mu_{32}\sigma_2 - \frac{g_5}{g_4}\mu_{43}\mu_{32}\sigma_2) - \sum_{i=1}^{3} \sigma_i(\mu_{5i}\delta_5 - \frac{g_5}{g_4}\mu_{4i}\delta_4) + (\delta_5^2\sigma_5 - \frac{g_5}{g_4}\delta_4^2\sigma_4)]n_e^3$$

$$+ \left[\left(\mu_{53} - \frac{g_5}{g_4}\mu_{43}\right)\mu_{32}\mu_{21}\sigma_1 \right.$$

$$- \sum_{i=2}^{3} \sum_{\substack{j=1 \\ i\neq j}}^{2} \left(\mu_{5i}\mu_{ij}\sigma_j \sqrt{\delta_5 + \delta_i + \delta_j} \right.$$

$$\left. - \frac{g_5}{g_4}\mu_{4i}\mu_{ij}\sigma_j \sqrt{\delta_4 + \delta_i + \delta_j}\right)$$

$$+ \sum_{i=1}^{3} \left(\mu_{5i}\sigma_i \sqrt{\delta_5^2 + \delta_i^2 + \delta_5\delta_i} \right.$$

$$\left. \left. - \frac{g_5}{g_4}\mu_{4i}\sigma_i \sqrt{\delta_4^2 + \delta_i^2 + \delta_4\delta_i}\right)\right] n_e^4$$

$$+ \text{---------} \qquad \text{(A5.20)}$$

which when written as a polynomial in n_e

$$\Delta n = C_1 n_e + C_2 n_e^2 + C_3 n_e^3 + C_4 n_e^4 + \text{-------} \qquad \text{(A5.21)}$$

From equation (5.6), the power output of the laser is given by,

$$P_{out} \alpha (\Delta n - \Delta n_{th}) \qquad \text{(A5.22)}$$

where Δn_{th} is the threshold inversion density which depends on the cavity losses etc. However, as discussed in the text, the current density J is linearly proportional to n_e so that using equations (A5.21) and (A5.22), the power output can be written as,

$$P_{out} = \text{constant} \times (C_1 J + C_2 J^2 + C_3 J^3 + C_4 J^4 + \text{---} - \Delta n_{th}) \qquad \text{(A5.23)}$$

The proportionality constant absorbs all the parameters like the average electron velocity in the discharge, the transition properties, mirror transmission coefficients, volume of the active medium etc. From the data obtained experimentally in the present work, it has been found that a polynomial of fourth degree in J gives the best fit. Therefore, terms of order higher than J^4 are neglected in equation (A5.23) and we write,

$$P_{out} = \text{constant} \times (C_1 J + C_2 J^2 + C_3 J^3 + C_4 J^4 - \Delta n_{th})$$

which can be recast as

$$P_{out} = \alpha_1 J + \alpha_2 J^2 + \alpha_3 J^3 + \alpha_4 J^4 - \alpha_{th} \qquad (A5.24)$$

The different coefficients α_i of equation (A5.24) obtained from the present experimental data are presented in the Table A5.1.

As the electron number density, n_e, is increased beyond a certain value, the assumption $D_i n_e < A_i(1-r_i)$ is no longer valid. However, by the time this value of n_e is reached, depletion of ground state atoms by electron collisions also begins to be significant. Then the population in the reservoir level can no longer be assumed to be constant. All the rate equations are now coupled through n_o and analytical solution of this problem becomes difficult. This situation has not been considered in the present analysis.

Table A5.1 : The Coefficients, α_i, for Different Wavelengths

Tube-bore Diameter : 4 mm
Energy Storage Capacitor : 1μF

Wavelength in Å	α_1	α_2	α_3	α_4
4954.13	-1.84	.65	- .06	.002
5007.8	-1.62	.49	- .04	.001
5159.08	-2.13	.66	- .06	.001
5260.19	-5.79	2.39	- .25	.008
5352.92	-9.52	3.31	- .33	.01
5394.62	-6.13	2.13	- .21	.007
5955.67	-3.24	3.24	- .16	.003

CHAPTER 6

EFFECT OF AXIAL MAGNETIC FIELDS

This chapter discusses the effect of an externally applied axial magnetic field in a short-pulse Xe IV laser. Axial magnetic fields affect the laser output both by changing the plasma parameters as well as by Zeeman splitting the lasing transition into two sets of left and right circularly polarised components. In a cavity employing Brewster windows this splitting causes the output light to become elliptically polarised. It further induces Faraday rotation near the transition frequency. In the present work an attempt has been made to study the variation in laser output due to effect of the magnetic field on plasma parameters. The polarisation characteristics of the output from a laser

using Brewster windows have also been studied by measuring the Faraday rotation and ellipticity of the output radiation.

For ion lasers operating cw the laser output has been found to be considerably enhanced on application of an external magnetic field. In pulsed operation the magnitude of the effect observed depends strongly on the operating conditions of the laser discharge. In all cases, at sufficiently high fields, the laser output decreases so that there is an optimum value of the field to be used for obtaining maximum output. This optimum field is, in general, smaller for pulsed operation than that for cw operation and further depends on tube diameter, gas pressure and discharge current. It also depends on whether a polarisation selecting element (e.g. a Brewster window) is used in the laser cavity.

The influence of magnetic field decreases with increasing pressure, discharge current and tube diameter and is greatest when the laser is operating near its threshold. All these conclusions are mainly based on studies performed on the Ar^+ laser [22,60,87,18]. Very few studies have been reported on the Xenon and Krypton ion lasers. However, the Xe II and Kr II transitions have been observed to be more critically dependent on the magnetic field and have lower values of optimum fields, presumably because of their lower ion mobility [22].

In pulsed operation the enhancement in the laser output is found to be not as marked as in the cw case and further varies from transition to transition. For example, in the pulsed Ar^+ laser it has been reported [84] that the output in the transition at 4954A shows an increase at low currents but a decrease at higher currents on application of magnetic field. The output in the other lines, however, showed an enhancement at all currents.

For the pulsed Xe IV laser Ames [66] has studied the effect of external magnetic fields. However, in that work only the variation of the all-line output power was reported and it was not specified whether Brewster windows were used in the laser. Further, it is difficult to appreciate the need of fields as high as are reported in his study. For a 6.3 mm tube, the optimum field value obtained by him at optimum pressure (3.3μ) was around 100 G while at lower pressures it was found to be more than 680 G. On the other hand, in the only report on cw operation of this laser, Bridges and Mercer have indicated that with a 2.3 mm diameter tube, fields used near threshold of operation were around 700 G [41].

6.1 Variation in Power Output due to Plasma Effects

The externally applied magnetic field can change the discharge parameters like the number density distribution,

the electron temperature etc. and thus affect the excitation processes. Theories of low pressure plasmas in magnetic fields have been given by Tonks and Langmuir [88,89], Forrest and Franklin [57,58] and others. Though these theories have been proposed for singly-ionised plasmas, the qualitative behaviour of a multiply-ionised plasma would probably be explained by similar theories. The results of these theories are briefly outlined below.

When an axial magnetic field is applied to a plasma, the electrons move along the discharge axis in spiral paths of average radius, $\bar{\gamma}_M$, given approximately by

$$\bar{\gamma}_M = 2.4(kT_e)^{\frac{1}{2}} B^{-1} \qquad (6.1)$$

where kT_e is in electron volts and B is in Gauss. If $\bar{\gamma}_M$ is smaller than the discharge tube radius then the electrons will move out towards the tube walls by diffusion across the field lines. In the presence of magnetic field, the electron diffusion coefficient is given by

$$D_e = \frac{D_{eo}}{1 + \omega^2 \tau_e^2} \qquad (6.2)$$

D_{eo} is the diffusion coefficient in the absence of magnetic field, ω is the electron cyclotron frequency and τ_e is the mean free time between electron collisions.

The change in electron number density distribution depends solely on the factor δ_M given by

$$\delta_M = \delta^* = \frac{kT_e}{2ZM_i D_e} \qquad (6.3)$$

where Z is the ionization rate and M_i is the mass of ions.

Increase of magnetic field increases δ_M. This causes the radial potential and charge distribution within the plasma tube to adopt the form that it would at higher pressures [59]. This profile is more peaked towards the centre of the discharge tube and corresponds to an increase in the axial electron density and a decrease in the axial electric field. Also the reduction in charged particle loss to the walls lowers the axial electric field required to maintain the same discharge current in the tube. This leads to a monotonic reduction in the average electron temperature which becomes smaller as the gas pressure is increased. It has been experimentally observed that the axial electric field decreases with increasing magnetic field [22]. This decrease is found to be sharper at low fields and levels off as the field is increased.

However, at high enough magnetic fields the electron diffusion coefficient, D_e, can decrease enough to be comparable to the ion diffusion coefficient neglected so far. In such a case the free-fall theory considered till now is not applicable and ambipolar diffusion is to be taken into account. Then the radial electrostatic field is given by

$$E_r = \left(\frac{D_{eo}}{1 + \omega^2 \tau_e^2} - D_i\right) \frac{1}{n} \frac{dn}{dr} \qquad (6.4)$$

Since the number density gradient (radial) dn/dr is monotonic, as $\omega^2 \tau_e^2$ increases to a value greater than D_{eo}/D_i, the sign of the field reverses. This has the effect of reducing the charged particle density at the axis and in turn can decrease the output from an ion laser.

6.1.1 Experimental Details

The tube diameter used in the present work is 6.3 mm. The choice of this diameter is based on our earlier results for optimum performance of the laser. The two ends of the tube have been fitted with quartz windows tilted at nearly 1°. This makes the cavity losses degenerate with respect to the polarization modes of the laser and the tilt prevents etalon effects. The tube has been placed in a solenoid driven by a dc or pulsed current source as described in Chapter 2. Power output from the laser at various wavelengths has been measured using a photo-diode along with a gated integrator as discussed earlier.

6.1.2 Results and Discussion

The effect of magnetic field has been studied on five transitions viz. 4954Å, 5260Å, 5353Å, 5395Å and 5955Å. The variation in power output with magnetic field is presented in Figures 6.1 - 6.6. Each figure shows the output variation at

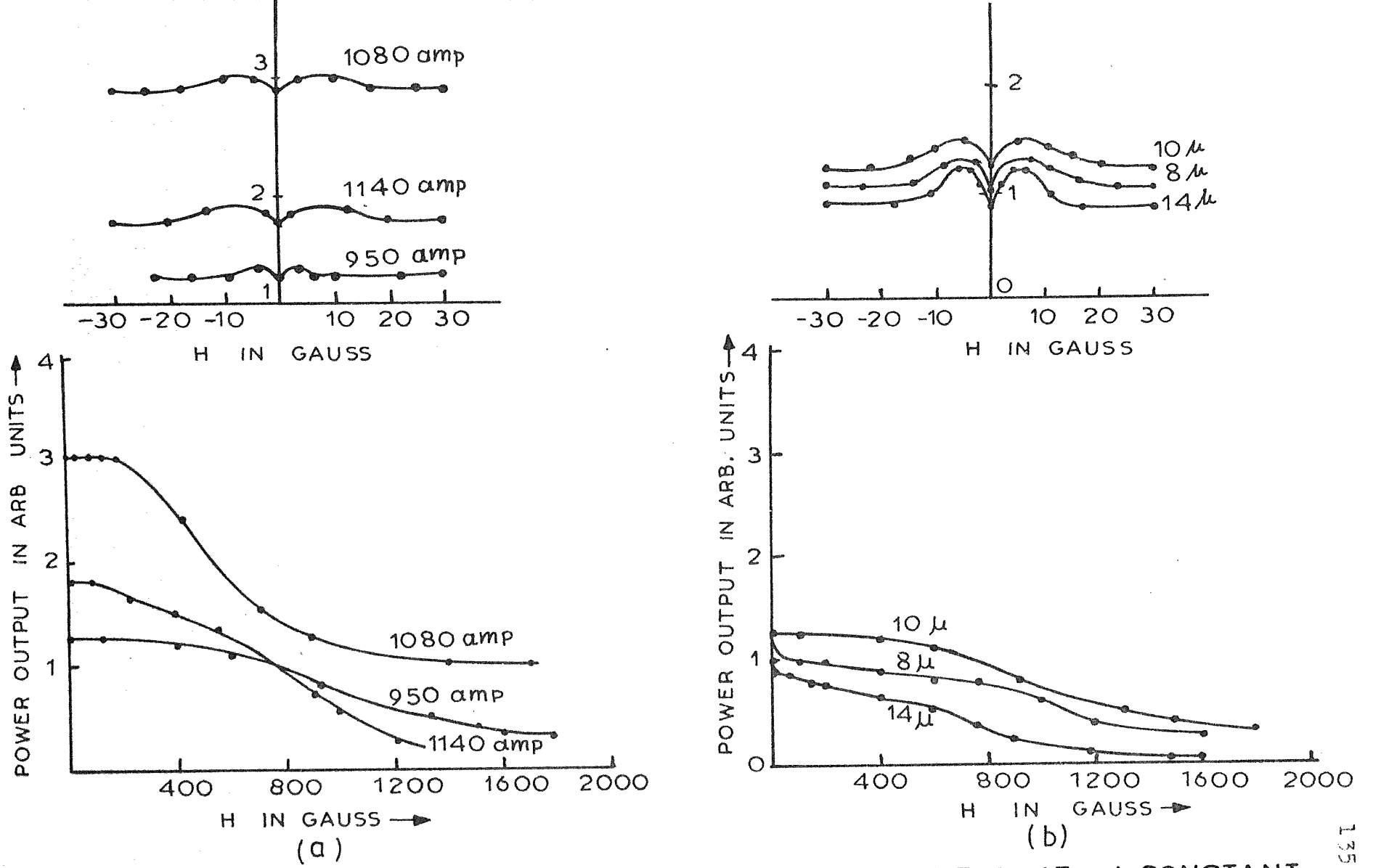

FIG. 6.2 POWER OUTPUT VARIATION WITH MAGNETIC FIELD AT a) CONSTANT PRESSURE: 10 μ, b) CONSTANT CURRENT: 950 amp. WAVELENGTH: 4954 Å°

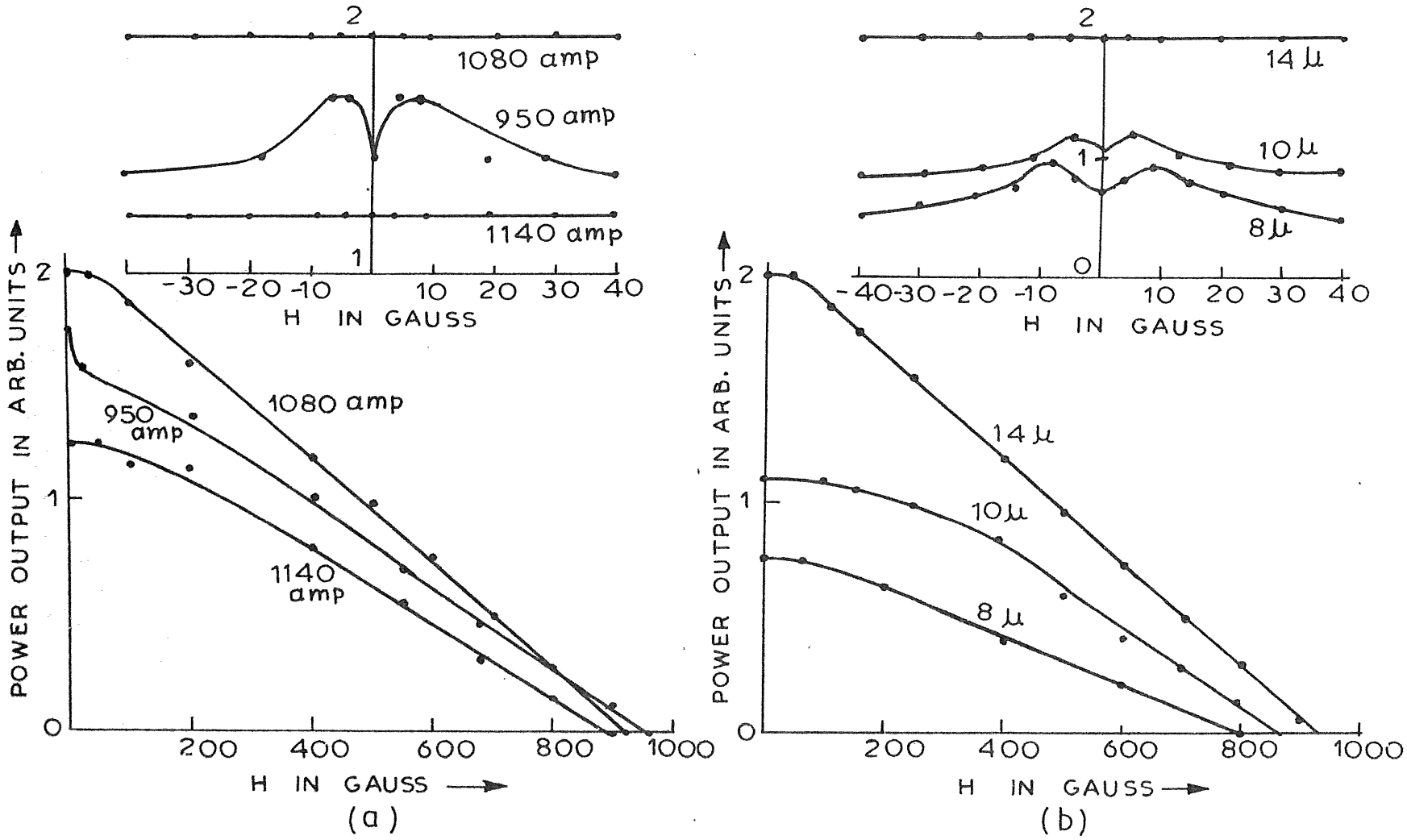

FIG. 6.3 POWER OUTPUT VARIATION WITH MAGNETIC FIELD AT a) CONSTANT PRESSURE: 14 μ, b) CONSTANT CURRENT: 1080 amp.
WAVELENGTH: 5260 A°

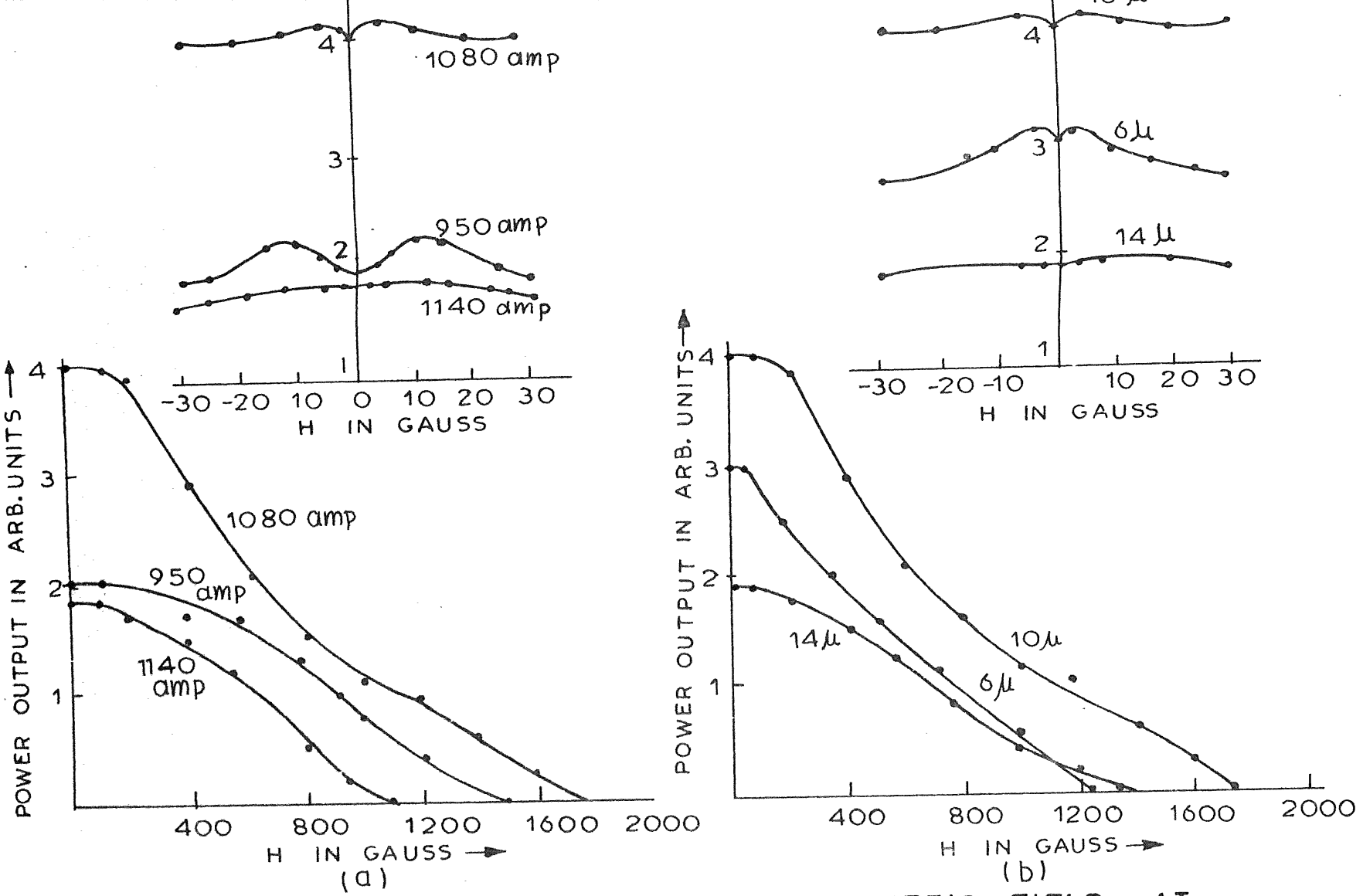

FIG.6.4 POWER OUTPUT VARIATION WITH MAGNETIC FIELD AT
a) CONSTANT PRESSURE: 10 μ , b) CONSTANT CURRENT: 1080 amp.
WAVELENGTH: 5353 A°

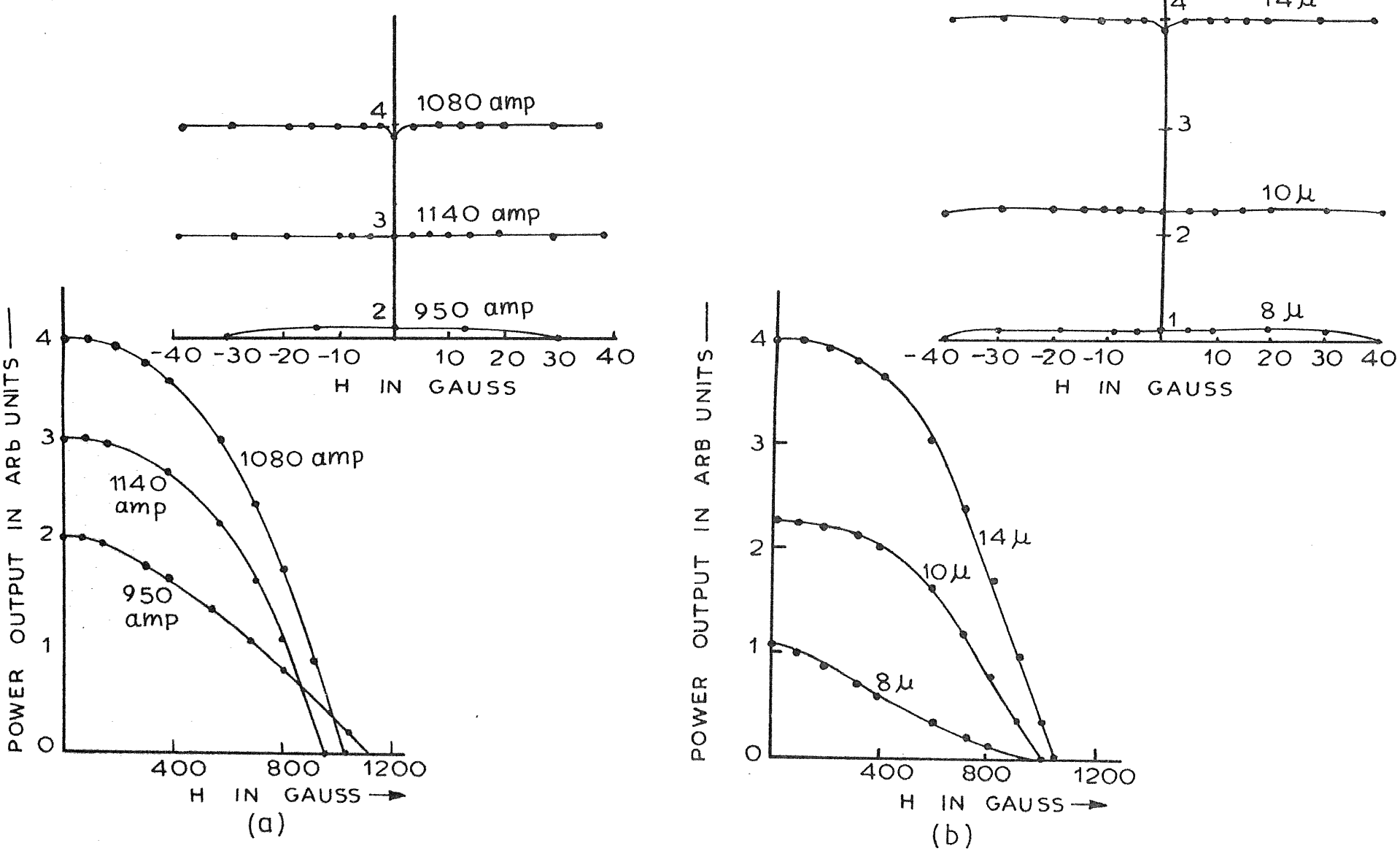

FIG.6.5 POWER OUTPUT VARIATION WITH MAGNETIC FIELD AT a) CONSTANT PRESSURE: 14 μ, b) CONSTANT CURRENT: 1080 amp.
WAVELENGTH: 5395 Å

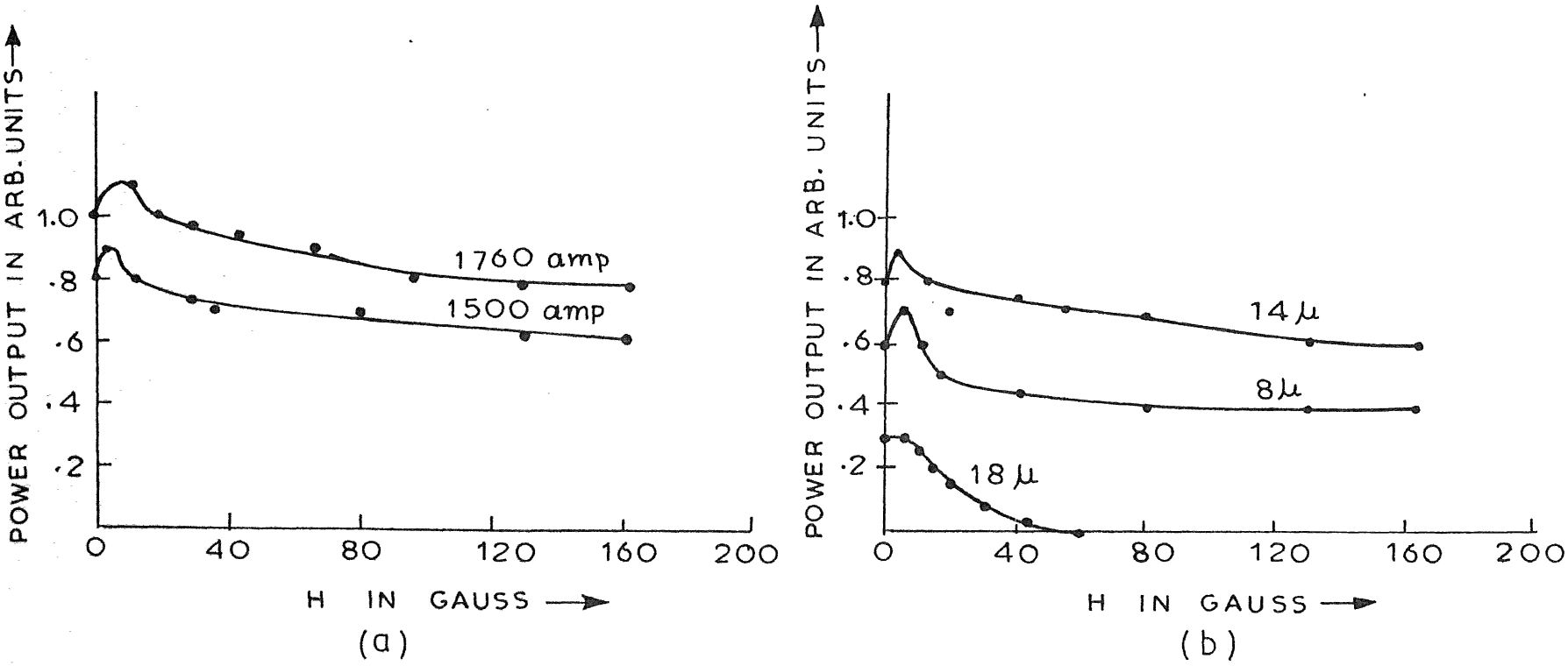

FIG. 6.6 POWER OUTPUT VARIATION WITH MAGNETIC FIELD AT
a) CONSTANT PRESSURE: 14 μ, b) CONSTANT CURRENT: 1500 amp.
WAVELENGTH : 5955 A°

different currents for a constant pressure as well as that at different pressures and a constant current. The variation in the all-line output is shown in Fig. 6.1 while Figures 6.2 - 6.6 represent the behaviour of individual lines. In figures 6.2 - 6.5, the variation at very low magnetic fields (0-40 G) has been shown in detail at the top. As indicated, data at these low field values have been taken by reversing the field direction also and the behaviour is found to be independent of the field direction. For the transition at 5955A, Fig. 6.6 shows the variation with magnetic fields upto 200 G. However, further increase in the field has continuously reduced the power output till lasing is quenched at fields of 600-1000 G, depending on the operating conditions. The data on this transition have been taken with He-Ne mirrors used to form the cavity.

It is observed that the power output in all the wavelengths is reduced by the application of the magnetic field. In some conditions there is a small increase in the power output at very low fields ($\sim$ 10 G). At high enough fields lasing is totally quenched. To confirm this behaviour supplementary observations (not shown in the figures) have been taken when the laser was operating just at threshold. There was no marked increase in the power output and the threshold is not observed to be lowered by the application of magnetic field.

As the magnetic field is increased (>200 G) the output beam shows a dark spot in the centre which increases in size with increasing field. At this stage lasing is observed to occur only in the higher order modes. This is similar to the effects observed in Ar^+ lasers by Gorog and Spong [59], Preobrazhenski and Shaparov [82].

At high pressures and currents, the laser pulse shows a double peak. The influence of the magnetic field is however different for the two peaks. This behaviour is very prominent for the line at 4954Å. It has been found that at all pressures, the output in the first peak reduces markedly on application of magnetic field whereas the output in the second peak first shows a slight increase (about ten percent at 150 Gauss) and then decreases slowly as the magnetic field is further increased. At pressurs slightly higher than the optimum, it has been observed that although there was only one peak at zero magnetic field, the second peak starts appearing as the magnetic field is increased. In all these cases, at still higher fields power output in both the peaks decreases and lasing is finally quenched.

These observations can be qualitatively understood as follows. When the magnetic field is applied, the consequent reduction in electron temperature reduces the excitation to the laser levels (the J^2 term) and hence the laser power decreases. The increase in the axial electron density is

probably not large enough to overcome this reduction except at very low fields ($\sim$10 G). A similar increase in the power output at very low fields has been reported by Fotiadi and Fridrikhov for the 4880A transition in the cw Ar^+ laser [65] and for the 1.15μ transition in the He-Ne laser [90]. The explanation given in the case of the IR transition is that the enhancement is due to the doubling of the number of holes in the gain curve when the separation between the σ^+ and σ^- Zeeman components is less than the homogeneous linewidth.

Attributing the reduction in power output with increasing magnetic field to the decrease in electron temperature is consistent with the fact that the second peak in the laser pulse is less affected by the magnetic field compared to the first one. It is to be recalled that the excitation for the second peak is attributed to a multi-step process so that reduction in the electron temperature would not be as significant at first and the increase in current density would probably enhance the excitation rate (the J^4 term) at moderate fields.

As the magnetic field is further increased, the 'anomalous' ambipolar diffusion reduces the charged particle density near the tube axis (defocussing). This opposes the action of pinch fields present in the discharge. This can be the reason for the appearance of a dark spot in the centre of the

output beam at high fields. As the field is further increased this effect becomes more predominant and the laser power decreases till it is quenched altogether. No apparent plasma instability has been observed to precede quenching of laser action in the present work.

6.2 Polarization Effects Due to the Magnetic Field

An externally applied magnetic field splits the laser transition into its σ^+ and σ^- components. Two effects arise due to this splitting. First, the gain coefficient of the medium is, in general, different for right- and left- circularly polarized radiation as can be seen by the intensity rules for Zeeman splitting. This causes the medium to exhibit circular dichroism. Also, since the real part of the index of refraction is generally different for the two components, the medium will exhibit Faraday rotation. In this condition , if a Brewster window (which selects linear polarization) is used in the laser cavity, then through circular dichroism the output radiation will become elliptically polarized. The axis of this ellipse will be rotated due to Faraday rotation.

The magnitude of the rotation depends on the gain coefficient of the laser medium (absorption coefficient for a passive medium) as given by Tobias and Wallace [62]. They have derived the expression for the polarizability of a dilute monoatomic gas for right- and left- circularly polarized radiation. To the first order in H, the polarizability is

given by

$$\alpha_{\pm} = \alpha_{\pm}^{o} + \alpha_{\pm}^{1} H \qquad (6.5)$$

The zero-order polarizability for a transition which is completely Doppler broadened is given by,

$$\alpha_{\pm}^{o} = - c\, k(\nu_o)\, F(\omega)/4\pi^{5/2}\, N \nu_o \qquad (6.6)$$

$k(\nu_o)$ is the absorption (gain) coefficient at the line centre, ν_o, N is the total number density of the atoms of the species under consideration and $F(\omega)$ and ω are given by,

$$F(\omega) = \exp(-\omega^2) \int_0^{\omega} \exp(y^2)dy \qquad (6.7)$$

$$\omega = [2(\ln 2)^{\frac{1}{2}}/\Delta\nu_o](\nu - \nu_o) \qquad (6.8)$$

Tobias and Wallace have further derived the first-order coefficients $\alpha_{\pm}^{1}$ for the three types of allowed transitions viz., $\Delta J = 0, +1, -1$. In each case the polarizability depends on the J values and degeneracies of the two levels, the Doppler width of the transition and is linearly proportional to $k(\nu_o)$. The single-pass Faraday rotation to the first-order is H is given by,

$$\theta = \frac{2\pi^2 N d \nu}{c} (\alpha_{-}^{1} - \alpha_{+}^{1})H \qquad (6.9)$$

d is the optical path length. The effective Verdet constant, V, of the active medium can be written as,

$$V = \frac{\theta}{Hd} \qquad (6.10)$$

However it has been observed in our work as well as by previous workers [61,65,63] that V depends on H. This shows the limited validity of the first-order theory.

6.2.1 Experimental Details

The plasma tube used for the present work has been described in Section 6.1.1. An additional quartz window has been placed at Brewster angle in the cavity to fix a reference axis for polarization selection. The output from the laser is passed through an analyzer and a polar plot of the radiation is drawn by measuring the power output at different orientations of the analyzer. Thus the ellipticity and the orientation of the major axis in the output at each wavelength have been measured for different values of the magnetic field.

The magnetic field produced by the solenoid has been found to be constant for over 90 percent of its length. The field variation at the ends has been taken into account by using an 'effective' length of the active medium in the calculation of the Verdet constant.

6.2.2 Results and Discussion

The variation in Faraday rotation with magnetic field is shown in Figures 6.7 - 6.11 for five of the lasing transitions. The magnitude of the rotation observed is quite high. As the field is increased, the rotation first increases to a maximum value, decreases and then saturates at some value.

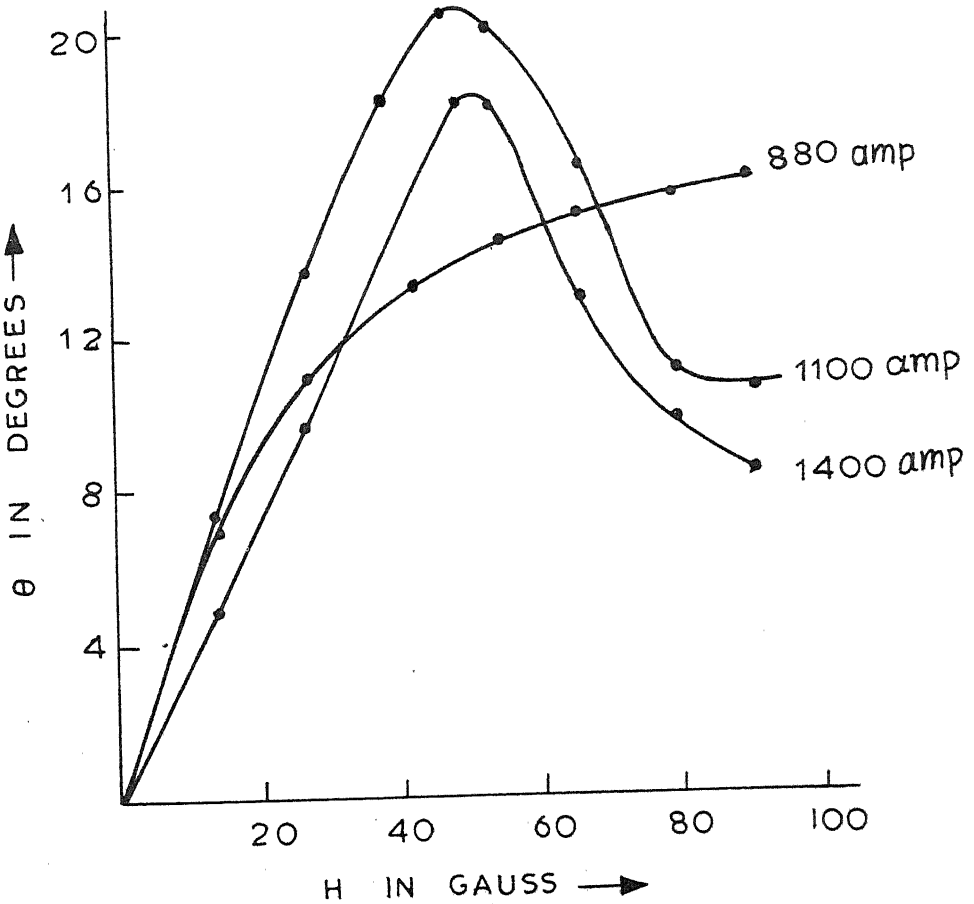

FIG. 6.7 FARADAY ROTATION Vs MAGNETIC FIELD FOR DIFFERENT DISCHARGE CURRENTS. WAVELENGTH : 4954 Å

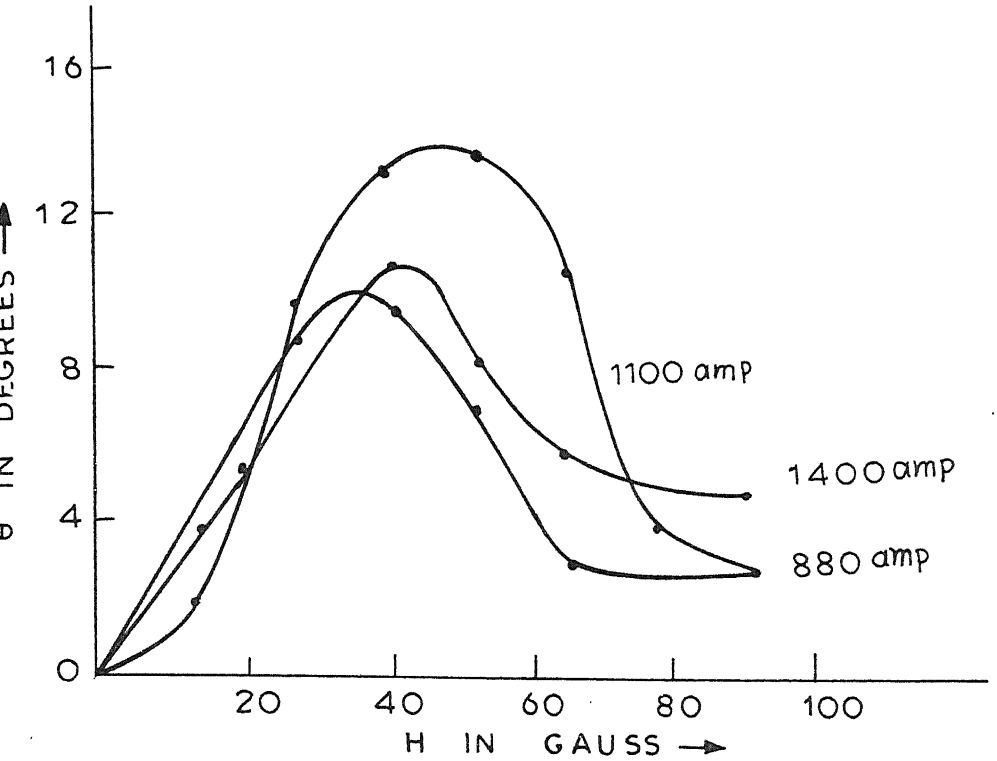

FIG.6.8 FARADAY ROTATION Vs MAGNETIC FIELD FOR DIFFERENT DISCHARGE CURRENTS
WAVELENGTH: 5260 Å

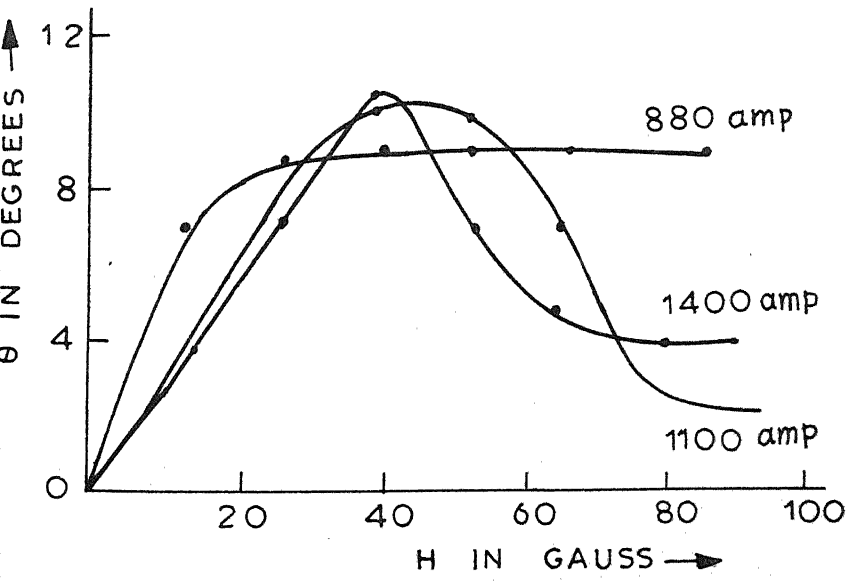

FIG.6.9 FARADAY ROTATION Vs MAGNETIC FIELD FOR DIFFERENT DISCHARGE CURRENTS.
WAVELENGTH: 5395 Å

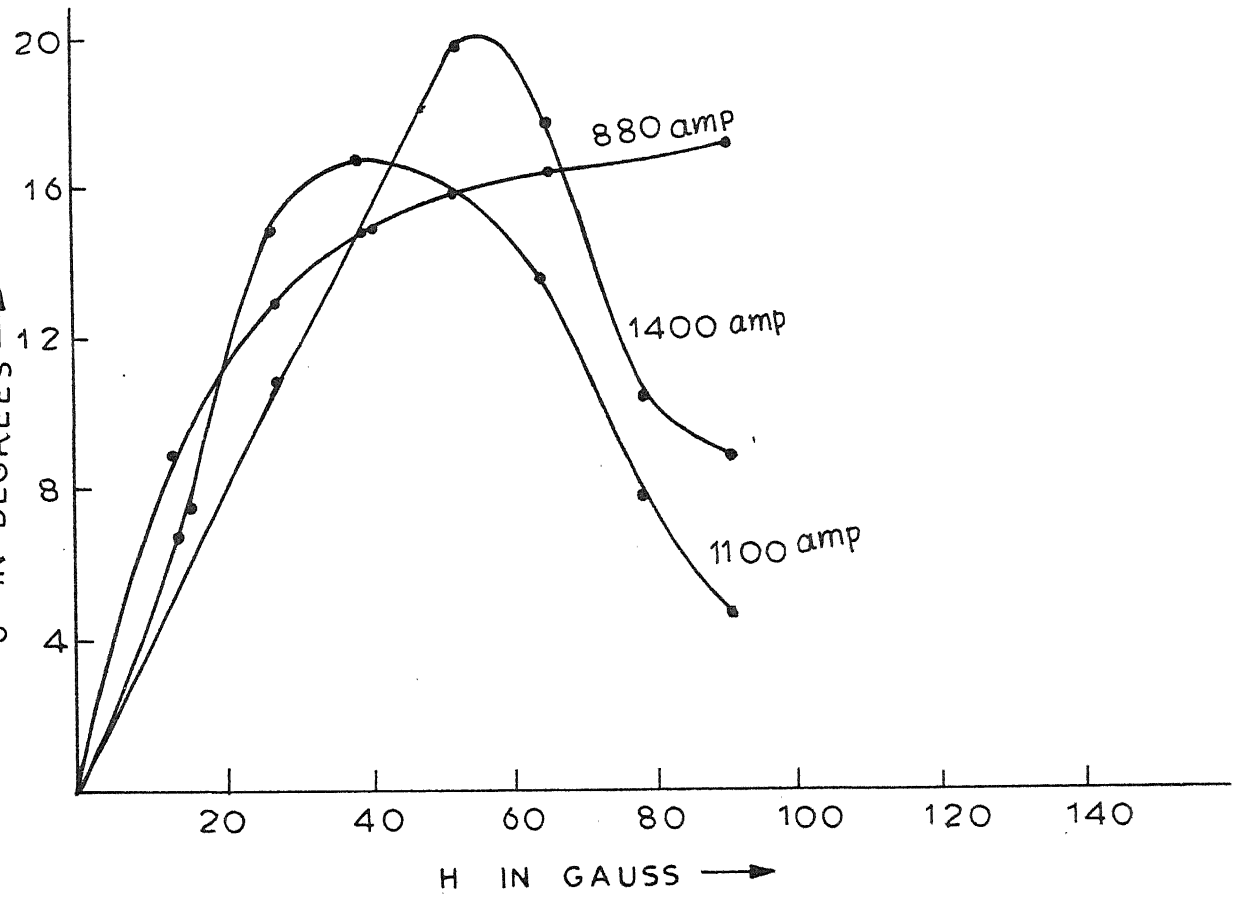

FIG.6.10 FARADAY ROTATION Vs MAGNETIC FIELD FOR DIFFERENT DISCHARGE CURRENTS WAVELENGTH : 5353 A°

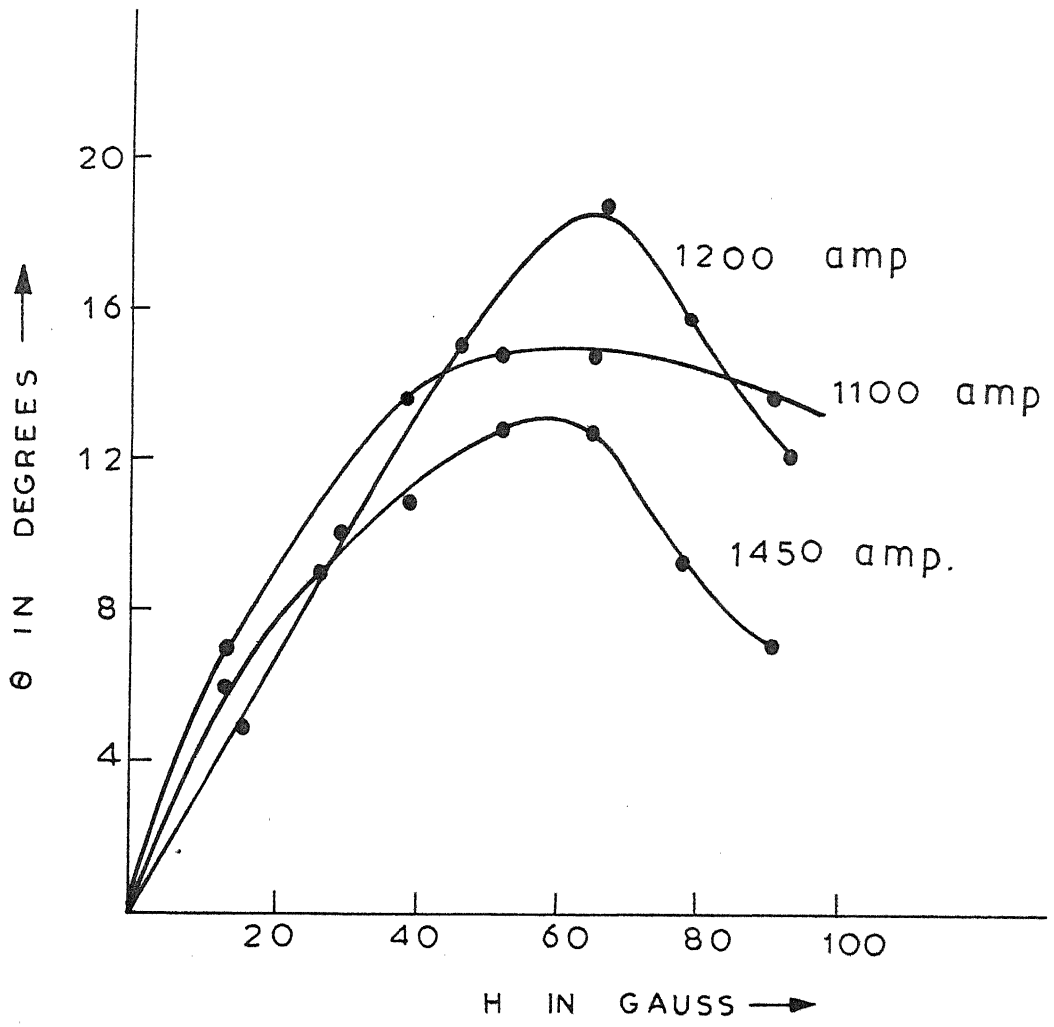

FIG. 6.11 FARADAY ROTATION Vs MAGNETIC FIELD AT DIFFERENT DISCHARGE CURRENTS WAVELENGTH : 5955 Å

At low currents, this variation is less pronounced. The ellipticity has been observed to be very small and shows a similar variation with magnetic field as that of the Faraday rotation (Fig. 6.12).

Equations 6.6 and 6.9 indicate that an increase in Faraday rotation implies an increase in gain, to a first-order approximation. However, the power output in each line has been observed to decrease with increasing magnetic field, (Fig. 6.13). One of the possible explanations for this behaviour can be given in the following manner. As discussed in Chapter 4, with no magnetic field the lines behave more like a homogeneously broadened one. When the magnetic field is applied, the σ^+ and σ^- components separate out, burning two different holes ('spin' packets) in the gain profile. This inhomogeneous behaviour reduces the efficiency of utilization of the inversion present in the medium; thereby decreasing the power output from the laser even if there is some gain enhancement. To confirm this a direct measurement of the variation in gain with magnetic field is required. However, the usual method of measuring gain in terms of the loss introduced through an additional Brewster window in the cavity does not give reliable results in this case due to the magnetic field induced Faraday rotation present in the medium. Efforts are underway to measure the gain using a cw probe beam from a tunable dye laser.

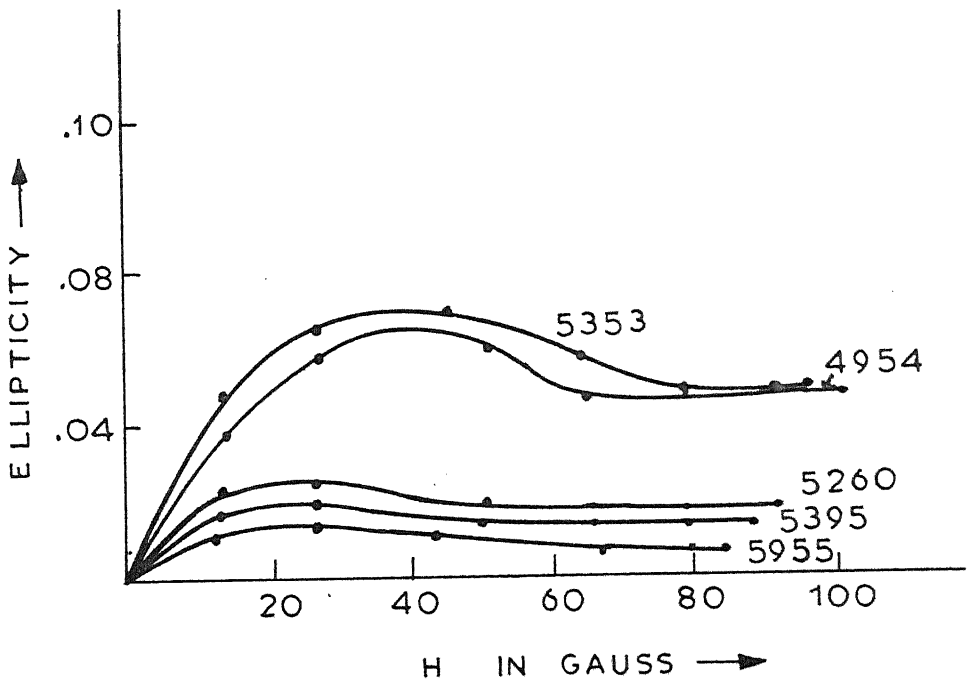

FIG. 6.12 VARIATION OF ELLIPTICITY WITH MAGNETIC FIELD.

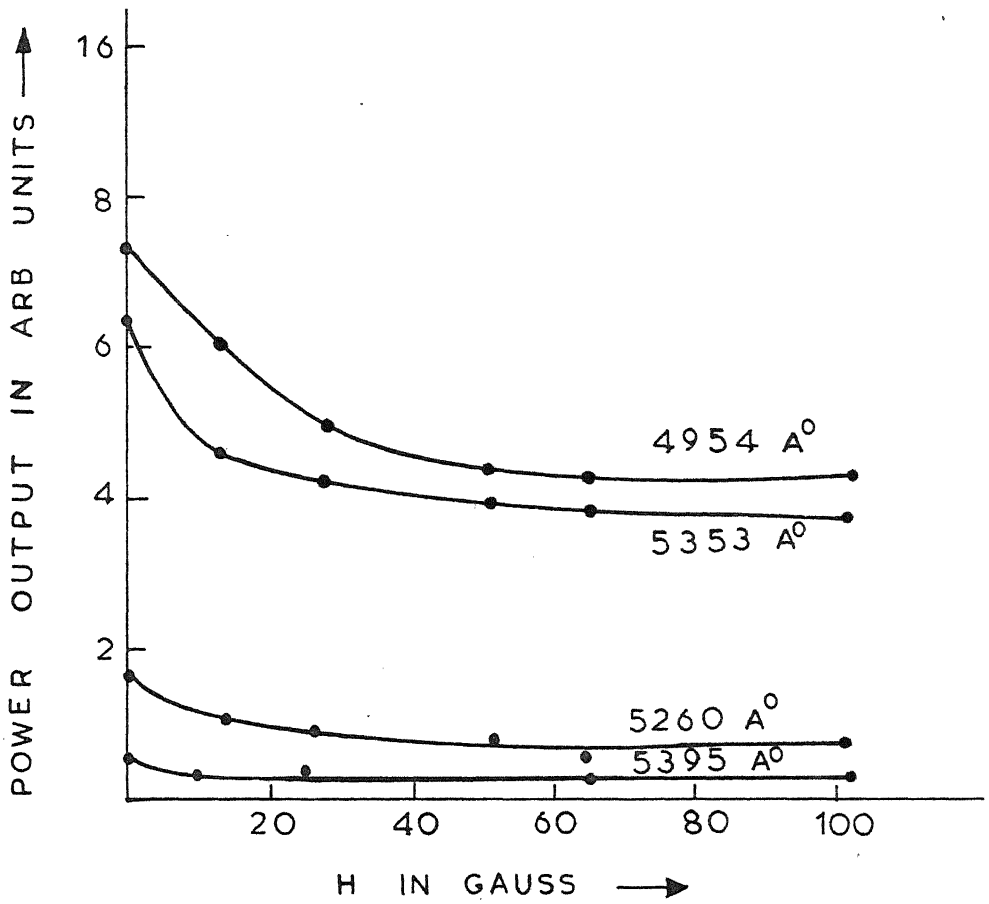

FIG. 6.13 VARIATION IN THE OUTPUT POWER WITH MAGNETIC FIELD WITH A BREWSTER WINDOW USED IN THE CAVITY, Current : 1080 amp., Pressure: 10 μ

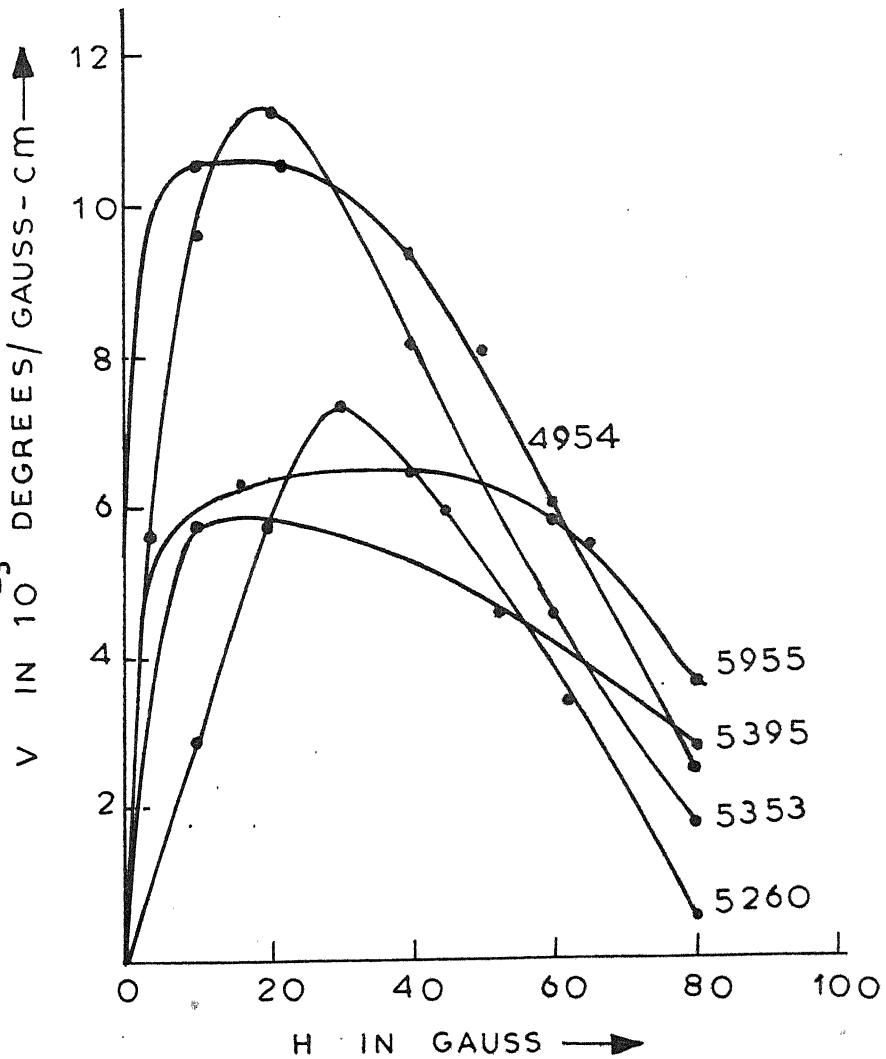

FIG.6.14 EFFECTIVE VERDET CONSTANT OF THE MEDIUM AT THE VARIOUS WAVELENGTHS Vs MAGNETIC FIELD.

CHAPTER 7

CONCLUSION

In this chapter, the main results of the present studies on some lasing transitions in the pulsed Xenon laser are presented.

The seven transitions studied are 4954.13 Å, 5007.8 Å, 5159.08 Å, 5260.19 Å, 5352.92 Å, 5394.62 Å and 5955.67 Å. As already mentioned, these transitions are assumed to belong to the Xe IV spectrum on the basis of empirical studies by many investigators. The fact that all these transitions belong to the same ionization species has been confirmed in our work also by the observation that the discharge conditions required for lasing are similar for all of them. Also, the very small spread in the E/p values where the output in the different lines optimises indicates that the upper levels of these transitions are close together.

In the Xe IV spectrum, very few energy levels are known. Using the data from the NBS tables of Atomic Energy Levels, energy differences have been calculated and compared with the wavenumbers of these transitions. It is to be noted that these transitions must be optically allowed ones as shown by their intensity in spontaneous emission and their high gains. From the listed levels (upto 23 eV above the Xe IV ground state) only the following closest coincidences were obtained within 20 cm^{-1}.

Wavelength in Å	Upper level energy, in cm^{-1}	Lower level energy in eV, in cm^{-1}	ΔJ	Difference in $\bar{\nu}$, in cm^{-1}
4954.13	165281	145107	-1	5.57
5394.62	167208	148684	-1	7.86
5352.92	173221	154532	+1	12.78
5159.08	179001	159643	+1 or -1	19.92

However none of these values are close enough to indicate a definite correlation. This lack of information about the spectroscopic parameters of the relevant levels is one of the main limitations in further quantification of the work on this laser.

All these transitions, though belonging to the same ionization species, have some characteristic differences as evidenced by their dependence on the operating parameters of the laser. In the first instance, there is no apparent

correlation in their lasing which indicates that they originate from different energy levels. For five of these transitions viz. 4954 Å, 5008 Å, 5160 Å, 5353 Å and 5395 Å, this has been shown to be the case by Bridges and Mercer using laser correlation spectroscopy.

The main characteristics of the different transitions observed in the present work are enumerated below.

1) The line at 4954 Å has the lowest operating threshold and the maximum unsaturated gain. This line lases at extremely low pressures also when all the other lines stop lasing and is least sensitive to contamination in the discharge. This can mean that the upper level for this transition is the most efficiently excited one.

2) The transition at 5395 Å, on the other hand, lases most strongly at the highest operating pressures and is then the dominant one. The line at 5260 Å shows a similar behaviour and both the lines optimise at nearly the same pressure. This indicates that probably the upper levels for these two transitions are very close-by and/or have the same symmetry properties for electron impact excitation.

3) The transition at 5008 Å also lases strongly at higher operating pressures, but it is not inherently as strong as the transitions at 5395 Å and 5260 Å.

4) The line at 5955 Å has the highest operating pressure

among all these lines. However, both the power output and gain are comparatively lower.

5) The transition at 5160 Å is the most sensitive one to changes in operating conditions and lases in the narrowest pressure range. The power output and the gain are again comparatively lower.

6) The transition at 5353 Å is the strongest one at the all-line optimum pressure. The gain of this line is comparable to that of 4954 Å.

There is also a slight but distinct difference in the optimum excitation voltage for each line and the power output in any particular line can be optimised by adjusting the pressure and the excitation voltage. The optimum pressure depends on the discharge current and the tube diameter also. With increasing current the optimum pressure increases in all cases. The variation with tube diameter is however very different. The optimum pressures of individual lines show a non-linear dependence on tube diameter. This dependence is not observed to follow any simple mathematical relationship. On the other hand, the all-line optimum pressure decreases linearly with increasing diameter.

The excitation processes for all these transitions are basically similar, at least in the short-pulse case, and involve multiple electron collisions. The main process

is probably a two-step excitation from the neutral atom ground state to the upper laser level with one of the Xe III levels being the intermediate level. Another excitation mechanism which involves a four-step excitation to the upper laser level is also present. This process could involve either cascade or recombination. It is normally not as efficient as the main process. However, the operating conditions required are slightly different for the two processes. The second one becomes more significant at high currents and pressures. Also, there is some delay between the inversion build-up due to the two processes, the second one taking a longer time. We believe that this is responsible for the double peak observed in the laser pulse at high currents and pressures.

Quenching of laser action is most probably due to increased deexcitation of the levels by electron collisions. Collisions/recombination at the tube walls also play a major role as shown by the following facts.

1) Lasing is not powerful in very small-bore tubes (1.5 mm). Even in wide-bore tubes the inversion is confined to a region more nearer the tube axis.
2) The optimum input energy density, as given by small-signal gain measurements, is larger for small-bore tubes and the efficiency of laser action decreases with decreasing diameter.

For the same reasons we believe that radiation trapping need not be the predominant process in deciding the laser behaviour. These conclusions about the excitation mechanism are further supported by the observed effects of axial magnetic fields on the laser output.

The application of a longitudinal magnetic field, in general, causes the electron temperature to go down while increasing the axial charged particle density. In the present case, no marked increase in the laser output has been observed on application of a magnetic field. However, the second peak in the laser pulse, when present, is observed to be less affected by the magnetic field as compared to the first one. At high magnetic fields, probably the anomalous ambipolar diffusion reduces the charged particle density, leading to a gradual quenching of laser action. A large Faraday rotation has been observed to be produced in the medium due to the magnetic field, possibly because of the high gains on these transitions. Magnetic field induced circular dichroism is also present although the observed ellipticity is small.

As an extension of the work presented in this thesis it is proposed to carry out the following studies on this laser.

1) Lineshape and linewidth parameter measurements and possibly the dynamic lifetime measurements on at least some of these transitions using a high-resolution

probe laser. Facilities for these experiments are being set-up.

2) Temporal and spatial variation of gain using direct as well as indirect techniques.

3) It is also desirable to carry out some plasma parameter measurements using suitable plasma probes or spectroscopic methods.

Finally, it has been observed in our work that there is a marked jitter in the power output of the laser due to pressure fluctuations in the discharge. Our experience indicates that closed-loop stabilisation of manifold pressure (using a cold trap and heater) alone is not entirely satisfactory as the percentage jitter in the output depends to some extent on the history of the tube also. The reason for this possibly lies in either the high adsorption/desorption of xenon by the glass walls of the plasma tube or the changes in the surface characteristics of the Indium cold cathode in course of time. We have not studied this problem in detail but we believe that it should be taken into account for any further technological developments on this laser.

REFERENCES

1. W.B. Bridges, Appl. Phys. Lett. 4, 128 (1964)
2. G. Convert, M. Armand and P. Martinot-Lagarde, Compt. Rend. Acad. Sci. Paris, 258, 3259 (1964)
3. G. Convert, M. Armand and P. Martinot-Lagarde, Compt. Rend. Acad. Sci. Paris, 258, 4467 (1964)
4. W.R. Bennett, Jr., J.W. Knutson, Jr., G.N. Mercer and J.L. Detch, Appl. Phys. Lett., 4, 180 (1964)
5. W.B. Bridges, Proc. I.E.E.E. (Correspondence) 52, 843 (1964)
6. E.I. Gordon, E.F. Labuda and W.B. Bridges, Appl. Phys. Lett. 4, 178 (1964)
7. D.C. Sinclair, J. Opt. Soc. Am. 55, 571 (1965)
8. F.A. Horrigan, S.H. Koozekanani and R.A. Paananen, Appl. Phys. Lett. 6, 41 (1965)
9. A.L. Bloom and W.E. Bell, Private Communication to Bridges and Chester, see ref. 12.
10. M. Birnbaum and T.L. Stockér, Private Communication to Bridges and Chester, see ref. 12.
11. L. Dana, P. Laures and R. Rocherolles, Compt. Rend. Acad. Sci. Paris, 260, 481 (1965)
12. W.B. Bridges and A.N. Chester, Appl. Opt. 4, 573 (1965)
13. P.K. Cheo and H.G. Cooper, J. Appl. Phys. 36, 1862 (1965)
14. R. Beck, W. Englisch, K. Gürs, 'Table of Laser Lines in Gases and Vapors', 3rd Ed., Springer-Verlag (1980)
15. R.A. Paananen, I.E.E.E. Spectrum 88,(1966)
16. V.F. Kitaeva, A.N. Odinstov, N.N. Sobolev, Sov. Phys. Usp. 12, 699 (1970)
17. W.B. Bridges and A.N. Chester, 'Ionised Gas Lasers' in 'Handbook of Lasers', CRC Press, Cleveland, Ohio (1971)

18. C.C. Davis and T.A. King, 'Gaseous Ion Lasers' in 'Advances in Quantum Electronics', Vol. 3, Academic Press, London and New York (1975)

19. M.H. Dunn and J.N. Ross, 'The Argon Ion Laser' in 'Progress in Quantum Electronics' Vol. 4, Pergamon Press, G.B. (1976)

20. W.B. Bridges and A.N. Chester, I.E.E.E. J. Quant. El. 1, 66 (1965)

21. C.S. Willett, 'Laser Lines in Atomic Species' in 'Prog. in Quant. El.', Vol. 1, Pt. 5, Pergamon Press, G.B. (1975)

22. W.B. Bridges, A.N. Chester, A.S. Halsted and J.V. Parker, Proc. I.E.E.E. 59, 724 (1971)

23. P. Laures, L. Dana and C. Frapard, Compt. Rend. Acad. Sci. Paris, 258, 6363 (1964)

24. P. Laures, L. Dana and C. Frapard, Compt. Rend. Acad. Sci. Paris, 259, 745 (1964)

25. L. Dana and P. Laures, Proc. I.E.E.E. (Correspondence) 53, 78 (1965)

26. L. Minnhagen, Ark. Fys. 25, 203 (1963)

27. M. Gallardo, J.G. Reyna-Almandoz, 'Xenon Lines in the Range from 2000Å to 7000Å', CIO_p Serie Monograficas Cientificas No. 1 (1981)

28. E.U. Condon and G.H. Shortley, 'The Theory of Atomic Spectra', University Press, Cambridge (1959)

29. H. Statz, F.A. Horrigan, S.H. Koozekanani, C.L. Tang and G.F. Koster, J. Appl. Phys. 36, 2278 (1965)

30. T.H.E. Cottrell, I.E.E.E. J. Quant. El. 4, 435 (1965)

31. C.C. Davis and T.A. King, Phy. Lett., 36A, 169 (1971)

32. W. Sasaki and S. Saito, Appl. Optics, 19, 5 (1980)

33. R.I. Rudko and C.L. Tang, J. Appl. Phys. 38, 4731 (1967)

34. M.B. Klein, Appl. Phys. Lett. 17, 29 (1970)

35. S. Hattori and T. Goto, I.E.E.E. J. Quant. El. 5, 531 (1969)

36. S.H. Koozekanani, Phy. Rev. 176, 160 (1968)

37. G.R. Levinson, V.F. Papulovskiy and V.P. Tychinskiy, Rad. Eng. Elec. Phys. 13, 578 (1968)

38. H.G. Heard and J. Peterson, Proc. I.E.E.E. 52, 1050 (1964)

39. L. Dana and P. Laures, Proc. I.E.E.E. 53, 193 (1965)

40. J.A. Dahlquist, Appl. Phys. Lett. 6, 193 (1965)

41. W.B. Bridges and G.N. Mercer, I.E.E.E. J. Quant. El. 5, 476 (1969)

42. S.M. Jarrett and G.C. Barker, I.E.E.E. J. Quant. El. (Notes and Lines) 5, 166 (1969)

43. W.W. Simmons and R.R. Witte, I.E.E.E. J. Quant. El. 6, 466 (1970)

44. P.K. Cheo and H.G. Cooper, Appl. Phys. Lett. 6, 177 (1965)

45. M. Gallardo, M. Garavaglia, A.A. Tagliaferri and E. Gallego Lluesma, I.E.E.E. J. Quant. El. (Correspondence) 6, 745 (1970)

46. W.B. Bridges and A.N. Chester, I.E.E.E. J. Quant. El. 7, 471 (1971)

47. E. Gallego Lluesma, A.A. Tagliaferri, C.A. Massone, M. Gallardo, J. Opt. Soc. Am. 63, 362 (1973)

48. C.C. Davis and T.A. King, I.E.E.E. J. Quant. El. (Correspondence) 8, 755 (1972)

50
49. A. Papayoanou, R.G. Buser and I.M. Gumeiner, I.E.E.E. J. Quant. El. 9, 580 (1973)

49
50. V. Hoffmann and P.E. Toschek, J. Opt. Soc. Am. 66, 152 (1976)

51. M. Gunderson and C.D. Harper, I.E.E.E. J. Quant. El. (Notes and Lines) 9, 1160 (1973) ; C.D. Harper and M. Gunderson, Rev. Sci. Instr. 45, 400 (1974)

52. A. Papayoanou and I. Gumeiner, Appl. Phys. Lett. 16, 5 (1970)

53. A. Papayoanou and I. Gumeiner, J. Appl. Phys. 42, 1914 (1971)

54. S. Hattori and T. Goto, J. Appl. Phys. 39, 5998 (1965)

55. E. Sakuma and T. Tako, Jap. J. Appl. Phys. 13, 1489 (1974)

56. V.F. Moskalenko, E.P. Ostaphenko, S.V. Pechurina, V.A. Stepanov Yu. M. Tsukanov, Opt. Spectr. 30, 201 (1971)

57. J.R. Forrest and R.N. Franklin, Br. J. Appl. Phys. 17, 1569 (1966)

58. J.R. Forrest and R.N. Franklin, Br. J. Appl. Phys. 17, 1061 (1966)

59. I. Gorog and F.W. Spong, Appl. Phys. Lett. 9, 61 (1966)

60. S.A. Ahmed, T.J. Faith and G.W. Hoffmann, Proc. I.E.E.E. (Letters) 55, 691 (1967)

61. D.C. Sinclair, J. Opt. Soc. Am. 56, 1727 (1966)

62. I. Tobias and R.A. Wallace, Phy. Rev. 134, No. 3A, 549 (1964)

63. D.K. Terekhin and S.A. Fridrikhov, Sov. Phys. - Tech. Phys. 14, 1444 (1969)

64. R.L. Fork and C.K.N. Patel, Phy. Rev. 129, 2577 (1963)

65. A.E. Fotiadi and S.A. Fridrikhov, Sov. Phys. - Tech. Phys. 14, 1292 (1970)

66. H.S. Ames, I.E.E.E. J. Quant. El. (Correspondence) 8, 808 (1972)

67. W.W. Simmons and R.S. Witte, I.E.E.E. J. Quant. El. 6, 648 (1970)

68. J.P. Goldsborough, E.B. Hodges and W.E. Bell, Appl. Phys. Lett. 8, 137 (1966)

69. P.O. Clark, I.E.E.E. J. Quant. El. 1, 109 (1965)

70. A. Maitland and M.H. Dunn, 'Laser Physics', North Holland Publishing Company, Amsterdam-London (1969)

71. W.W. Rigrod, J. Appl. Phys. 34, 2602 (1963)

72. A.D. White, E.I. Gordon and J.D. Rigden, Appl. Phys. Lett. 2, 91 (1973)

73. P.W. Smith, I.E.E.E. J. Quant. El. 2, 62 (1966)

74. T.F. Johnston Jr., I.E.E.E. J. Quant. El. 5, 616 (1969)

75. E.I. Gordon, E.F. Labuda and R.C. Miller, I.E.E.E. J. Quant. El. 1, 273 (1965)

76. H. Boersch, G. Herziger, W. Seelig and I. Volland, Phy. Lett. 24A, 695 (1967)

77. E. Skurnick and H. Schacter, J. Appl. Phys. 43, 3393 (1972)

78. C.P. Wang and S.C. Lin, J. Appl. Phys. 43, 5068 (1972)

79. H. Boersch, J. Boscher, D. Hoder and G. Schafer, Phy. Lett. 31A, 188 (1970)

80. P.C. Thoneman and W.T. Cowhig, Proc. Phys. Soc. BG-4, 345 (1951)

81. I. Gorog and J.R. Singer, J. Appl. Phys. 37, 4141 (1966)

82. N.G. Preobrazhenski, N.Ya. Shaparov, Opt. Spectr., 25, 172 (1968)

83. M.I. Dyakonov and V.I. Perel, Sov. Phys. JETP, 23, 298 (1966)

84. M. Birnbaum, Appl. Phys. Lett. 12, 86 (1968)

85. V.A. Burmakin, F.A. Korolev, V.V. Lebedeva, A.I. Odintsov, V.M. Salimov and L.N. Sinitsa, Rad. Eng. Elec. Phys. 16, 1228 (1971)

86. I. Gorog, RCA Review, 32, 88 (1971)

87. E.I. Gordon, E.F. Labuda, R.C. Miller, C.E. Webb in 'Physics of Quant. El.', Ed. Kelley, Lax, Tannenwald, McGrawhill Inc. (1966)

88. L. Tonks, Phy. Rev., 56, 360 (1939)

89. I. Langmuir and L. Tonks, Phy. Rev., 34, 876 (1929)

90. A.E. Fotiadi, S.A. Fridrikhov, Sov. Phys. Tech. Phys., 11, 416 (1966)

PHY-1984-D-CHA-STU